2014

The evaluation of the hindered settling behavior of the ground calcium carbonate suspension

Raj Jain
University of Toledo

A Thesis

entitled

The Evaluation of the Hindered Settling Behavior of the Ground Calcium Carbonate Suspension

by

Raj Jain

Submitted to the Graduate Faculty as partial fulfillment of the requirements for the Master of Science Degree in

Industrial Pharmacy

_____

Kenneth Alexander, PhD., Committee Chair

_____

Sai Hanuman Sagar Boddu, PhD., Committee Member

_____

Jerry Nesamony, PhD., Committee Member

_____

Patricia R. Komuniecki, PhD, Dean
College of Graduate Studies

The University of Toledo

May 2014

An Abstract of

The Evaluation of the Hindered Settling Behavior of the Ground Calcium Carbonate Suspension

by

Raj Jain

Submitted to the Graduate Faculty as partial fulfillment of the requirements for the Master of Science Degree in
Industrial Pharmacy

The University of Toledo

May 2014

The purpose of this study is to examine the effects of a non-ionic surfactant, Labrasol®, on the settling behavior of suspensions prepared from ground calcium carbonate. Suspensions were prepared with Labrasol® concentrations of 0%, 0.05%, 0.5%, 1.0%, and 2.0% and containing Calcium carbonate at weights of 20 to 50 grams in increments of 5 grams. The settling behavior of the suspensions were analyzed by using modified Stokes' laws, specifically the Steinour's equation, Richarson and Zaki's equation and Dollimore-McBride's equations. The Kozeny and Carman equation was used to analyze the permeability of the suspension. In addition to the previous equations, the suspensions were also analyzed using laser diffraction, scanning electron microscopy, zeta potential determination, differential scanning calorimetry, and powder x-ray diffraction. Based on the modified Stokes' Laws, it is shown that increasing concentrations of Labrasol® led to a decrease in particle size and increased deflocculation of the suspension. Laser diffraction gave results that were inconsistent with data provided from the modified Stokes' laws, most likely due to the homogenizer disturbing the suspension. Powder x-ray diffraction showed that the surfactant

concentration had no effect on the crystallinity of the calcium carbonate. Kozeny and Carman showed a decrease in permeability which was consistent with the reduction in particle size. Differential Scanning Calorimetry shows an overall trend of decreasing heats of vaporization. This is possibly due to the surfactant causing an increase in the heat transfer in the suspension by increasing the wettability between the suspension media and the crucible surface. The deflocculation of the suspension causes a decrease in particle size which allows for more surface area for water adsorption, but DSC results obtained here cannot confirm that without further testing. Zeta potential measurements show that increased surfactant led to a more negative zeta potential, possibly due to deflocculation leading to more ion adsorption sites for the electric double layer.

Table of Contents

List of Tables

List of Figures

Chapter 1

Introduction

In the pharmaceutical and chemical industries, when working with suspensions, the sedimentation behavior is considered one of the more important aspects of the suspension stability. Sedimentation or more specifically the hindered settling of suspensions is used as an analytical tool to determine various characteristics of the suspension. This research project focuses on the preparation and analysis of ground heavy calcium carbonate suspensions. Ground calcium carbonate is a term used to describe calcium carbonate prepared from natural sources, usually mined from rocks which include chalk, limestone and marble. Ground calcium carbonate has a wide variety of uses, however, in regards to pharmaceuticals, synthetic or precipitated calcium carbonate is preferred due to the energy intensive process of grinding and pulverizing natural sources into particle sizes that are acceptable for use.

In this project high concentrations of ground heavy calcium carbonate are used. This is due to the fact that at low concentrations, the hindered settling phenomenon is not observable. High concentrations of suspended calcium carbonate lead to particle-particle interactions which allow for hindered settling to be visible to the naked eye. Also, at high concentrations of calcium carbonate, the particle-particle interactions lead to the

formation of aggregates which are referred to as flocs. The suspensions prepared were composed of varying concentrations of heavy calcium carbonate and a non-ionic surfactant. The sedimentation rates in the prepared suspensions were used to determine the particle size using modified Stokes' law equation such as the Dollimore-McBride, the Richardson- Zaki, and the Steinour equations. In addition to particle size, the permeability of the suspension is analyzed using the Kozeny-Carman equation.

A non-ionic surfactant, Labrasol®, was used at varied concentrations to determine what effects it would produce in the calcium carbonate suspensions. Variables that were studied included particle size, zeta potential, bound and unbound water, surface morphology, and crystal lattice structures. Particle size was determined using the aforementioned modified Stokes's laws in addition to laser diffraction. Zeta potential was measured to determine if the non-ionic surfactant had an effect on the difference in electric potential between the dispersion medium and the fluid layer around the suspended particles. Differential Scanning Calorimetry was used to analyze the effects that Labrasol® had on the bound and unbound water in the suspensions. Analysis of the thermogram produced via Differential scanning calorimetry allows for the determination of the heats of crystallization, vaporization, and fusion. Scanning electron microscopy was used to study the effects on the surface morphology of calcium carbonate that resulted from varied concentration of Labrasol®. Powder x-ray diffraction was a tool used to show whether or not Labrasol® produced any variability in the crystallinity of the calcium carbonate.

Chapter 2

Ground Calcium Carbonate

2.1 Calcium Carbonate

Calcium carbonate is a chemical with the formula $CaCO_3$. It is a compound found abundantly in many natural as well as biological sources. Biological sources include sea shells, oyster shells, coral, and egg shells. Natural sources of calcium carbonate are found in rocks, mainly limestone, marble and chalk. Calcium carbonate is a polymorph meaning it is able to exist in several different crystal lattice formations. Its different polymorphs are calcite, aragonite, vaterite, and ikaite, with stability going from most stable to least stable, respectively. Calcite and aragonite are the two main polymorphs found in nature, however, compared to calcite, the other three forms are thermodynamically unstable and will eventually convert to the more stable calcite form.

There are two primary ways for preparing calcium carbonate for use in industry. The first method is to mine it directly from a natural source such as chalk which usually presents the most pure natural source, in some cases up to 99% purity. A second method for the preparation of calcium carbonate is through calcination. Calcination is the heating of calcium carbonate sources, such as limestone, to 825 °C. When calcium carbonate is

heated it will undergo decomposition forming calcium oxide. The calcium oxide is dissolved in water at which point it will convert to calcium hydroxide. Carbon dioxide is then passed through the solution, and it will react with the calcium hydroxide to form calcium carbonate which is insoluble and will precipitate out of the water.

$$CaCO_3 \rightarrow CaO + CO_2 \qquad \text{Eq. 2.1}$$
$$CaO + H_2O \rightarrow Ca(OH)_2 \qquad \text{Eq. 2.2}$$
$$Ca(OH)_2 + CO_2 \rightarrow CaCO_3 + H_2O \qquad \text{Eq. 2.3}$$

A third method for the production of calcium carbonate is to react molar equivalents of calcium chloride and sodium bicarbonate in solution to precipitate calcium carbonate

$$2NaHCO_{3(aq)} + CaCl_{2(aq)} \rightarrow CaCO_3 + 2NaCl_{(aq)} + H_2O + 2CO_2 \qquad \text{Eq. 2.4}$$

. If mined directly from a natural source it is labeled as ground calcium carbonate, and if it is produced via chemical reaction, it is labeled as precipitated or synthetic calcium carbonate. Either source of calcium carbonate can be used in pharmaceutical preparations as long as it meets purity standards for use.

2.2 Properties of Calcium carbonate

2.2.1 Physicochemical Properties:

Calcium carbonate appears as a fine white chalk-like powder. It has a molecular weight of 100.09 g/mol, and a melting point of 825°C. In its calcite form, it has a density of 2.711 g/cm^3, and in its aragonite form, it has a density of 2.8 g/cm^3. It possesses a solubility of 15 mg/L, but at acidic pH its solubility increases greatly. Its increased solubility at acidic pH's is due to the equilibrium shift between it soluble and insoluble form. The dissolved form of calcium carbonate is in the form of a calcium ion and carbonate ion. In an acidic environment, the carbonate ion will react with hydrogen ions to form bicarbonate ions. The removal of carbonate ions from solution causes the equilibrium to shift leading to more calcium carbonate dissolving and ionizing to calcium and carbonate ions.

2.2.2 Uses:

Calcium carbonate has a variety of uses in and out of the pharmaceutical industry. One of the most common uses in the pharmaceutical industry is as a cheap calcium supplement or antacid. Another common use is as a bulking agent for pharmaceutical preparations. It can also act as an anti-diarrheal. It does so by binding water in the intestines leading to a firmer stool. It can also be used as a food preservative. Due to the extent of use of calcium carbonate as a calcium supplement, antacid, anti-diarrheal, preservative, or in fortifying foods with calcium, it is wholly possible to develop

hypercalcemia. Hypercalcemia is marked by an elevated amount of calcium in the blood. In serious cases it can lead to abnormal heart rhythms and/or renal failure.

Calcium carbonate also has many uses in other industries. In the construction industry it was once widely used in cement compositions, however, that has since subsided due to the ability of acid rain to dissolve calcium carbonate, thus weakening any cement formulation in which it was used. In the oil industry it can be used as a bulking agent to increase the density of drilling fluids to control the pressure within the drill hole. It is commonly used as a filler in papermaking due to its low cost. Another use is in the processing of iron ore to give purified iron. This is accomplished by calcination. The calcium oxide produced from the heating of calcium carbonate forms a slag with impurities and removing them from the iron ore.

Chapter 3

Hindered Settling Theory

3.1 Introduction:

Suspensions are dosage forms used to facilitate the delivery of insoluble dugs in a dispersion media, commonly water in the case of pharmaceuticals. Suspensions are heterogeneous mixtures of insoluble solids with varying particle sizes. Depending on the particle size and concentration of the solids in suspension, the rates of settling will vary along with the sedimentation behavior. When the concentration of the suspended solid is low enough, the particles settle independent of one another, and the suspension can be analyzed with Stokes' law. This type of sedimentation is termed "free settling." With higher concentrations, different sedimentation behaviors are exhibited and Stokes' law can no longer be applied. For instance, high concentrations of suspended solids lead to particles interacting with each other, creating a hindered settling sedimentation. In hindered settling, due to the particles interacting with each other, a visible interface is produced in the suspension. Above the interface is a clear supernatant of the dispersion media, and below is the mass of particles settling en bloc [1]. When studying hindered settling, a marked interface is key to its analysis, as without it, accurate sedimentation

rates cannot be determined. Determining at what concentrations of suspended solids will incur hindered settling is important when it comes to pharmaceutical formulation designs, however, with increasing concentrations sedimentation behavior will gradually change from free settling to hindered leaving a concentration range in the middle where it is difficult to clearly distinguish between the two settling behaviors.

In analyzing the settling of suspended solids, there are a number of factors to consider that can affect the rate of sedimentation and final sedimentation volume. These include: concentration of the suspension, particle size and shape, range of particle sizes, ability of particles to form flocs, and physicochemical properties of the suspending media [1].

A common method to study sedimentation and determine whether the suspension exhibits free settling or hindered settling is to use a large clear graduated cylinder that is filled with the suspension that is to be studied. The suspension is mixed and agitated in the cylinder to ensure homogeneity, at which point the height of the interface, if it is present, and its rate of decline can be measured. The data gathered is graphed on an xy-plot with height of the interface on the y-axis and time on the x-axis. Using the plot of height versus time, three regions of the data can be distinguished. Region A, which is the first, is the initial settling of the suspension where the particles are compressing before they settle en bloc and before the interface is visible. Region B is the second region. It is where hindered settling occurs with a linear rate of sedimentation. Region B is the most important as it provides the data to be used for determining particle size. Region C, the third, is the region where there is so much particle-particle interaction, the rate of

sedimentation drops drastically and the suspension is nearing its final sedimentation volume. These three regions are seen in Figure 3-1.

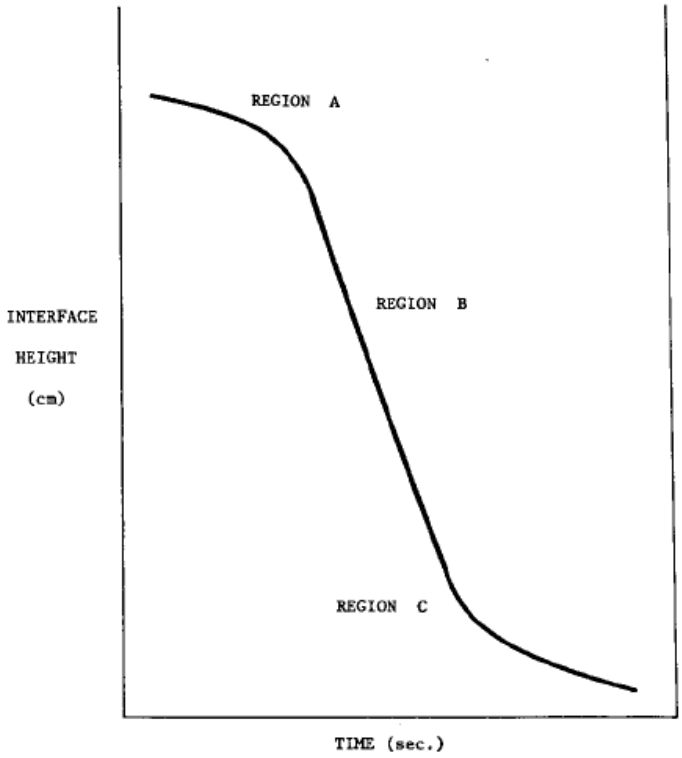

Figure 3-1 A plot showing the initial region, A, the linear region showing rate of sedimentation, B, and the final region showing the decrease in the compressibility of the suspension, C [1].

3.2 Stokes' Law

In suspensions containing low concentrations of solid particles, below the threshold for hindered settling, sedimentation occurs by means of gravitational forces causing the particles to settle. Suspensions that have free settling sedimentation behavior can be examined with Stokes' law, given as:

$$V_s = \frac{2gr^2(\rho_s - \rho_l)}{9} \qquad \text{Eq. 3.1}$$

Where, (Vs) is the spherical particles settling velocity;

(r) is the radius of the particle;

(g) is the acceleration due to gravity;

(ρs) is the density of the solid;

(ρl) is the density of the liquid medium; and

(η) is the coefficient of viscosity.

Stokes' law, in practical usage, applies only to perfectly ideal suspensions containing spherical particles. In real world applications, solid particles are not spheres. The particles vary in shape, size, and spatial orientation, which in turn causes particles to sediment at different rates [2]. Stokes law has been modified numerous times to encompass non-spherical particles, which then includes a dimensionless factor. When dealing with non spherical particles, the radius of the particle is determined by the radius of a sphere having the same volume of the particle in suspension. For suspensions that have very low particle-particle interactions, Stokes law is applicable. It does not hold true when the particle-particle interactions increase. The greater the particle-particle interactions, the less reliable Stokes law become.

When dealing with suspensions that have concentrations that produce sedimentation behavior between free settling and hindered settling, a haze effect is produced. The haze effect is observed as a cloudy boundary separating from the supernatant and another boundary composed of sediment accumulation [3]. When observed, it appears as if the upper cloudy boundary is rapidly falling while the lower boundary of sediment buildup is slowly increasing in height. Eventually the two boundaries merge at which point sediment volume remains fairly stable. The haze effect

demonstrates that if the concentration is not high enough to produce hindered settling, then the particles sediment based on their particle size with smaller particles forming the upper boundary and the larger particles forming the lower boundary. Other factors such as viscosity or dielectric constant of the dispersion media can alter the sedimentation behavior producing the haze effect. A viscous dispersion media would increase the occurrence of the haze effect as it would create a larger gap between the sedimentation rates of large and small particles. McKay [3] has stated that this happens due to the small particles escaping from larger particulate clouds.

Bhatty and Dollimore [4] studied particle behavior of suspensions at low concentrations with focus on free settling and cluster forming regions. In free settling, non-spherical particles showed rotation. Larger particles with higher settling velocities created vortices in their wake during sedimentation. Smaller particles would move into the vortex wake of larger particles forming temporary clusters. If the settling velocity of the larger particle and the cluster in its vortex differed too much, the cluster would break apart as it could not be sustained by the vortex. Doublets were found to be the most readily formed cluster compared to larger ones. Clusters larger than four were very rare [4].

The effect noticed was a greater terminal velocity of clusters because of the decreased drag on individual particles. At increased concentrations, the sedimentation rate of the particle is always less than the sedimentation rate of a single particle in free settling due to the hindrance effect. Zimmels [5] stated the hindered effect resulting from an increase in concentration is due to various factors: a decrease in the open cross section for the upward flow of the dispersion media, which results in an increased fluid approach

velocity; increased apparent viscosity; and a decrease in gravitational forces due to a decrease in the difference in apparent specific gravity between the particles and the medium

Particle sizing of suspensions can be carried out through the use of various equations which account for variables such as suspension concentration, rate of sedimentation, final sediment volume, and container dimensions.

3.2.1 Steinour's equation

Steinour's equation is a modified Stokes' law. It can be used to examine a suspension in which particles are suspended in a fixed arrangement and the velocity of the settling is fairly constant. A laminar flow is established by the fluids movement around the particles. If the particles are well dispersed in the media uniformly and have similar particle sizes, the suspension will have a settling velocity that can be represented by Stokes' law multiplied by a term which is a function of concentration. In real suspensions, particles are not completely uniform, however, under good conditions, a stable arrangement and constant velocity can be assumed. This allows for a stable laminar flow to be maintained by the consistent fluid space shape [6]. This equation is given as:

$$V_1 = \frac{2gr^2(\rho_s - \rho_l)\varepsilon\emptyset(\varepsilon)}{9} \qquad \text{Eq. 3.2}$$

Where, (ε) = liquid volume fraction of the uniformly mixed suspension (the initial porosity of the suspension). At infinite dilution, $\varepsilon \rightarrow 1$ (tends to 1) and [ø (ε)] also becomes one, when Eq. 3.2 reduces to Eq. 3.1.

V_l = The average relative velocity between the spherical particles and the liquid.

(Q) = The measured velocity is that of the particle relative to a fixed horizontal plane.

The volumes of the solid and fluid that move in opposite directions in a unit time gives the relationship between (Q) and (V), i.e.

$$[(1-\varepsilon)\, Q] = [\varepsilon\, (Vl-Q)] \qquad \text{Eq. 3.3}$$

$$Q = \varepsilon\, V_1 \qquad \text{Eq. 3.4}$$

Substituting Eq. 3.4 into Eq. 3.2 gives:

$$Q = \frac{2gr^2(\rho_s-\rho_l)\varepsilon\emptyset(\varepsilon)}{9} \qquad \text{Eq. 3.5}$$

The relationship between (Vs) and (Q) was derived by Steinour, with potential energy loss because of various resistances during the fall of a sphere:

$$\frac{4}{3}\pi r^3(\rho_s - \rho_l)gQ = \frac{4}{3}\pi r^3(\rho_s - \rho_l)gV_s \qquad \text{Eq. 3.6}$$

Which simplifies to:

$$\frac{Q}{V_s} = \frac{(\rho_s-\rho_b)}{(\rho_s-\rho_l)} \qquad \text{Eq. 3.7}$$

Where, (ρ_b) is the density for computing buoyancy

For the hydraulic radius of the suspension, Steinour deduced:

$$\phi(\varepsilon) = \frac{\varepsilon}{1-\varepsilon}\phi(\varepsilon) \qquad \text{Eq. 3.8}$$

Where, [ϕ (ε)] represents those effects of shape that are not evaluated by using the hydraulic radius.

Substituting Eq.3.8 in Eq 3.5 gives,

$$Q = \frac{2gr^2(\rho_s-\rho_l)\varepsilon^3\emptyset(\varepsilon)}{9\ (1-\varepsilon)} \qquad \text{Eq. 3.9}$$

or

$$Q = \frac{V_s\varepsilon^3\phi(\varepsilon)}{1-\varepsilon} \qquad \text{Eq. 3.10}$$

Rearrangement of Eq. 3.9 gives:

$$r = \left[\frac{9Q\eta(1-\varepsilon)}{2g(\rho_s-\rho_l)\varepsilon^3\phi(\varepsilon)}\right]^{1/2} \qquad \text{Eq. 3.11}$$

This equation was modified by Steinour for instances when spherical particles are settling in the presence of an attached immobile liquid [7].

$$Q = V_s\frac{(\varepsilon-W_1)^3\phi(\varepsilon)}{(1-W_1)^2-(1-\varepsilon)} \qquad \text{Eq. 3.12}$$

Where, (W_1) is the ratio of the volume of the immobile liquid to the total volume of solid, with pore volume, plus immobile liquid:

$$W_1 = \frac{\alpha}{1+\alpha} \qquad \text{Eq. 3.13}$$

Where, (α) is the quantity of liquid in millimeters per unit bulk volume of solid.

Steinour expressed this equation in another form:

$$Q = V_s\varepsilon^2 10^{A(1-\varepsilon)} \qquad \text{Eq. 3.14}$$

Where, (A) is a characteristic constant. It can be calculated from plots of log (Q/ε)2 against (ε) for each experiment and fitted his experimental results with a constant calculated to be A=1.8

Comparison of the coefficients in Eq. 3.14 and Eq. 3.5 gives

$$\left[\frac{1-\varepsilon}{\varepsilon}\right] 10^{A(1-\varepsilon)} = \phi(\varepsilon) \qquad \text{Eq. 3.15}$$

This can be rearranged to:

$$\left[\frac{1-\varepsilon}{\varepsilon\,\phi(\varepsilon)}\right] = 10^{A(1-\varepsilon)} \qquad \text{Eq. 3.16}$$

Eq. 3.16 is then inserted into Eq. 3.11:

$$r = \left[\frac{9Q\eta 10^{A(1-\varepsilon)}}{2g(\rho_s-\rho_l)\varepsilon^2}\right]^{1/2} \qquad \text{Eq. 3.17}$$

Taking the logarithm of Eq. 3.14 and rearranging it gives:

$$\log\frac{Q}{\varepsilon^2} = A\varepsilon + [\log V_s - A] \qquad \text{Eq. 3.18}$$

When log (Q/ε^2) is plotted against (ε), the intercept of the equation is [logVs-A] and slope is (A). The particle size is calculated by extrapolating the relationship to unit porosity where $Q=V_s$.

3.2.2 Richardson and Zaki Equation

The Richardson and Zaki empirical equation is:

$$Q = V_s\varepsilon^n \qquad \text{Eq. 3.19}$$

In this equation, (n) is a dimensionless factor. A graph of [Q (1-ε)] versus (ε) will reach a maximum at (ε_1) because the value of (1-ε) decreases with an increase in ε, and will

eventually be zero. The value for ([Q (1- ε)] ρ_s) is the solid flux which is the mass transfer of solid per unit cross section per unit time. The maximum value for [Q(1-ε)] is given by:

$$0 = \frac{d[Q(1-\varepsilon)]}{d\varepsilon} \quad \text{Eq. 3.20}$$

If porosity is defined as (ε_1) then:

$$V_s\varepsilon_1^n = V_s\varepsilon_1^n n\epsilon_1^{-1}(1-\varepsilon_1) \quad \text{Eq. 3.21}$$

Which is simplified to:

$$\varepsilon_1 = \frac{n}{n+1} \quad \text{Eq. 3.22}$$

Here it is shown that (n) is a function of the porosity (ε_1) where [Q (1-ε)], and the maximum value for solid flux is attained for the system.

The Richardson and Zaki equation is now given as:

$$Q = V_s\varepsilon^{\varepsilon_1/(1-\varepsilon_1)} \quad \text{Eq. 3.23}$$

The log of this equation gives:

$$\log Q = \log V_s + n\log\varepsilon \quad \text{Eq. 3.24}$$

In ideal situations, the plot of (log Q) versus (log ε) should give a straight line. This demonstrates that (ε_1) is an important variable in describing the sedimentation rate for suspensions. The magnitude of (ε_1) can be determined by the relationship between (ε_1) and the parameters of the chemical system. The factor, (ε_1) is as important as the initial suspension concentration for maximum solid flux.

The settling rate will decrease with an increase in concentration on the basis of mechanical and physical interference. Due to this, the experimental relationship that

(Q/V_s) is proportional to (ε) should be expected. It is more significant than the influence of concentration:

(liquid volume fraction)/ (solid volume fraction) which is $[\varepsilon_1(1- \varepsilon_1)]$ Eq. 3.25

If the hindered settling were only an effect of the solid concentration, then it would be more sensible for the solid volume fraction to be in the numerator of Eq. 3.25. When (ε_1) approaches its theoretical maximum value of infinity, there is a decrease in the interface settling rate along with a decrease in initial porosity. When observing hindered settling systems, it is seen that it usually occurs when particulate concentrations are high, which corresponds to (ε_1) being proportional to hindered settling [8]. Hindered settling is not just a function of particle concentration. It is also related to the range and intensity of many different forces present within the system. Davies et. al [9] stated that hindrance would be expected at a maximum with charged or polar particles of large surface areas per gram in polar solvents and at a minimum with uncharged or non-polar solids of small specific surface in non-polar solvents. Hindered settling should also be related to interactions of the particles with the dispersion media [10]. This goes hand in hand with this concept of long range electrostatic interactions previously developed. However, this concept implies that particle-particle repulsions act only as the cause of hindrance. This model also suggests particle-liquid attractions. Particle-particle repulsions cause the relatively slow settling because electrostatic repulsions are preventing particle-particle cohesion. Particle-liquid attractions would affect hindrance due to particle-liquid attraction reducing the effective density of the solid. Charge density of the particle

surface is another factor in determining hindrance as it is exposed to the dispersion media.

3.2.3 Dollimore-Mcbride Equation:

The Dollimore-Mcbride equation was proposed to relate the rate of fall of the interface to the concentration of the suspension [11]. Using this equation, Dollimore and Mcbride were able to show that suspensions exhibiting hindered settling behavior provided information on particle size, particle packing, and sedimentation mechanisms. Graphing the logarithm of the rate of fall against the concentration of the suspension should show a linear trend for a hindered settling system. If the plot is extended to a zero concentration, it presents the rate of fall for a single particle in an infinite fluid system which can be represented as stokes velocity (V_s). The linear representation of this equation is:

$$\log Q = a - bC \qquad \text{Eq. 3.25}$$

Here, (a) and (b) are represented as constants.

In an infinite fluid system the equation becomes:

$$\log Q = a \qquad \text{Eq. 3.26}$$

Also:

$$Q = V_s \qquad \text{Eq. 3.27}$$

and:

$$10^a = 10^{\log Vs} = V_s \qquad \text{Eq. 3.28}$$

Therefore:

$$Q = V_s 10^{-bc} \quad \text{Eq. 3.29}$$

Initial porosity (ε) can also be determined as follows:

$$\varepsilon = \frac{V_{sn} - V_{sd}}{V_{sn}} \quad \text{Eq. 3.30}$$

Where V_{sn} is the suspension volume and V_{sd} is the volume of the suspended solid.

$$V_{sd} = \frac{M_s}{\rho_s} = \frac{Mass\ of\ solid}{Density\ of\ solid} \quad \text{Eq. 3.31}$$

and:

$$\varepsilon = \frac{V_{sn} - \frac{M_s}{\rho_s}}{V_{sn}} \quad \text{Eq. 3.32}$$

or can be written as:

$$\varepsilon = \frac{1 - M_s}{\rho_s V_{sn}} \quad \text{Eq. 3.33}$$

Since mass (M_s) divided by volume (V_{sn}) is concentration (C):

$$\varepsilon = 1 - \frac{C}{\rho_s} \quad \text{Eq. 3.34}$$

If the initial porosity (ε) is substituted in for the concentration then:

$$Q = V_s 10^{-b\rho_s(1-\varepsilon)} \quad \text{Eq. 3.35}$$

If this equation is compared to Steinour's equation (Eq. 3.4), and if (ε) is close to (ε^2) then:

$$A = b\rho_s \quad \text{Eq. 3.36}$$

If (ε^2) and (ε) are not uniform, then the relationship between (A) and (b) is derived as follows.

If Equation 3.35 is put into logarithmic form, then:

$$\log Q = \log V_s - b\rho_s(1-\varepsilon) \quad \text{Eq. 3.37}$$

Also:

$$\log Q = \log V_s + 2\log\varepsilon - A(1-\varepsilon) \quad \text{Eq. 3.38}$$

Which can also be seen as:

$$b\rho_s(1-\varepsilon) = \log V_s + 2\log\varepsilon - A(1-\varepsilon) \quad \text{Eq. 3.39}$$

Therefore:

$$A = b\rho_s + \frac{2\log\varepsilon}{(1-\varepsilon)} \quad \text{Eq. 3.40}$$

If the system is being considered at infinite dilution then log (ε) = 0 and the equation is simplified to:

$$A = b\rho_s \quad \text{Eq. 3.41}$$

Data resulting from using the Dollimore-Mcbride equation are similar to data from the Richardson-Zaki equation. In a uniform suspension, the weight to volume solids concentration can be calculated for maximum solid flux which occurs at the initial porosity (ε_1).

$$\varepsilon = 1 - \frac{1}{2.303b} \quad \text{Eq. 3.42}$$

When, $C = C_{\varepsilon 1}$:

$$2.303(b)C_{\epsilon 1}(1-\varepsilon_1) = (1-\varepsilon_1) \quad \text{Eq. 3.43}$$

and:

$$C_{\epsilon 1} = 1 - \frac{1}{2.303b} \quad \text{Eq. 3.44}$$

Based on this, a plot of Log (Q) against (C) for maximum solid flux is obtained, where (–b) is the slope using Equation 3.44.

3.3 Permeability

Permeability is another method that can be used to explain sedimentation behaviors observed in suspensions. Using the permeability approach, the suspended solids are considered as a packed bed through which the dispersion media flows [12]. The equation that best describes this phenomenon is the Kozeny-Carman equation, which is given below.

$$\upsilon = \frac{\varepsilon^3}{K\eta s^2}\left(\frac{\mathrm{P}}{L}\right) \qquad \text{Eq. 3.45}$$

In the above equation:

(υ) is the volume of the fluid permeating through the packed bed in ($cm*s^{-1}$)

(ε) is the porosity of the packed bed

(K) is the Kozeny constant

(η) is the viscosity of the dispersion media ($gm*cm^{-1}*s^{-1}$)

(S) is the particle surface area

(P) is the pressure gradient across the depth of the bed

(L) is the depth of the bed

When a suspension follows hindered sedimentation behavior, the particles move under laminar flow through the dispersion media with a Reynolds number of less than 0.2, with a solid flux velocity (Q) relative to a fixed plane, which can be compared to the velocity (υ) of the dispersion media permeating through a motionless bed. A modified form of the Kozeny-Carman equation was proposed by Happel to correct for problems in sedimentation influenced by hindered settling [13].

$$Q = \left(\frac{1}{2K}\right)\left(\frac{\varepsilon^3}{1-\varepsilon}\right)V_s \quad \text{Eq. 3.46}$$

Also written as:

$$Q(1-\epsilon) = \left(\frac{1}{2K}\right)\varepsilon^3 V_s \quad \text{Eq. 3.47}$$

Davies and Dollimore [14] demonstrated that (K) reaches its minimum value (K_{min}) at a value (ε_k) which is less than (ε_1). The following equation is used to demonstrate the relation between ε_k and ε_1.

$$\varepsilon_k = \frac{4\varepsilon_1 - 3}{3\varepsilon_1 - 2} \quad \text{Eq. 3.48}$$

Based on this, the values for (ε_K) and (ε_1) converge as (ε_1) increases and attains virtual identity, when (ε_1) is equal to unity, which is to say in highly hindered systems.

3.4 Packing factor

In suspensions, solid particles that are settling out are said to carry a certain amount of liquid down along the laminar flow. It is an important factor in examining sedimentation behavior. Increased sedimentation volume after settling usually indicates the amount of dispersion media that was carried down with the particles since the calculated solid volume determined from the weight and density of the solid differs from the observed solid volume seen during experimentation. Factors such as surface morphology, flocculation of the particles, and surface charges can affect the amount of liquid carried down during sedimentation [3]. McKay [3] presented the packing factor term which was considered not to be related to flow units. Instead, the liquid is said to be present in the voids between flow units. McKay describes the flow units as:

$$p = \frac{1-\varepsilon}{V} \qquad \text{Eq. 3.49}$$

Where (p) is the packing factor

(ε') is the corrected volume of (ε)

(V) is the final settled volume

(1- ε') is the volume fraction of the flow unit\

The packing factor term can be evaluated by performing serial dilutions on a single master suspension. In this way, only the concentration of the dispersion is changed and the packing factor can be studied from (Q) and (V) as shown in the following equation.

$$Q = \left(\frac{2g}{9\eta}\right)(\rho_s - \rho_l)\left(\frac{C}{pv}\right)(1 - pV_s)^2 r^2 (10^{-1.82pv}) \qquad \text{Eq. 3.56}$$

When P >1, the liquid associated with the solid flux will be forced, and when P<1, a small portion of the associated dispersion media remains where there is tight packing of incompressible solids. From this, it can be stated that the larger the amount of associated liquid, the larger the packing factor (p) value will be, resulting in greater hindrance due to lower density of flocs.

3.5 Final Settled Volume

The final settled volume is the volume of the settled solids including void spaces present between the particles in the sediment. The density of the settled bed varies based on the height of the settled bed with higher densities at the lower parts of the bed and

lower densities at the upper areas of the bed. The porosity of the settled bed is also greater at the upper portions of the bed as compared to the lower area. Liquid trapped in the pores tends to move up and out of the bed during sedimentation where it is undergoing compression. More liquid remains in the upper boundaries of the settled bed due to there being less compressive forces acting on it relative to the lower portions of the bed.

Particle morphology also affects the final settled volume. It controls what arrangements in which particles can pack, which in turn affects the void spaces present in the bed. Particle packing is differentiated according to their coordination number, which is the number of nearest particles in contact with the central particle. Coordination numbers less than six have increased void spaces, which increases instability. Smaller particles have lower coordination numbers. The electrostatic interaction between particles can also cause a decrease in the coordination number. It was concluded by Steinour that, for higher concentrations, porosity ranges from 0.26 to 0.95, but only under the condition that the shape factor is known. Final sedimentation volume can also be used to determine particle size.

Surface energy is a factor of the cohesive forces between adjacent particles. Greater cohesive forces lead to great surface energy, and vice versa. It is a directly proportional relationship. Particle size and cohesive force is an inversely proportional relationship. Based on this, it can be said that small particles will have large cohesive forces, which means that smaller particles will not break up or fragment. Due to the high nature of cohesive forces in small particles, a large amount of voidage will be present in

the sediment, leading to a larger final settled volume. To maintain stability, small particles have finer geometry and high voidage.

Dispersion media that is bound or associated with the settled particle will also affect the final sediment volume. If liquid is associated with the particle, it will lead to a larger floc with a lower density. The density of these particles can be calculated with the following equation.

$$\rho_c = \frac{\rho_s + \partial \rho_l}{1 + \partial} \qquad \text{Eq. 3.57}$$

Where (∂) is the quantity of bound liquid per centimeter cubed of solid. The value of (∂) is calculated by measuring the final settled volume and calculating the amount of liquid within this volume present as liquid associated to the particles surface and unbound liquid trapped in the void spaces of the floccules.

3.6 Calculating Particle size

The particle size can be determined as a function of the rate of sedimentation. Factors affecting the rate of sedimentation such as viscosity, shape, and density are all studied closely and used to calculate the particle size. Calculations were performed using the modified Stokes' laws.

3.6.1 Steinour's Method

Steinour's equation can be used to calculate particle size where:

$$Q = V_s \varepsilon^2 10^{A(1-\varepsilon)} \quad \text{Eq. 3.56}$$

Taking the logarithm of Eq. 3.56 and rearranging gives:

$$\log \frac{Q}{\varepsilon^2} = A\varepsilon + [\log V_s - A] \quad \text{Eq. 3.58}$$

Using Equation 3.58, a graph of log (Q/ε^2) versus (ε) is constructed. The graph should be linear. Using this plot, the slope and intercept will give the values for (V_s) and (A), respectively. This (V_s) value is then inserted into the Stokes' law equation and the average particle radius is calculated.

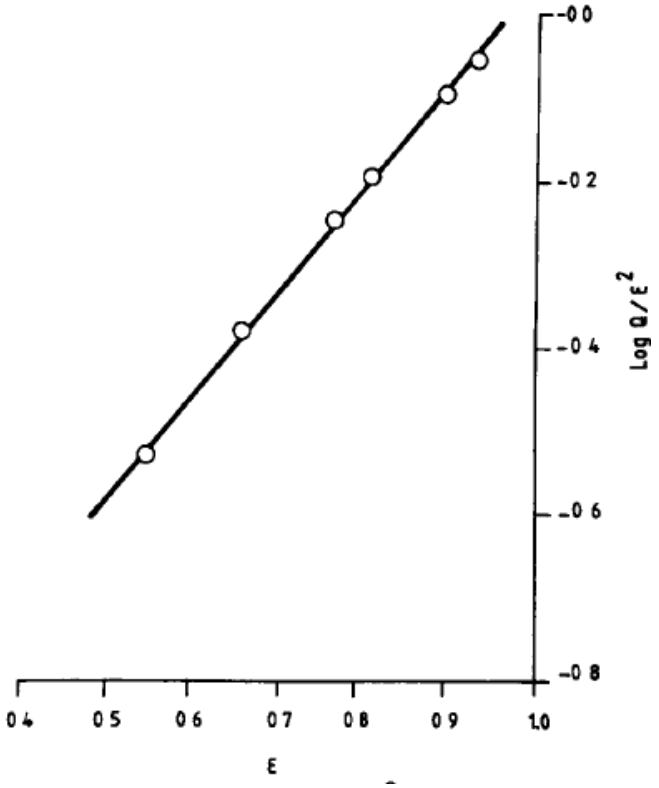

Figure 3-2: Linear plot of log (Q/ε^2) versus (ε)

3.6.2 Richardson and Zaki Method

The Richardson and Zaki equation can be used to calculate (V_s) and (r) by plotting log(Q) versus loh(ε). The slope of the plot gives the value (n) and the intercept value of (V_s)

$$\log Q = \log V_s + n \log \varepsilon \qquad \text{Eq. 3.59}$$

3.6.3 Dollimore and Mcbride's Method

Using the Dollimore and Mcbride's Method, plots of log(Q) versus concentration were graphed. The plot was extended out to zero concentration and (Q) was related to (V_s) to obtain the particle size as follows:

$$\log Q = a - bC \qquad \text{Eq. 3.60}$$

where, (a) and (b) are represented as constants.

In an infinite fluid system the equation is given as:

$$\log Q = a \qquad \text{Eq. 3.61}$$

and:

$$Q = V_s \qquad \text{Eq. 3.62}$$

Chapter 4

Flocculation of Suspensions

4.1 Introduction

When preparing a pharmaceutical suspension, there are several factors to take into consideration. The first is that the suspended solid should not form a hard cake in the container. The second, the solid particulate should remain suspended for a period of time in a fairly uniform manner so that it may be dispensed from the container. The third is that while the suspension may be thickened to delay the settling of particles, increasing the viscosity too much will make the suspension difficult to remove from the container, and from an organoleptic standpoint, it will not be appealing. For pharmaceutical preparations, since sedimentation cannot be completely removed from the formulation, it should be made to be fairly easy to re-disperse the sediment [1]. Flocculation of the suspension is a common way to increase re-dispersibility.

4.2 Flocculation

The rate of sedimentation follows Stokes law, as previously discussed. It was also shown that smaller particles settle at a decreased rate. However, the reduction of

particle size causes the suspension to become unstable do to the large surface area of the particles leading to increased surface area charge. The smaller particles will have much greater cohesive forces compared to the larger particles, meaning that when they settle, the smaller particles are more likely to form a hard cake that is difficult to re-disperse, if it can be re-dispersed. Though smaller particles will mean sedimentation will be much slower, it is counterproductive since the suspension is unstable and once it does sediment, it will be become difficult to break up the sediment cake. In a flocculated system, the particles come together to form large loose aggregates held together by weak Van der Waals forces [2]. In a deflocculated system, the suspended matter has very little or no cohesive forces. Repulsive forces control particle-particle interactions in a deflocculated system. Due to the high repulsive forces, particles will settle slowly and remain as single particles. The strong repulsive forces make the individual particles completely controlled by Brownian motion and gravity when it comes to sedimentation [3]. Since the particles repel each other, when they sediment, the continual repulsion maximizes the packing efficiency of the particles and they form highly dense cakes with low very void space. The agglomeration of particles, forming either floccules or aggregates is a measure of tendency of the system to move toward thermodynamic stability [3,4]. Work (W) or Gibbs free energy (∂G) is related to total free surface area (∂A) and the solid liquid interfacial surface tension (γ_{SL}) through the equation below.

$$\partial \mathrm{G} = (\gamma_{SL})(\partial \mathrm{A}) \qquad \text{Eq. 4.1}$$

For thermodynamic stability, the tendency is to reduce the surface free energy by reducing the interfacial tension or interfacial area. Interfacial tension can be reduced

through the use of a surfactant. The forces at the surface of the particle affect the degree of flocculation and agglomeration in a suspension. Forces of attraction are of the London-Van der Waal's type [3]. Repulsive forces arise from the interaction of the electric double layers surrounding individual particles [2]. Factors like hydration, hydrophobicity, steric interactions, polymer bridging, and electrostatic interactions are some of the numerous variables which can affect attractive and repulsive forces which control the flocculation and deflocculation of the system

4.3 Electrical double layer and Zeta potential

Electric charges can be formed several ways when at the solid liquid interface. The most common method is by altering the pH causing functional groups on the dispersed phase to be ionized. Also, charges are formed when there is a difference in the dielectric constants of the liquid and dispersed phase. The electrical charges contribute greatly to the stability of suspensions as they determine the strength of attractive and repulsive forces, which in turn controls the levels of flocculation or deflocculation. The surface charges present causes an uneven distribution of charges in the surrounding space of the particle, creating an electric potential between the surface of the particle and the bulk of the dispersion media. This phenomenon is known as the electric double layer [7].

Figure 4-1 demonstrates how the electric double layer is composed. An Electric Double Layer consists of three parts. The first is the surface charge, which is compromised of charged ions adsorbed on the particles surface. The second is the stern layer, these are the counter-ions attracted to the particles surface charge and attached to it by the electrostatic force. The third is the diffuse layer, which is a film of the dispersion

medium adjacent to the particle. The diffuse layer contains free ions with a higher concentration of the counter-ions. The ions of the diffuse layer are affected by the electrostatic force of the charged particle. When the particle moves in the dispersion media, a layer of liquid

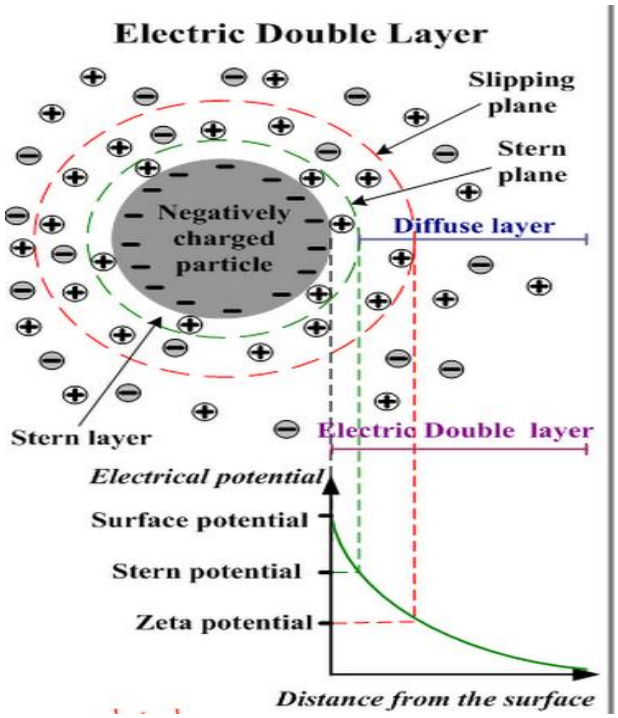

Figure 4-1 Diagram demonstrating the electric double layer [5]

remains attached to the particle, this layer is called the slipping plane.[5] The electric potential at the slipping plane is also known as the zeta potential (ζ)

Zeta potential gives a measure of the net surface charge on the particle and interfacial potential distribution. It serves as an important parameter in characterizing the electrostatic interaction between particles in dispersed systems and the properties of the suspension which are affected by this electrical phenomenon. If the zeta potential is

below a certain value, the attractive forces exceed the repulsive forces and the particles come together, thereby causing the suspension to flocculate.

4.4 DLVO Theory

In the 1940s the DLVO theory was developed by Deryagin, Landau, Vewey and Overbeel. It was based on the stability of colloidal systems. The DLVO theory makes several assumptions related to colloidal systems [5]:

- The dispersion is dilute;
- The only two forces that act on the particles are Van der Waals forces and electrostatic forces;
- The electric charge and other properties are uniformly distributed over the solid surface;
- The distribution of the ions is determined by the electrostatic forces and brownian motion.

Based on this theory, the potential energy is represented by the equation below where V_T is the total potential energy, V_a is the potential energy of attractive interaction, and V_r is the potential energy of the repulsive interactions.

$$\mathbf{V_T = V_a + V_r} \qquad \textbf{Eq. 4.2}$$

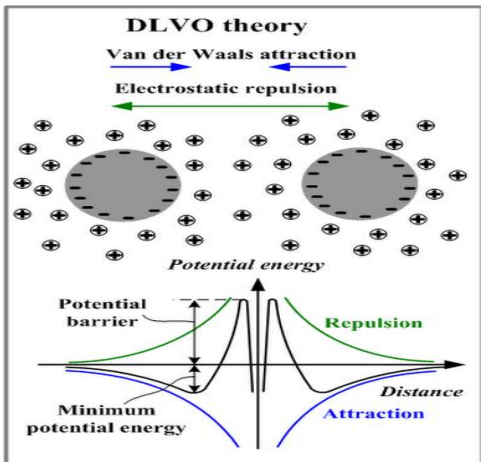

Figure 4-2 Diagram demonstrating DLVO theory [5]. The minimum potential energy determines the distance between the particles.

Figure 4.2 diagrams the forces in play which demonstrate the DLVO theory and the potential energy and determines the distance between particles.

4.5 Flocculating Agents

4.5.1 Electrolytes

Electrolytes are used to decrease the electrical potential barrier between particles to allow them to form floccules [6]. The solid particles posses a surface charge which induces repulsion between individual particles. The adsorption of the multi-valent ions creates the surface charge and encourages aggregation between adjacent particles leading to the formation of floccules. There is a decrease in the zeta-potential of the particles to almost zero. There is also a formation of a bridge between the adjacent particles. Further addition of electrolytes makes the zeta potential more negative leading to deflocculation.

For particles with a low surface charge, a monovalent ion can be used to induce flocculation, however, when there is a high surface charge, di- and tri-valent ions work

better. Trivalent ions, though effective, are not used much due to their toxicity. The concentration of electrolyte used is based on what degree of flocculation is desired.

4.5.2 Surfactants

Surfactants are compounds which can be added in low concentrations to suspensions. Surfactants work by reducing the interfacial surface tension and surface free energy of the particle [8]. They adsorb on the surface of the particles and reduce the interfacial energy between the particle and the dispersion media. The particles having less surface energy are attracted towards each other by Van der Waal's forces and forms loose aggregates.

There are several classes of surfactants: anionic, cationic, zwitterionic, and non-ionic. Ionic surfactants can create flocculation in suspensions [8]. This is accomplished by using an ionic surfactant that acts as a counter-ion to the surface charges of the suspended particles. The surfactant will counter the surface charge, and because surfactants have large hydrocarbon chains, ions will be prevented from gathering around it and the zeta potential will be minimized. This will allow Van der Waals attractive forces to flocculate the systems. Non-ionic surfactants don't affect the charge density of suspended particles much, however, they can absorb onto the surface of the particles, if they have linear configurations, they can link up with more than more molecule, bridging the molecules together into loose flocs. These types of surfactants are usually polymeric, meaning they have very long repeating chains which is what allows them to link up multiple particles.

4.5.3 Polymeric flocculants

Polymers are long chain, high molecular weight compounds that have active groups spaced along their length. These soluble polymeric materials adsorb onto the surface of multiple particles. This is due to the repeating nature of the basic monomeric unit in the polymer structure and their very high molecular weight. Synthetic and natural polymers can behave as surfactants by stabilizing or flocculating the particles in suspension [8].

The most important characteristics are the molecular weight and charge density of the polymer. A problem associated with polymeric flocculants is that molecular weights are given as a range, and the range might be quite broad in terms of how it affects the polymers flocculating ability. If the chain isn't long enough, then it won't have much effect on flocculation as it won't be able to bridge multiple particles together. Polymers can greatly affect factors like sediment volume and viscosity.

Chapter 5

Instrumentation

5.1 Laser Diffraction Analysis

Laser diffraction is a simple technique that is very useful determining particle size. It can scan over a broad range of particle sizes and is capable of operating with a number of different dispersion media. [1]

5.1.1 Principles of Laser Diffraction

Laser diffraction operates on the principle that when the particles are passed through a laser beam, the light is scattered at an angle corresponding to the particle size. Decreasing particle size causes the light scattering angle to increase logarithmically [2]. The intensity of the scattered light is also particle size dependent. Large particles will scatter light at high intensity but low angles while small particles will scatter the light at low intensity but wide angles. This light scattering behavior is what allows the determination of the particle size.

Particle size is determined by comparing the suspensions scattering pattern to an appropriate model. Two commonly used models are the Mie theory [3] and Fraunhofer

approximation theory [4]. The Mie theory is used for smaller particles. It allows for primary scattering from the surface of the particle, using the intensity predicted by the refractive index difference between the particle and dispersion media. Secondary scattering caused by light refracted within the particle is also predicted. The Fraunhofer theory is used mostly for larger partle size distributions because it assumes the particles are opaque and scatter low angles.

5.1.2 Instrumentation

The Malvern Mastersizer 2000® Laser Diffraction Grain Size Analyzer has optics that allow it to scan a particle size range from 0.2 - 2000 microns. It has two dispersion units, one unit used for small amounts of sample, with the other dispersion unit used for large sample volumes. The dispersion units have automatic stirrers attached to them which are set to 3000 rpm, which is what is recommended for most samples.

A helium neon laser is employed as the light source. The sample which is placed in the dispersion units/homogenizer is sent through the machine into the main body where it is hit with the laser which is scattered and detected by the detector. The signals received from the detector are sent to the computer and the software send out data showing mean particle size, range, median, and mode [5,6].

5.1.3 Sample Preparation

The sample used is in the form of a suspension. No special treatment is needed to prepare the sample any further. The homogenizer is filled with distilled water prior to sample addition, so no dilution of the sample is needed. When the sample is added,

however, care needs to be taken not to overload the homogenizer, otherwise the software will not be able get a uniform reading of the sample.

5.1.4 Applications

The main application of laser diffraction is for determining particle sizes. Laser diffraction allows for size ranges within numerous types of pharmaceutical formulations to be accurately determined.

5.2 Nicomp ZLS 380

The Nicomp ZLS 380 is used for the quantitative measurement of charge and electric mobility of the suspended particles. The technique used by this machine is called electrophoretic light scattering [7]. Electrophoretic light scattering is used to measure electrophoretic mobility. The potential difference between the surface of the diffusion layer and the stern layer is called the zeta potential.

5.2.1 Principles of Electrophoretic Light Scattering

Electrophoretic light scattering is based on electrophoresis. The electrophoretic mobility of charged particles in suspension is measured under an electrical field. To determine the speed of the particles, the sample is irradiated with a laser which is scattered by the particles and detected. The scattering of the light by the particles in suspension causes the frequency to shift proportionally to the movement of the particle. Based on this shift in frequency, the electrophoretic mobility can be measured, and from

the electrophoretic mobility, the zeta potential can be calculated using the Helmholtz-Smoluchowiski equation [9].

$$\zeta = \eta \mu / \epsilon \qquad \text{Eq. 5.1}$$

(ζ) is the zeta potential

(η) is the viscosity of the solvent

(μ) is the electrophoretic mobility

(ε) is the dielectric constant of the solvent

5.2.2 Instrumentation

Key components of the Nicomp 380 ZLS are a laser, delivering optics, electrophoretic cell, collecting optics, and a photomultiplier tube which is the detector. A laser beam passes through the electrophoretic cell which irradiates the particles. The particles causes the light beam to scatter and shift frequencies, and this scattered beam is then detected by the photomultiplier. Figure 5-1 gives a schematic of the electrophoretic light scattering machine

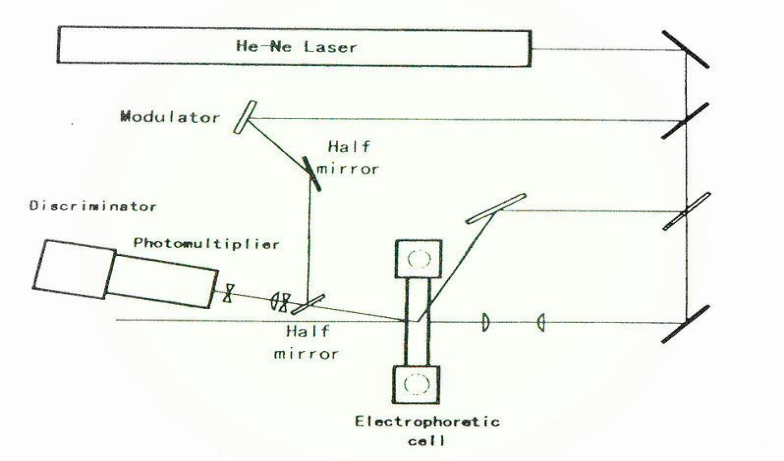

Figure 5-1 Diagram of an electrophoretic light scattering machine [10]

5.2.3 Sample Preparation

When performing electrophoretic light scattering, no special sample preparation techniques are needed other then dilution. The sample needs to be diluted enough to prevent particle-particle interactions. If particle-particle interactions are present, it could alter the calculated zeta potential due to the possibility that increased interactions will affect the mobility of the suspended particles. Any mobility that isn't a caused by the electric field or light scattering could potentially result in incorrect zeta potentials [7].

5.2.4 Application

The determination of zeta potential is the main scope of electrophoretic light scattering. Zeta potential is a key factor in understanding inter-particulate electrostatic interactions. Zeta potential determination is mainly done when studying dispersions since it can give insight into how stable a suspension may be and if it will be prone to flocculation or deflocculation and subsequent caking [8].

5.3 Scanning Electron Microscopy

Scanning electron microscopy allows for the topological observation of particulate matter [11]. It is a powerful tool for the characterization of surface morphologies for all types of samples. It is very useful for qualitative analysis of samples. It operates by imaging the sample by bombarding it with a high energy electron

beam which is conducted by the gold coated sample. Gold is used as a coating since it conducts electrons well to give a good image.

5.3.1 Instrumentation

A scanning electron microscopes' key components are an electron gun with a tungsten filament which serves are the electron source, visual photo-recording cathode ray tubes, sample stage, electron collector, and a vacuum pump [11]. Scanning electron microscopes often have multiple detectors [11]. Depending on the power of the electron source, the scanning range can go from 1000x optics up to 100000x optics. Another scale to measure the scanning range is from micrometers down to nanometers [12]. Figure 5-2 gives the schematic for a scanning electron microscope

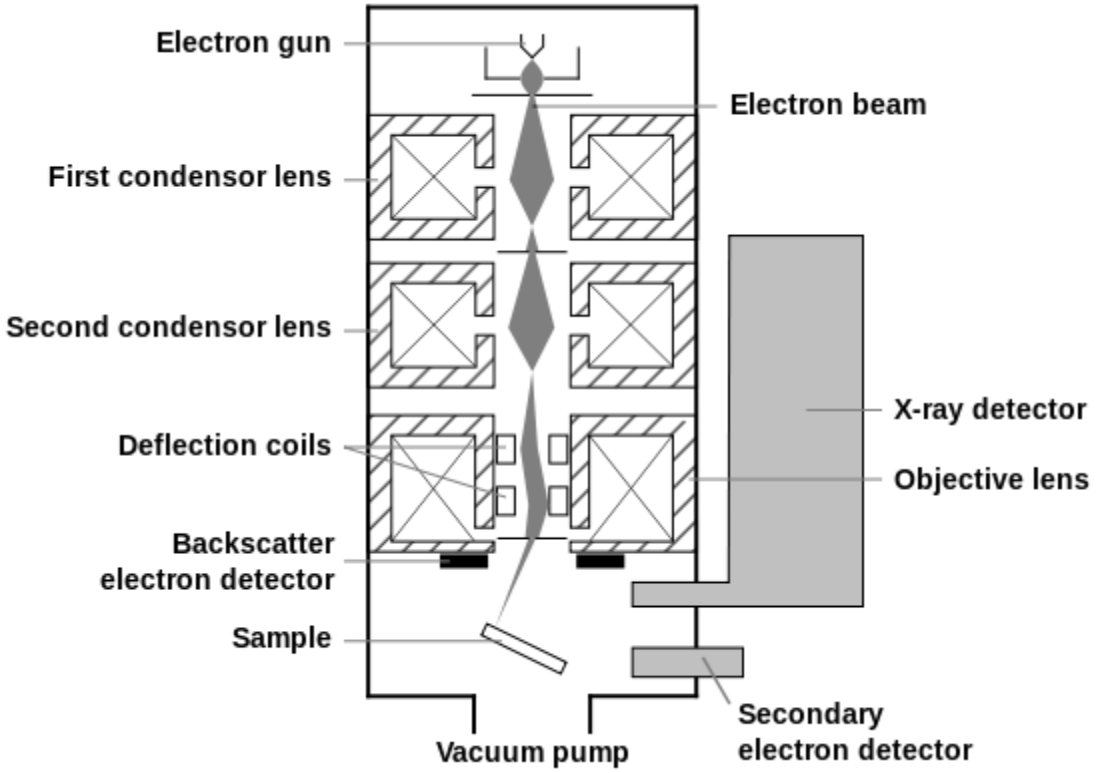

Figure 5-2 Schematic of a scanning electron microscope.

5.3.2 Sample Preparation

If the sample is conductive then there is not any special sample preparation needed other than making sure the sample is dry. If the sample is wet with water or contains a volatile material, then upon bombardment with electrons, the liquid would vaporize and that could damage the equipment as it is a sensitive machine. Carbon tape or double sided tape is applied to an aluminum stage. The sample is sprinkled on the tape. If the sample is not conductive, then a conducting coating is applied to the sample to allow for the electrons to be properly conducted to produce an image with good resolution. Gold is a common coating material as it is a good conductor which allows for a clear image to be taken [13].

5.3.3 Applications

The uses for scanning electron microscopy are widespread. Physical structure, surface morphology, size, texture, and composition can be examined used scanning electron microscopy [13]. With proper software or training, it can even be used for quantitative analysis. Particle sizing is possible with SEM, but a high number of pictures are needed for it to be accurate. Something like that would only be done in conjunction with other more well established techniques like laser diffraction, though it could be used to show reliability from one test to another

5.4 Powder X-ray Diffraction (PXRD)

Powder x-ray diffraction is an analytical tool that is used to study the crystalline nature of a material and any other phases shown in the material [15]. The material is bombarded with x-rays at varying angles stepwise. The x-rays are diffracted from atoms within the sample and produce a unique diffraction pattern specific to the composition of the sample. The diffraction pattern provides information on the arrangement of atoms within the sample, but only for a crystalline sample. An amorphous sample will produce no diffraction pattern and return only a flat line.

5.4.1 Principles of PXRD

X-rays are electromagnetic radiation of about 1 angstrom which is in the same range as an atom [14]. With the same size range as atoms, x-rays are well suited for studying structural arrangements of atoms. Crystalline solids have a three dimensional structure of repeating planes of atoms that make up its crystal lattice. When x-ray beams are focused on the sample, interaction with the planes of atoms occurs. When the x-ray wavelength is similar to that of the atomic spacing of the sample diffraction occurs. This diffraction gives rise to constructive interference as given by Braggs Law.

$$n\lambda = 2dsin\theta \qquad \text{Eq. 5.1}$$

(λ) is the wavelength of the incidence x-ray;

(n) is an integer;

(d) is the spacing between the planes in the crystal lattice structure;

(θ) is the angle between the incident ray and the scattering planes.

Braggs law relates the x-ray's wavelength to the diffraction angle and the lattice spacing [15]. The diffraction of the x-rays happens at specific angles when constructive interference occurs. Each crystal has its own diffraction pattern, much like a fingerprint, which allows for database searches to compare unknowns to known diffraction patters for identification purposes.

5.4.2 Instrumentation

PXRD's have three basic components, an x-ray tube, a sample hold, and an x-ray detector. X-rays are generated by a cathode ray tube in which a filament is heated to produce electrons [16]. The electrons are accelerated towards a target when voltage is applied. The high energy electrons continue to bombard the target material. When enough energy is applied to dislodge inner shell electrons, x-ray spectra are produced. Figure 5-3 provides a schematic for the PXRD analysis.

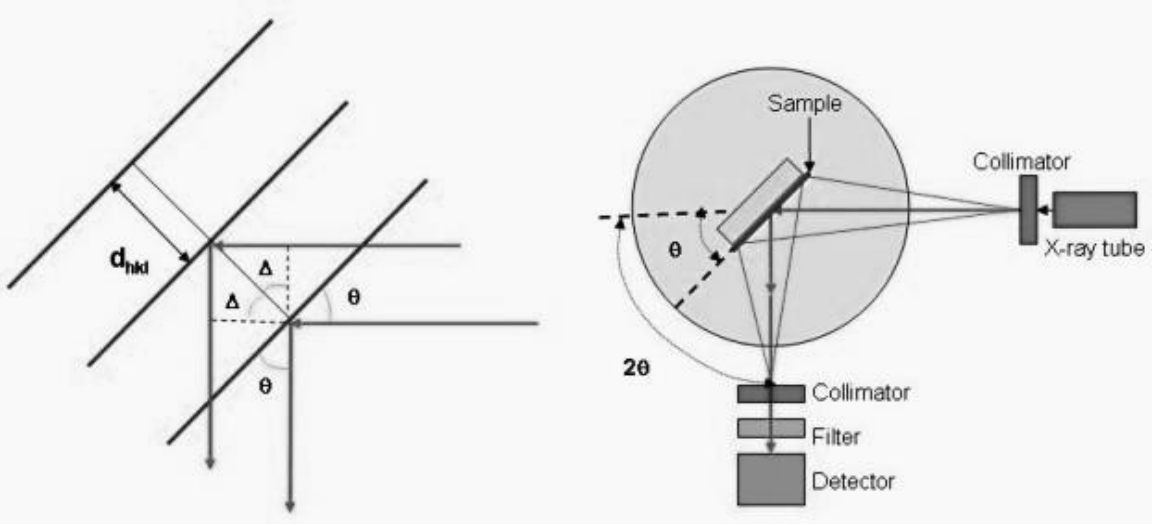

Figure 5-3 Left side: Diffraction of x-ray, Right side: schematic of PXRD [18]

The wavelength of the x-ray is determined by the type of target material used. Some common materials are copper, iron, nickel, molybdenum, and chromium. The x-rays are collimated and directed at the sample through a slit aperture. A goniometer, a device that measures angles, rotates the x-ray source and detector around the sample to produce different angles of incidence. As the angles of incidence are varied stepwise, the detector records the intensity of the x-rays. When the angle of incidence matches up with lattice spacing, constructive interference occurs as a peak in intensity recorded by the detector (θ) is the incidence angle, and (2θ) is the angle between incident and the diffraction beam before it enters the detector. The x-ray source and detector are rotated to maintain the (θ) to (2θ) geometry

5.4.3 Sample preparation

The sample should be ground into a very fine powder, preferably with a particle size less than 10 μm [15]. The powder should be placed into the sample holder and spread into it to produce a flat surface. If the surface is not flat, it will interfere with the x-ray diffraction, and the pattern may be off or shifted from its true point

5.4.4 Applications

PXRD is heavily used in the development of drugs and their delivery systems. It is used to identify unknown crystalline samples, and also to determine the purity of crystalline samples. PXRD can be used to determine the drug form when compounded into its formulation. It can also be used to determine if interactions are present between

different compounds in the formulation based on the diffraction patterns of the pure substance compared to the diffraction patterns of the substances after compounding.

5.5 Differential Scanning Calorimetry (DSC)

Differential scanning calorimetry is a thermoanalytical technique used to analyze the transition states of substances when heated [16].

5.5.1 Principles of Differential Scanning Calorimetry

Differential scanning calorimetry is a technique used to examine thermal transitions for materials. Transitions involved include solid-solid, solid- liquid, and liquid gas. In a DSC study, the temperature and heat flow associated with the transition states of the sample are measured relative to a reference standard. When a thermal transition takes place in the sample (glass transition, crystallization, melting, vaporization) the sample will require either more or less heat to maintain a temperature equal to the reference standard. The basis for whether more heat or less heat is needed to maintain a set temperature depends on if the transition state is exothermic or endothermic. The thermogram produced will show negative or positive peaks if the event was exothermic or endothermic [16].

5.5.2 Instrumentation

A DSC instrument consists of a furnace in which two crucibles sit on a thin plate. One crucible is for the sample and the other crucible is the reference pan to which the

sample is measured against [16]. The crucibles are usually made from aluminum however when higher temperatures are required for DSC, platinum or ceramic pans are used as they can withstand much greater temperatures [16]. Beneath the crucibles are thermocouples which register any difference in temperature between the two pans. The pans are heated at a specific rate programmed into the machine before the study, and an inert gas, such as nitrogen, is used as a purge gas to remove any gasses evolved from the heating of the sample. Figure 5-4 gives a schematic for a DSC.

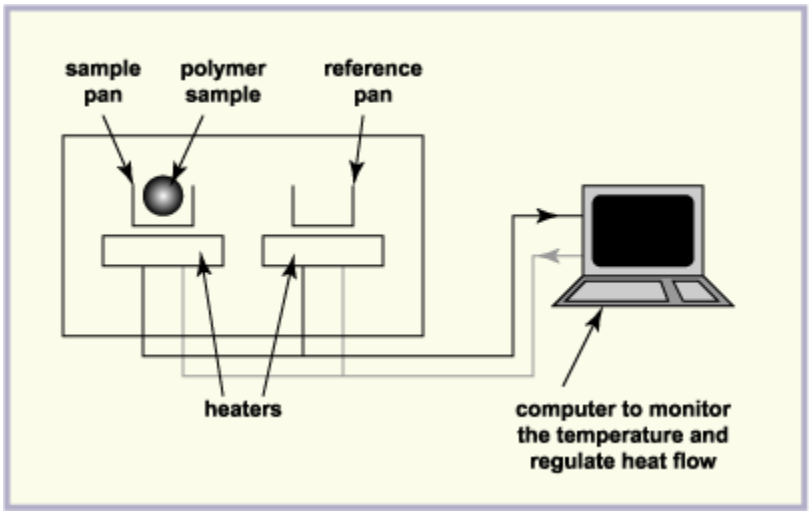

Figure 5-4 Simplified schematic of a DSC[17]

5.5.3 Sample Preparation

Solid and liquid samples can be analyzed using DSC. Between 1-10 mg of the sample is weighed into the crucible. The crucible is covered with a lid. The crucible is then re-weighed. The DSC temperature program will need the weight of the empty crucible and lid, and the weight of the crucible and lid with the sample. If the sample is volatile or likely to degrade and expend and gas, a small hole can be poked into the lid of

the pan to prevent it from bursting in the oven. The melting point of aluminum is 660^0C, if the temperature program will come within 100^0C of that, then an aluminum crucible should be replaced by a crucible with a higher melting point, such as platinum. An empty pan and lid are used as the reference sample

5.5.4 Applications

In the industry, DSC is primarily used for drug development as well as continuing drugs studies for shelf life. By measuring heat flow during transition states for all the pure substances in a drug compound and then comparing that to the heat flow thermogram for the final formulation of a drug product, any interactions between drugs and excipients can be determined. If the intensity of the peaks at transition states are shifted, reduced, or enlarged, then we can use that data to infer something about the type of interaction taking place. Many times, drugs are mixed with only a single other excipient to perform individual compatibility studies to determine if any interactions occur. In this way, problems can be determined before too much work has been done for a formulation that may not work.

Chapter 6

Methods and Materials

6.1 Materials

6.1.1 Calcium Carbonate

Ground Calcium Carbonate was used in the hindered settling experiments. It was sourced from Letco Medical. The Calcium Carbonate was produced from natural sources, specifically Limestone [1].

Source: Letco Medical

Lot no: 11240219

Cas no: 471-34-1

Appearance: White Powder

Formula: $CaCO_3$

pH: 8.4 – 10.2 at 5% water suspension

Water solubility: 1.3 mg/L

Density: 2.7 gm/cm^3

Median Particle size: 12 μm [4].

Decomposition temperature: 700 – 900^0C

LETCO MEDICAL

Certificate of Analysis

Letco Medical Item(s)/Lots: 692756/Lot: 11240217, 692755/Lot: 11240218, 690941/Lot: 11240219, 686308/Lot: 11240220

Item:	Cust. Order #:	Lot Number:
Calcium Carbonate USP	21098	180201310
Ship Date:	**Production Date:**	**Expiration Date:**
March 15, 2010	January 28, 2010	January 28, 2013

Test Description	Unit of Measure	Min	Tested Value	Max
Identification (XRD)	Positive		Positive for Calcite	
Calcium Carbonate (USP)	Percent	98.0	99.4	100.5
Magnesium & Alkali Salts (USP)	Percent		0.42	≤1.0
Acid Insoluble's (USP)	Percent		0.04	≤0.2
Loss on Drying (USP<731>)	Percent		0.07	≤2.0
Lead (ICP-MS)	Parts per million		0.063	≤0.3
Arsenic[1](ICP-OES)	Parts per million		≤3.0	≤3.0
Fluoride[1] (specific ion electrode)	Percent		≤0.005	≤0.005
Barium[1](ICP-OES)	Not detected		Pass	Pass
Iron[1](ICP-OES)	Parts per million		≤1000	≤1000
Mercury[1](ICP-MS)	Parts per million		≤0.5	≤0.5
Heavy Metals (asPb)(USP <231>)	Parts per million		<20	<20.0
Total Plate Count (USP<61>)	CFU per gram		50	<1000
Total Combined Yeast & Mold (USP<61>)	CFU per gram		10	<200
USP Pathogens (Staphylococcus aureus, Pseudomonas aeruginosa, Salmonella, Escherichia coli)	Negative		Negative	

All products will meet the indicated specifications, based on demonstrated process capability and periodic testing.
Residual Solvents: Ground calcium carbonate sold under this manufacture contains no Class I, II, or III residual solvents.
Irradiation/Radioactivity: This product or its components have not been subjected to irradiation, ethylene oxide or any other method of sterilization.
Country of Origin: USA

WE HEREBY CERTIFY THAT THIS IS A TRUE COPY OF THE MANUFACTURERS ORIGINAL CERTIFICATE OF ANALYSIS

Letco Medical • 1316 Commerce Dr. NW • Decatur, AL 35601 • (800) 239-5288
www.letcomedical.com

Figure 6-1 Certificate of Analysis of Calcium Carbonate provided by Letco Medical [2].

6.1.2 Labrasol®

Labrasol® is a non-ionic water dispersible surfactant. It is composed of Polyethylene glycol esters, glycerides, and free Polyethylene glycol [3]. It is soluble in ethanol, chloroform, methylene chloride, and water at room temperature. It is insoluble in mineral oil. It is an oil in water surfactant and it is used as a solubility and wettability enhancer for active pharmaceuticals. In solutions with water it, excessive agitation causes foaming, so care should be taken when mixing suspensions containing Labrasol® to minimize this occurrence.

Source: Gattefosse

Batch No: 136935

Chemical name: Caprylocaproyl poloxyl-8 gycerides USP NF

Cas No: 61791-29-5

Appearance: Oily Liquid at room temperature

Specific Gravity: 1.060 – 1.070

Viscosity: 80 – 110 mPa

Boiling point: 250^0C

6.1.3 Deionized Water

Deionized water was used in the hindered settling experiments. Its purpose was to minimize the possible effects that impurities in the water would have on sedimentation. It was provided by the University of Toledo.

6.1.4 Equipment

Graduated cylinders with a volume of 250 mL made by Fisher Scientific were used in the hindered settling experiments. The cylinders were made of Pyrex glass.
Volumetric flasks measuring 100 mL were used to produce the Labrasol® solutions used in the experiment.

An electronic balance, ER 120A, made by American Scientific Products was used for all weighings.
An Ostwald-Viscometer was to measure the viscosity of the solutions of varying Labrasol® concentration. It was made by E.H. Sergent & Co. No. S-83305, Chicago, IL.

A 10 mL pycnometer was used to determine the density of the solutions containing different concentrations of Labrasol®. It was Kimble brand, Item No. 15123-ST.

A stop watch was used for determining the time it took for complete sedimentation. It was made by, Fisher Scientific.

Parafilm was used to seal the graduated cylinders to prevent the suspensions from spilling during experimentation. It was made by American National Can Co. Chicago, IL.

Zeta potential measurements were made using a Nicomp 380 ZLS, Particle Sizing Systems, CA

Differential Scanning Calorimeter measurements were made using a Mettler Toledo DSC 822e with TS0801RO sample robot

A Sputter Coater –Denton vacuum, Desk II and JSM 5200 Scanning Electron Microscope was used to produce SEM samples and images

A Laser diffraction instrument was use to measure particle seize, Malvern Metasizer 2000e®

A X-ray powder diffractometer was used for PXRD measurements of powdered samples, PANalytical X'Pert Pro MPD

6.2 Methods

6.2.1 Preparation of Suspensions

First, A 100 mL 10% stock solution of Labrasol® was prepared. Experiments were performed at Labrasol® concentrations of 0.05%, 0.5%, 1.0%, 2.0%, and a control at 0.0%. Sedimentation was measured in a suspension volume of 200 mL with masses of 20 g, 25g, 30 g, 35 g, 40g, 45 g, and 50 g of Calcium carbonate at each concentration of Labrasol® listed above. Graduated cylinders were first filled with the varying amounts

of Calcium carbonate which were previously listed. The cylinder was the filled with Deionized water up to 100 mL and allowed to sit for 24 hours to allow the Calcium carbonate to become wetted. After 24 hours the Labrasol® stock solution was added to the graduated cylinder to produce concentrations of 0.05%, 0.5%, 1.0%, 2.0%. Following the addition of the stock solution, Deionized water was added to the suspensions to produce a final volume of 200 mL. The suspensions were then allowed to set for 48 hours with periodic mixing to allow the Calcium carbonate, water, and Labrasol® to equilibrate before any sedimentation experiments were performed.

6.2.2 Measuring Density

The densities of the various suspensions were determined by using a 10 mL pycnometer. The empty pycnometer was weighed and then filled with the Labrasol® solution and then weighed again. The difference in the weights between the empty pycnometer and the filled pycnometer was used to determine the density by dividing the weight difference by the pycnometer volume, 10 mL. This procedure was done for all Labrasol® concentrations, (0.0%, 0.05%, 0.5%, 1.0%, 2.0%) and performed in triplicate. All measurements were taken at 25^0C.

6.2.3 Measuring Viscosity

Viscosity of the suspending media was measure using an Ostwald-viscosimeter. This is done by measuring the time it takes for the liquid in the viscosimeter to drop between to calibrated marks. This is performed for the suspending media and a reference standard with a known viscosity, which is usually water. This measurement was performed at all concentrations of Labrasol®, (0.0%, 0.05%, 0.5%, 1.0%, 2.0%). All measurements were taken at 25^0C. Viscosity was then determined using the following equation.

$$\frac{\eta_1}{\eta_2} = \frac{\rho_1 t_1}{\rho_2 t_2} \qquad \text{Eq. 6.1}$$

Where:

η_1 is the viscosity of water;

η_2 is the viscosity of suspending media;

ρ_1 is the density of water;

ρ_2 is the density of the suspending media;

t_1 is the time of fall for water; and

t_2 is the time of fall for the suspending media

6.2.4 Hindered settling experiments

The hindered settling experiments were performed using the suspensions previously described in section 6.2.1. After the suspension was equilibrated for 48 hours, experimentation proceeded. The suspension was first agitated by inverting it back and

forth 30 times and then placed on a flat level surface. The height of the interface between the supernatant and the falling calcium carbonate was measured every 30 seconds. This continued until the sediment volume remained relatively steady. The experiment was performed in triplicate for each combination of various weights of Calcium carbonate and concentrations of Labrasol®. The data was plotted with the x-axis measuring time in minutes and the y-axis measuring the height of the interface in millimeters. The linear portion of the plotted data is then used to determine particle size according to previously discussed methods in Chapter 3 Section 5.

6.2.5 Scanning Electron Microscopy

Scanning electron microscopy was used to study the morphology of calcium carbonate in combination with Labrasol®. This was done using a JSM – 5200 scanning electron microscope. Samples of the Calcium carbonate suspensions used in the hindered settling experiment were dried overnight in an oven at 30^0C. The dried samples were then placed on a metal sample holder and made conductive with gold using a vacuum sputter coater. Images were taken with the microscope operating at 10 kV.

6.2.6 Laser Diffraction

Small quantities of the calcium carbonate suspensions used in the hindered settling experiment were taken and the particle size was measured using a Malvern Metasizer 2000e®. Small amounts of the sample were added to the homogenizer attached to the

metaziser, which was previously filled with deionized water. A computer attached to the metaziser provided output data showing when enough sample was added to the homogenizer to be within the machines operating range. Once the proper amount of sample was in the homogenizer, the measurement process was initiated. The samples used were taken from the suspensions containing 40 grams of Calcium carbonate and at all concentrations of Labrasol®. The metaziser automatically measured each sample in triplicate. The process was repeated in triplicate for all samples. Data was exported to an excel spreadsheet and graphs were produced from the measurements.

6.2.7 Zeta potential measurement

A Nicomp 380 ZLS, particle sizing system was used to measure the zeta potential of the suspensions. Samples from suspensions containing 30 grams of calcium carbonate and all Labrasol® concentrations were taken and diluted down to 2% calcium carbonate to obtain an accurate zeta potential measurement. A culture tube, Durex borosilicate, was used to hold the sample in order to obtain the zeta potential measurements. The zeta potential was determined by placing the sample in the path of a helium neon laser of wavelength 658 nm at a scattering angle of 90^{o}.

6.2.8 Differential scanning calorimetry

Differential scanning calorimetry was performed on samples taken from the suspensions with 30 grams of calcium carbonate that were used in the hindered settling experiments.

Samples were carefully weighed into 100 μL aluminum crucibles. The crucibles were pre-weighed. The weight of the reference aluminum pan was 75.407 mg. The weight of the empty sample pan and the weight of the suspension samples were inputted into the DSC software for measurement purposes. A Mettler Toledo DSC 822e with TS0801RO sample robot was used to perform the studies equipped with a TS0800GCI gas flow system attached to a Nitrogen gas cylinder. Nitrogen gas was used as the purge gas. The method was divided into three segments. The first segment was from 25°C to -20°C at 1°C/min. The second segment was from -20°C to 50°C at 2°C/min and third segment was from 50°C to 200°C at 10°C/min. The method was kept constant for all the samples. The flow of the purge gas was set to a rate of 20 mL/min. After the program method finished, the curves were saved and further evaluated using STARe software. The study was used to analyze the bound and unbound water found in the suspensions and to determine if varying the Labrasol® concentrations had an effect.

6.2.9 Powder x-ray diffraction

Samples of all the calcium carbonate suspensions used in the hindered settling experiments were taken to study the x-ray diffraction pattern using a PANalytical X'Pert Pro MPD. X-ray spectra were recorded using a Cu X-ray source at a voltage of 45 kV, a current of 40 mA, with 0.04 rad Soller slits, 1/4° divergence slit,10 mm mask, 1/2^{o} anti scattered slit, Nickel filter and X'Celerator detector over a 2Θ range of 10^{o} to 70^{o} with a continuous speed of 4 degrees per minute. The samples were dried and then ground in a mortar and pestle to obtain a uniform more free flowing powder. The powder was placed on an aluminum sample holder and

carefully smoothed over to obtain a flat powder surface. The peak pattern for each sample was evaluated using the X'Pert Data High Score Plus software. Diffractograms were automatically produced by the software to show the crystallinity of the samples and if there were any noticeable changes between them.

Chapter 7

Results and Discussion

7.1 Rate of Sedimentation

7.1.1 Density and Viscosity of Suspension media

The density and viscosity of the suspension media were calculated according the methods described in Chapter 6. All measurements were taken at 25^0C. The results are listed below in Table 7.1. The density and viscosity of water were obtained from reference literature.

Table 7.1 Density and Viscosity measurements of suspension media

Suspending media	Density(gm/cm^3)	Viscosity(poise)
Deionized Water	0.997	0.0091
0.05% w/v Labrasol®	1.03	0.0093
0.5% w/v Labrasol®	1.030	0.0093
1.0% w/v Labrasol®	1.030	0.0095
2.0% w/v Labrasol®	1.031	0.0101

7.1.2 Sedimentation Results

The hindered settling experiments were performed with the methods outlined in chapter 6. Suspensions were made up to 200 mL, and Labrasol® concentrations of 0%, 0.05%, 0.5%, 1.0%, and 2.0% were produced by adding the appropriate amount of stock solution. Due to the nature of Labrasol® as a non-ionic surfactant, foaming was observed when the suspensions were agitated, so extra care was taken to only shake the suspensions as much as needed to thoroughly homogenize the Calcium carbonate.

The graphed data from the experiments typically shows three segments, however, for this study only the middle linear portion of the graph is needed to calculate the rate of fall (Q) and subsequent particle size. Hindered settling was visible at all concentrations ranging from 20 grams to 50 grams of Calcium carbonate. At concentrations of 2% Labrasol®, hindered settling was still visible, however, during the first few minutes of settling the supernatant near the interface was relatively cloudy compared to the other Labrasol® concentrations. This could be due to the slightly increased viscosity at the higher Labrasol® concentrations shown in Table 7.1. This could also be due to Labrasol® causing deflocculation. The Labrasol® acts to increase wettability of the Calcium carbonate by reducing the interfacial tension between the particles and the water. This decreased interfacial tension could lead to water particle interactions overtaking particle particle interactions causing less aggregation of the suspended media. With less particle aggregation, there will be an increased amount of smaller particles relative to larger particles causing a hazier supernatant. The following figures in this section will show the hindered settling data plots and the following tables in this section will show the calculated velocities (Q), average velocity and initial porosity (ε).

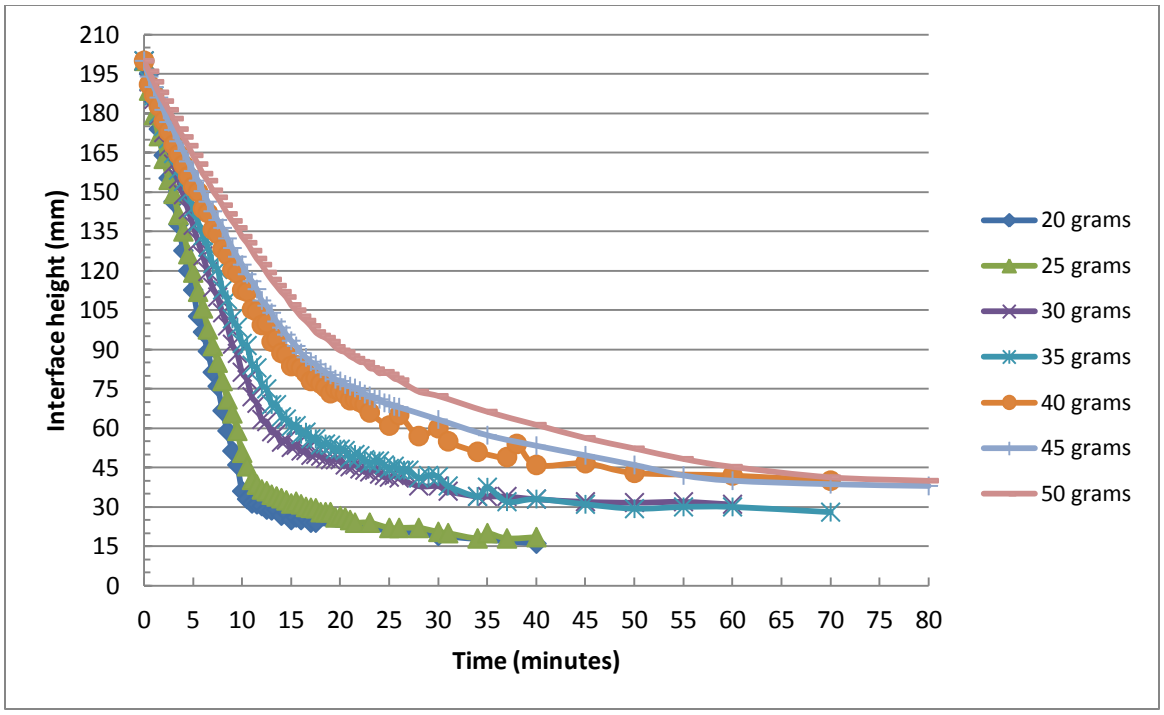

Figure 7-1: A plot of height of the interface (mm) against time (min) for ground calcium carbonate suspensions in deionized water

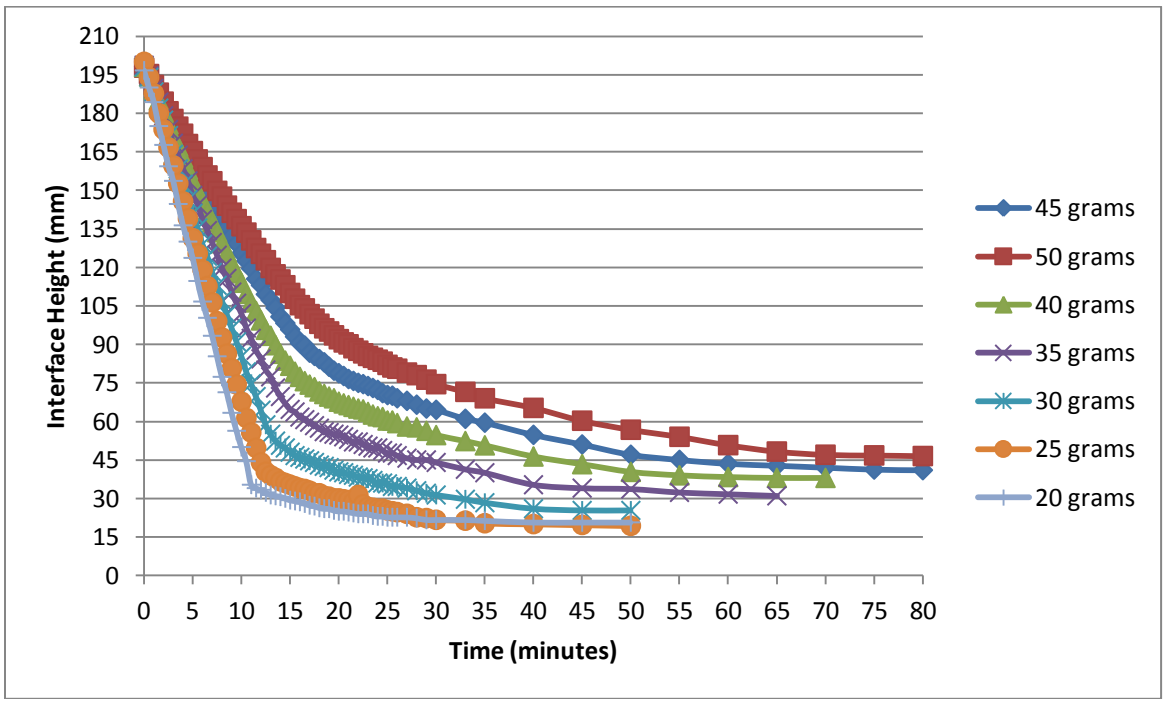

Figure 7-2: A plot of height of the interface (mm) against time (min) for ground calcium carbonate suspensions in 0.05% Labrasol® solution.

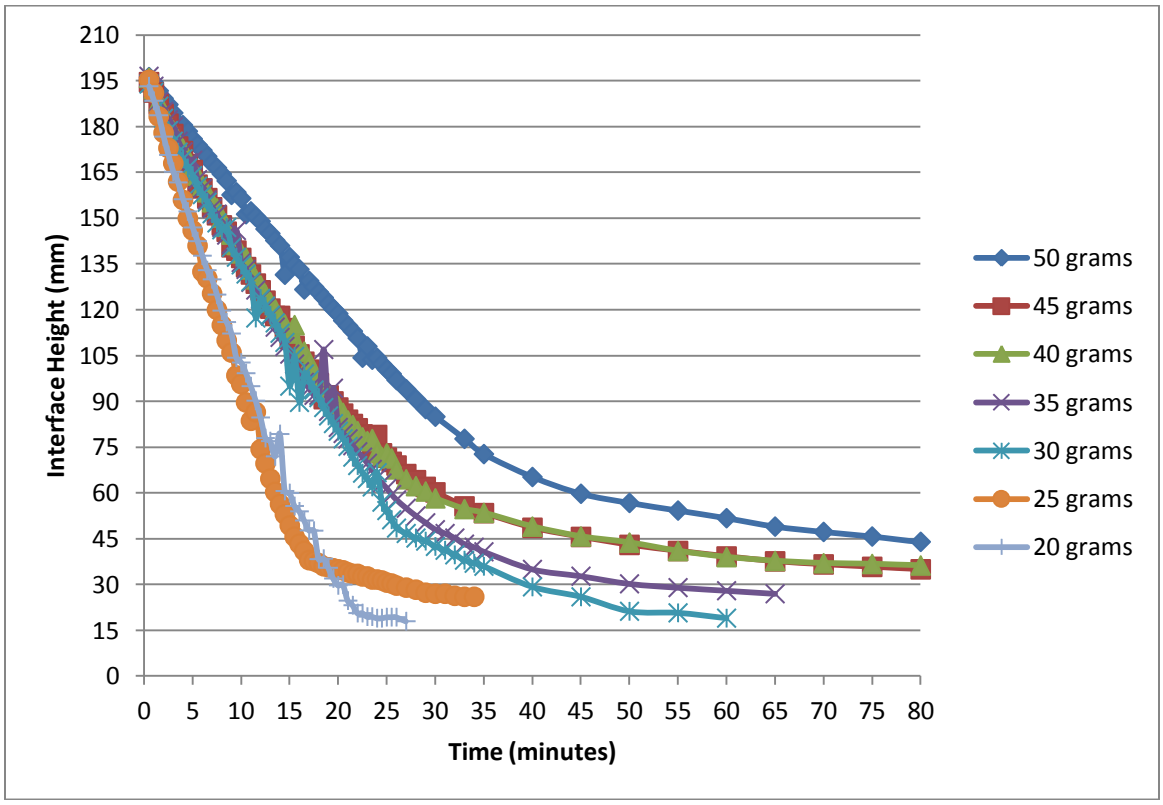

Figure 7-3: A plot of height of the interface (mm) against time (min) for ground calcium carbonate suspensions in 0.5% Labrasol® solution.

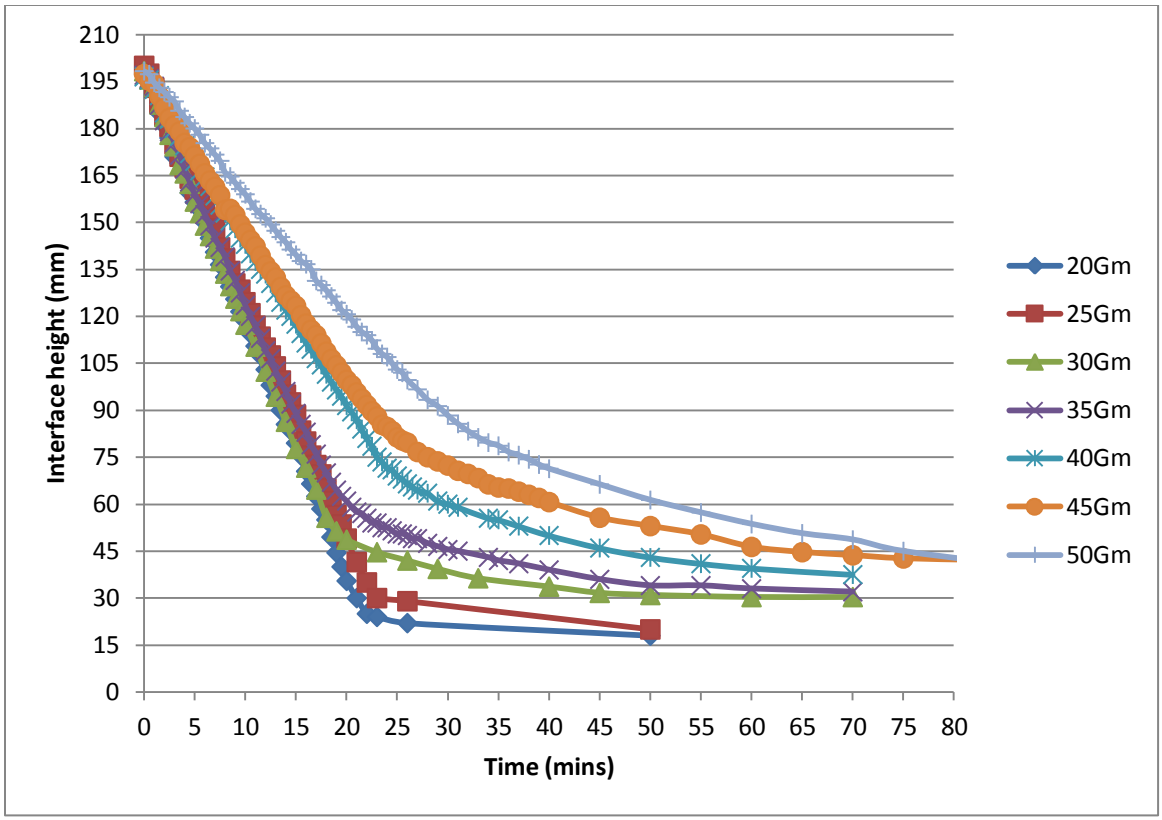

Figure 7-4: A plot of height of the interface (mm) against time (min) for ground calcium carbonate suspensions in 1.0% Labrasol® solution

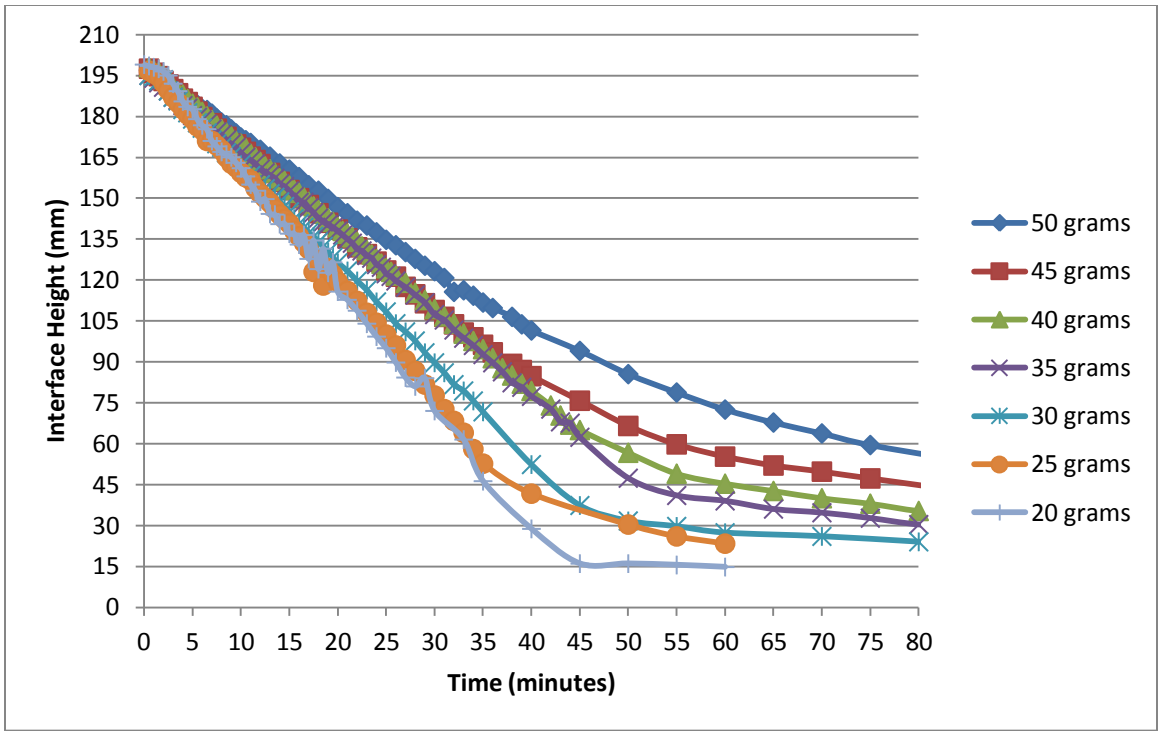

Figure 7-5: A plot of height of the interface (mm) against time (min) for ground calcium carbonate suspensions in 2.0% Labrasol® solution

Table 7.2 Hindered settling values for concentration, Q_1, Q_2, Q_3, Q_{avg}, standard deviation and porosity derived from different weights of calcium carbonate suspended in water

Wt (gm)	Conc. (gm/mL)	Q_1 (mm/min)	Q_2 (mm/min)	Q_3 (mm/min)	Q_{avg} (mm/min)	Std. Dev.	ε
20	0.1	16.38	16.97	17.304	16.885	0.468	0.962
25	0.125	14.642	14.335	14.372	14.449	0.168	0.953
30	0.15	11.887	11.395	11.27	11.517	0.326	0.944
35	0.175	10.715	10.108	10.077	10.3	0.359	0.935
40	0.2	7.608	7.669	8.295	7.857	0.380	0.925
45	0.225	6.859	6.959	6.994	6.938	0.0702	0.917
50	0.25	6.374	6.229	6.357	6.32	0.079	0.907

Table 7.3 Hindered settling values for concentration, Q_1, Q_2, Q_3, Q_{avg}, standard deviation and porosity derived from different weights of calcium carbonate suspended in 0.05% Labrasol®

Wt (gm)	Conc. (gm/mL)	Q_1 (mm/min)	Q_2 (mm/min)	Q_3 (mm/min)	Q_{avg} (mm/min)	Std. Dev.	ε
20	0.1	14.879	14.721	14.767	14.789	0.0812	0.962
25	0.125	13.004	13.032	13.046	13.027	0.0213	0.953
30	0.15	11.143	11.169	11.11	11.140	0.0295	0.944
35	0.175	9.431	9.344	9.647	9.474	0.155	0.935
40	0.2	7.990	7.869	8.098	7.986	0.114	0.925
45	0.225	6.783	6.825	6.772	6.793	0.027	0.917
50	0.25	5.647	5.638	5.708	5.664	0.0383	0.907

Table 7.4 Hindered settling values for concentration, Q1, Q2, Q3, Qavg, standard deviation and porosity derived from different weights of calcium carbonate suspended in 0.5% Labrasol®

Wt (gm)	Conc. (gm/mL)	Q_1 (mm/min)	Q_2 (mm/min)	Q_3 (mm/min)	Q_{avg} (mm/min)	Std. Dev.	ε
20	0.1	7.755	9.005	7.698	8.152	0.738	0.962
25	0.125	11.228	10.018	9.785	10.343	0.774	0.953
30	0.15	6.646	6.531	5.814	6.330	0.450	0.944
35	0.175	4.435	5.347	5.842	5.208	0.713	0.935
40	0.2	4.934	5.770	4.753	5.152	0.542	0.925
45	0.225	4.521	4.476	4.695	4.564	0.115	0.917
50	0.25	3.653	4.152	4.137	3.981	0.283	0.907

Table 7.5 Hindered settling values for concentration, Q1, Q2, Q3, Qavg, standard deviation and porosity derived from different weights of calcium carbonate suspended in 1.0% Labrasol®

Wt (gm)	Conc. (gm/mL)	Q_1 (mm/min)	Q_2 (mm/min)	Q_3 (mm/min)	Q_{avg} (mm/min)	Std. Dev.	ε
20	0.1	7.905	7.949	7.968	7.940	0.032	0.962
25	0.125	7.440	7.429	7.417	7.429	0.012	0.953
30	0.15	7.813	7.718	7.850	7.794	0.068	0.944
35	0.175	7.127	7.235	7.020	7.127	0.107	0.935
40	0.2	5.262	5.210	5.236	5.236	0.025	0.925
45	0.225	4.905	4.940	4.794	4.880	0.075	0.917
50	0.25	3.814	3.814	3.892	3.840	0.045	0.907

Table 7.6 Hindered settling values for concentration, Q1, Q2, Q3, Qavg, standard deviation and porosity derived from different weights of calcium carbonate suspended in 2.0% Labrasol®

Wt (gm)	Conc. (gm/mL)	Q_1 (mm/min)	Q_2 (mm/min)	Q_3 (mm/min)	Q_{avg} (mm/min)	Std. Dev.	ε
20	0.1	3.935	4.663	3.749	4.116	0.482	0.962
25	0.125	3.054	4.456	4.497	4.002	0.821	0.953
30	0.15	3.574	3.456	3.725	3.585	0.134	0.944
35	0.175	2.856	3.019	3.018	2.964	0.093	0.935
40	0.2	3.179	2.774	3.077	3.010	0.210	0.925
45	0.225	3.309	2.513	3.600	3.141	0.562	0.917
50	0.25	3.069	2.250	2.809	2.709	0.418	0.907

After examining Figures 7-1 to 7-5 and Tables 7.2 to 7.6, it is clearly visible that increased concentrations of calcium carbonate in the suspensions causes the rate of sedimentation to decrease. This is due to the increase particle-particle interaction taking place causing a greater hindrance effect, thus slowing the rate of fall. By examining the tables and figures and comparing the different concentrations of Labrasol® added with the same amount of calcium carbonate, it can be shown that increased concentrations of Labrasol® can lead to a decreased rate of sedimentation. This is most likely due to the Labrasol® increasing the wettability of the Calcium carbonate. With this increased wettability and decreased interfacial tension between the water and particles, the particles are less likely to aggregate and form flocs. The rate of fall is also affected by the increase in viscosity. The pure water has a viscosity of 0.0091 poise and the 2.0% Labrasol® suspension had a viscosity of 0.0101 poise. Though the change is viscosity is not large, so its contribution to the change in sedimentation is most likely limited. The change in sedimentation rates will be further explored with the examination of particle size and zeta potential.

7.1.3 Particle Size Calculation

7.1.3.1 Steinour Method

Particle size can be calculated from the Steinour method by using the following equation:

$$\log \frac{Q}{\varepsilon^2} = A\varepsilon + [\log V_s - A] \qquad \text{Eq. 7.1}$$

Using this equation a plot of Log (Q/ε^2) versus (ε) is made and the slope and intercept are derived from the graph. The slope is equivalent to the (A) value in the Steinour equation and the intercept is equal to the ($LogV_s - A$) term from the equation. The plots and data are listed below in tables 7.7 to 7.12 and figures 7.6 to 7.10.

7.1.3.2 Richardson & Zaki Method

The Richardson & Zaki method can be used to calculate particle size with the equation shown below:

$$\log Q = \log V_s + n \log \varepsilon \qquad \text{Eq. 7.2}$$

A plot of (Log Q) versus (Log ε) is graphed, and from it the slope and intercept are determined, equaling (n) and (Log V_s), respectively, from the Richardson & Zaki equation. The data and graphs derived from this equation are show in Figures 7.7 to 7.11 and Table 7.13 and Figures 7.11 to 7.15.

7.1.3.3 Dollimore-Mcbride's equation

The Dollimore-Mcbride method can be used to calculate particle size using the following equation:

$$\log Q = \log V_s - b\rho_s(1-\varepsilon) \qquad \text{Eq. 7.3}$$

A plot of (Log Q) versus (1-ε) is graphed and the slope and intercept are determined. The slope is equal to the ($-bp_s$) term and the intercept is equal to the (Log V_s) term. The data and plots derived from this equation are listed below in Tables 7.7 to 7.11 and Table 7.14 and Figures 7.16 to 7.20.

With the data derived from the three different equations, particle size can be calculated by inputting the data into Stokes law, which is listed below. The method for using Stokes law was described in Chapter 3. Particle sizes calculated from Stokes law are listed in tables 7.15 to 7.19

$$V_s = \frac{2gr^2(\rho_s-\rho_l)}{9} \qquad \text{Eq. 7.4}$$

Table 7.7: The values for the hindered settling parameters for different weights of calcium carbonate suspended in water.

Weight (g)	Q_{avg} (mm/min)	log(Q)	ε	log(ε)	log(Q/ε^2)	(1 - ε)
20	16.884	1.227	0.962	-0.016	1.260	0.037
25	14.449	1.159	0.953	-0.020	1.201	0.046
30	11.517	1.061	0.944	-0.024	1.111	0.055
35	10.300	1.012	0.935	-0.029	1.071	0.064
40	7.857	0.895	0.925	-0.033	0.962	0.074
45	6.937	0.841	0.917	-0.037	0.916	0.083
50	6.320	0.800	0.907	-0.042	0.885	0.092

Table 7.8: The values for the hindered settling parameters for different weights of calcium carbonate suspended in 0.05% Labrasol®.

Weight (g)	Q_{avg} (mm/min)	log(Q)	ε	log(ε)	$\log(Q/\varepsilon^2)$	(1 - ε)
20	14.789	1.169	0.962	-0.016	1.202	0.037
25	13.027	1.114	0.953	-0.020	1.156	0.046
30	11.140	1.046	0.944	-0.024	1.096	0.055
35	9.474	0.976	0.935	-0.029	1.034	0.064
40	7.986	0.902	0.925	-0.033	0.969	0.074
45	6.793	0.832	0.917	-0.037	0.907	0.083
50	5.664	0.753	0.907	-0.042	0.837	0.092

Table 7.9: The values for the hindered settling parameters for different weights of calcium carbonate suspended in 0.5% Labrasol®.

Weight (g)	Q_{avg} (mm/min)	log(Q)	ε	log(ε)	$\log(Q/\varepsilon^2)$	(1 - ε)
20	8.152	0.911	0.962	-0.016	0.944	0.037
25	10.343	1.014	0.953	-0.020	1.055	0.046
30	6.330	0.801	0.944	-0.024	0.851	0.055
35	5.208	0.716	0.935	-0.029	0.774	0.064
40	5.152	0.712	0.925	-0.033	0.778	0.074
45	4.564	0.659	0.917	-0.037	0.734	0.083
50	3.981	0.600	0.907	-0.042	0.684	0.092

Table 7.10: The values for the hindered settling parameters for different weights of calcium carbonate suspended in 1.0% Labrasol®.

Weight (g)	Q_{avg} (mm/min)	log(Q)	ε	log(ε)	$\log(Q/\varepsilon^2)$	(1 - ε)
20	7.940	0.899	0.962	-0.016	0.932	0.037
25	7.429	0.870	0.953	-0.020	0.912	0.046
30	7.794	0.891	0.944	-0.024	0.941	0.055
35	7.127	0.852	0.935	-0.029	0.911	0.064
40	5.236	0.719	0.925	-0.033	0.785	0.074
45	4.880	0.688	0.917	-0.037	0.764	0.083
50	3.840	0.584	0.907	-0.042	0.668	0.092

Table 7.11: The values for the hindered settling parameters for different weights of calcium carbonate suspended in 2.0% Labrasol®.

Weight (g)	Q_{avg} (mm/min)	log(Q)	ε	log(ε)	$\log(Q/\varepsilon^2)$	(1 - ε)
20	4.116	0.614	0.962	-0.016	0.647	0.037
25	4.002	0.602	0.953	-0.020	0.643	0.046
30	3.585	0.554	0.944	-0.024	0.604	0.055
35	2.964	0.472	0.935	-0.029	0.530	0.064
40	3.010	0.478	0.925	-0.033	0.545	0.074
45	3.141	0.497	0.917	-0.037	0.572	0.083
50	2.709	0.432	0.907	-0.042	0.517	0.092

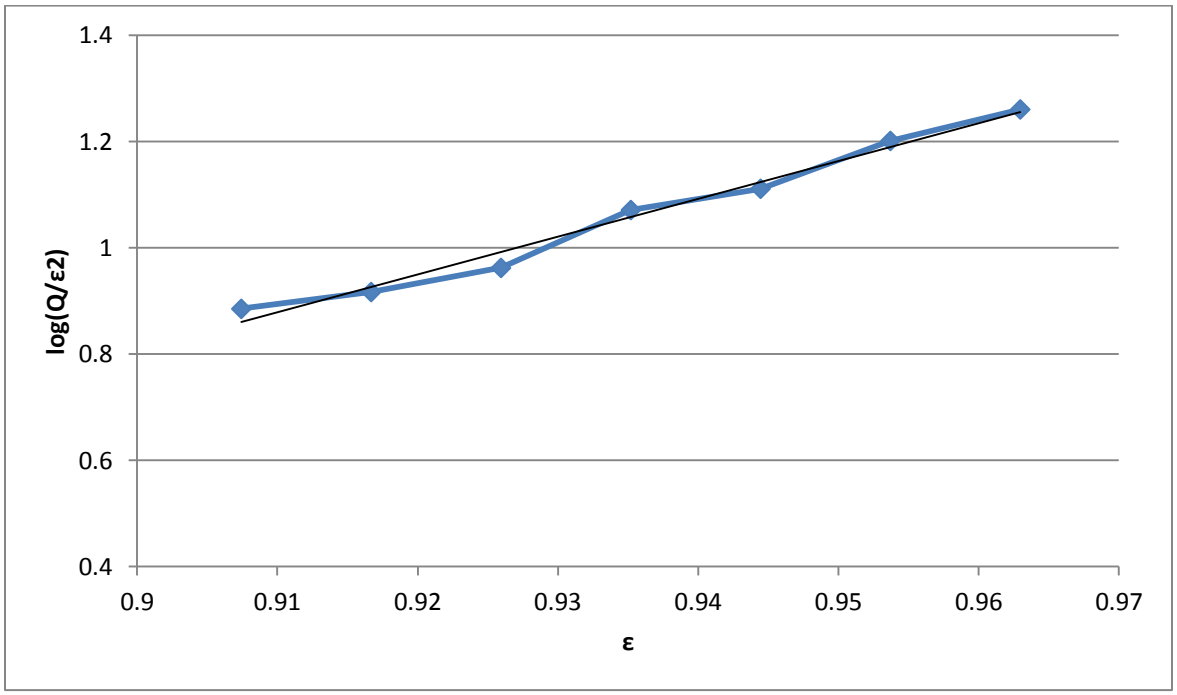

Figure 7-6: The linear plot of the Steinour equation for different weights of calcium carbonate in water, where slope = 7.1093; intercept = -5.5904; and R^2 = 0.9831

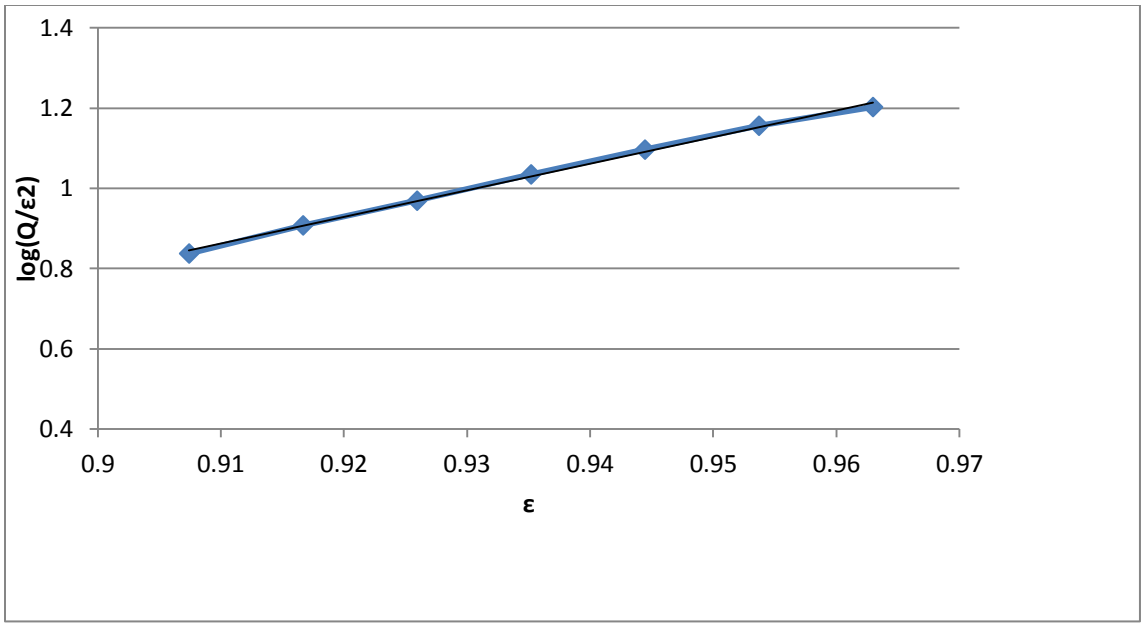

Figure 7-7: The linear plot of the Steinour equation for different weights of calcium carbonate in 0.05% Labrasol®, where slope = 6.6333; intercept = -5.1742; and R^2 = 0.9976

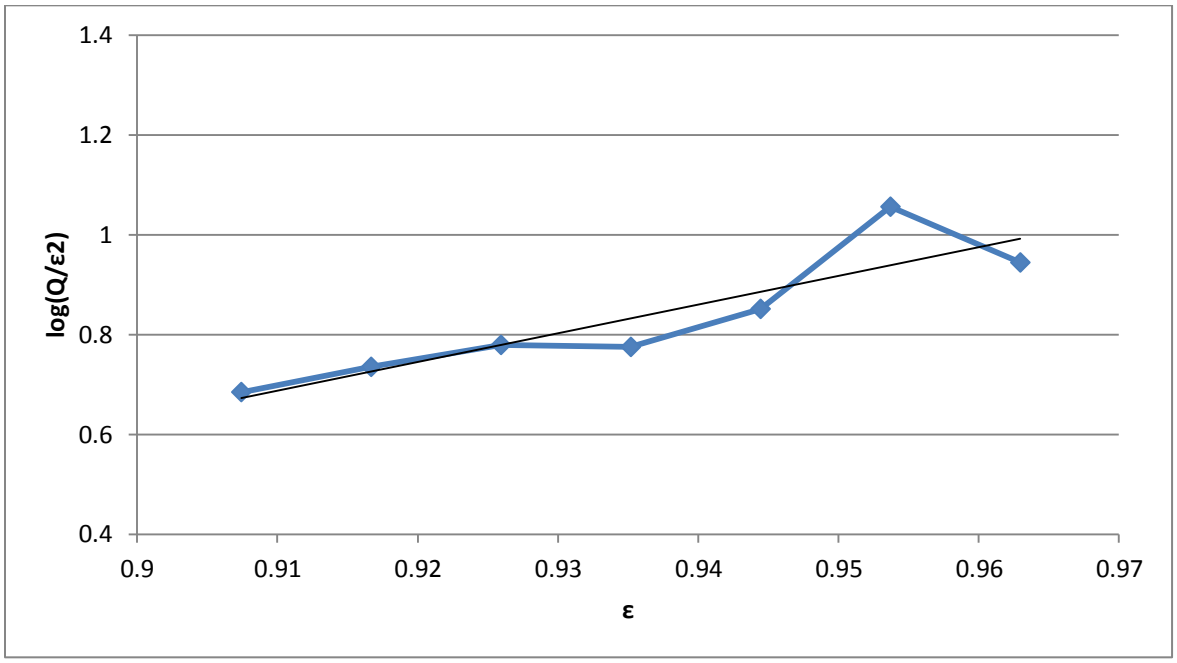

Figure 7-8: The linear plot of the Steinour equation for different weights of calcium carbonate in 0.5% Labrasol®, where slope = 5.7599; intercept = - 4.5546; and R^2 = 0.7936

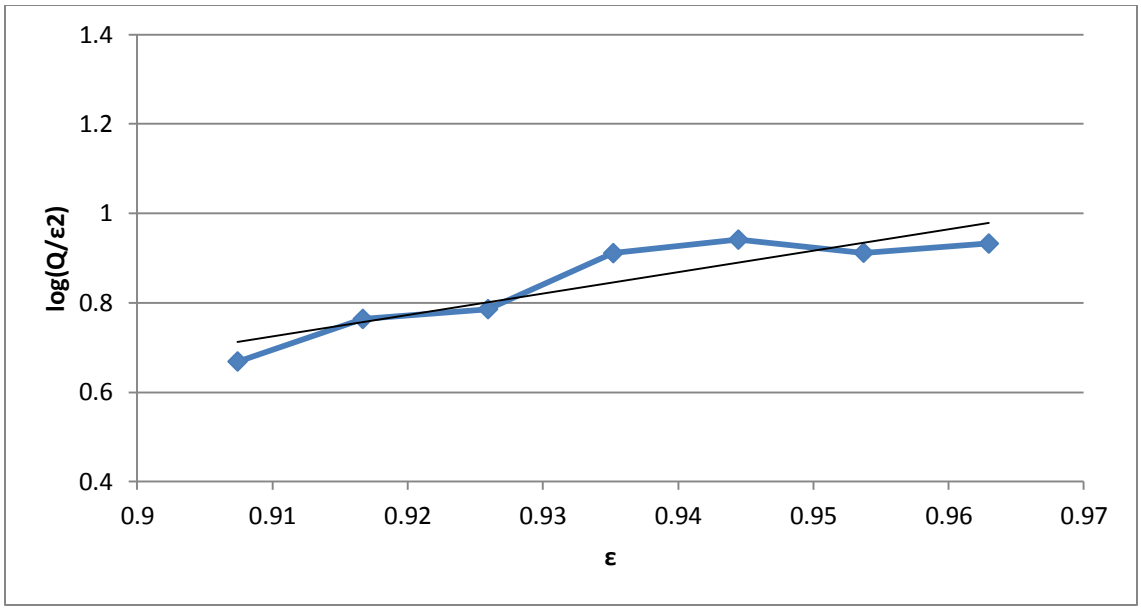

Figure 7-9: The linear plot of the Steinour equation for different weights of calcium carbonate in 1.0% Labrasol®, where slope = 4.7968; intercept = - 3.6407; and R^2 = 0.8245

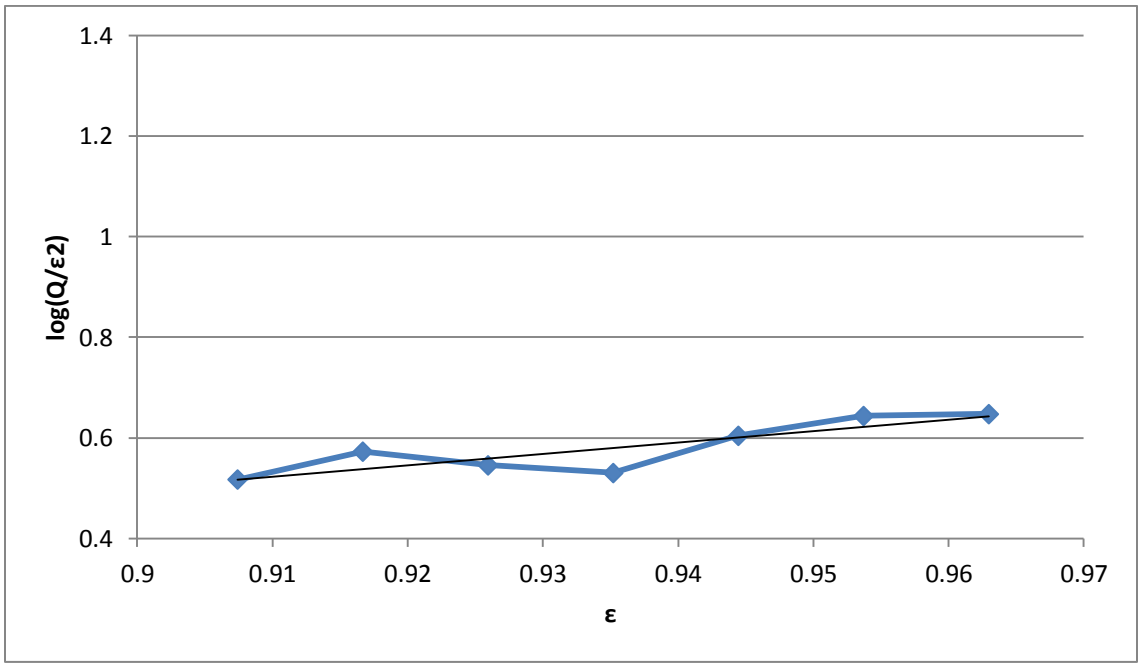

Figure 7-10: The linear plot of the Steinour equation for different weights of calcium carbonate in 2.0% Labrasol®, where slope = 2.2768; intercept = - 1.5497; and R^2 = 0.7405

Table 7.12: Hindered settling parameters obtained by Steinour's equation for calcium carbonate suspended in different media.

Suspension Media	A	Log V_s	V_s (mm/min)
Water	7.109	1.518	33.029
0.05% Labrasol®	6.633	1.459	28.780
0.5% Labrasol®	5.759	1.205	16.043
1.0% Labrasol®	4.796	1.156	14.325
2.0% Labrasol®	2.276	0.727	5.3419

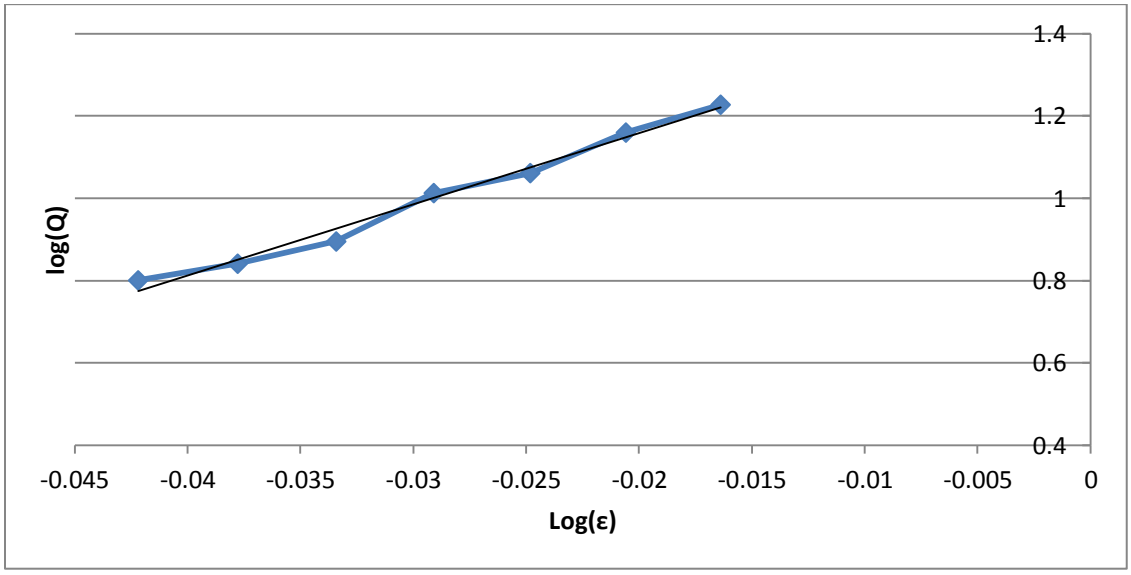

Fig. 7-11: The linear plot for the Richardson & Zaki equation for different weights of calcium carbonate in water, where slope = 17.295; intercept = 1.5046; and R^2 = 0.9857

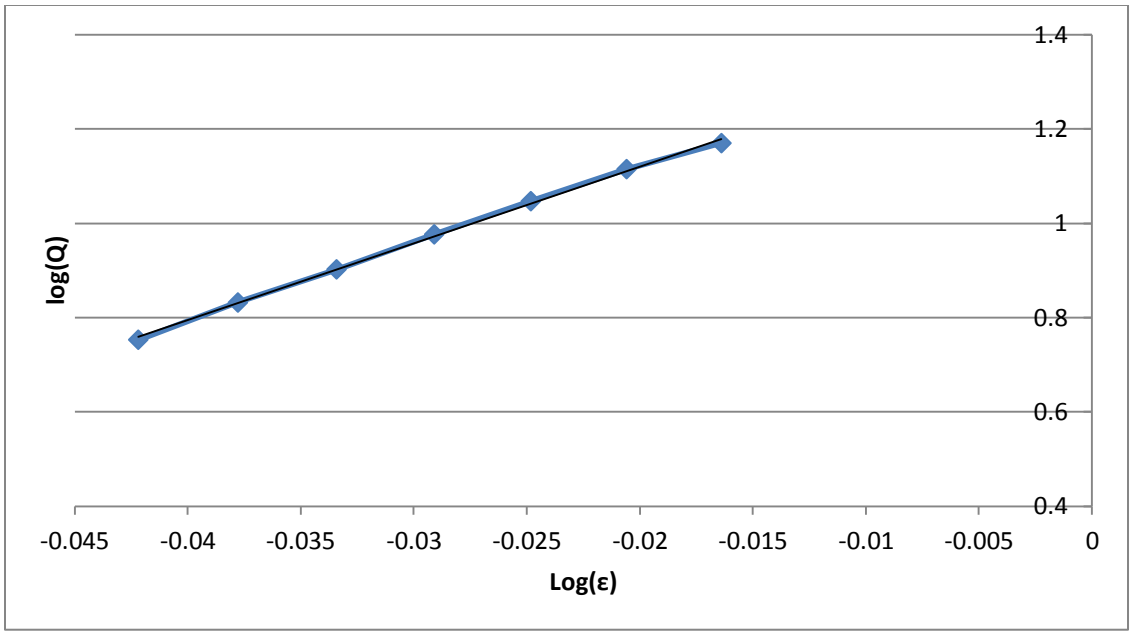

Fig. 7-12: The linear plot for the Richardson & Zaki equation for different weights of calcium carbonate in 0.05% Labrasol®, where slope = 16.285; intercept = 1.4462; and R^2 = 0.9987

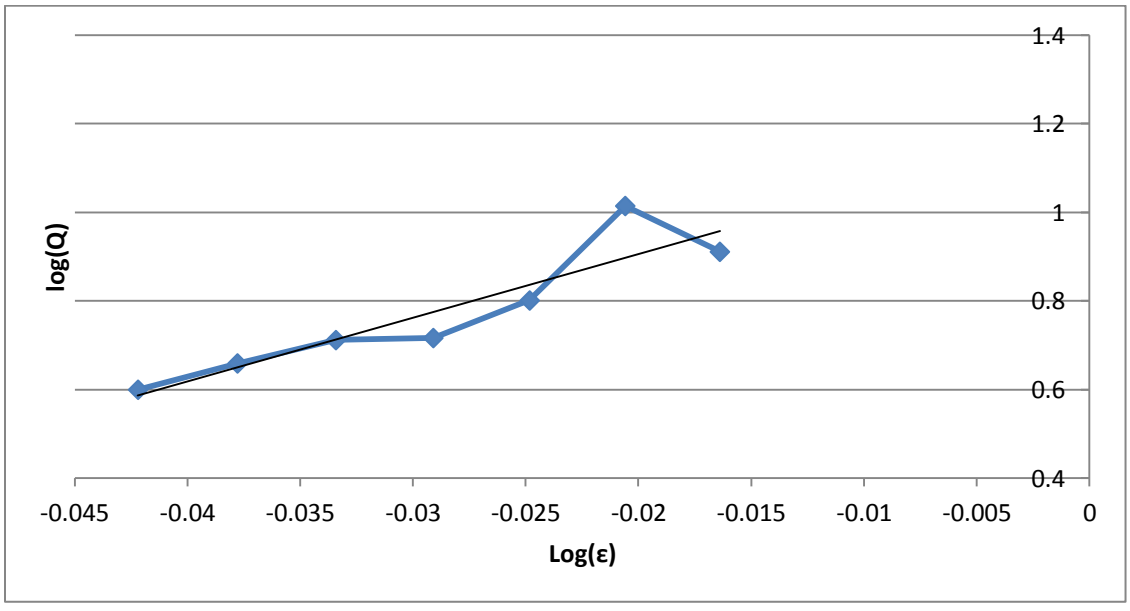

Fig. 7-13: The linear plot for the Richardson & Zaki equation for different weights of calcium carbonate in 0.5% Labrasol®, where slope = 14.393; intercept = 1.1937; and R^2 = 0.8376

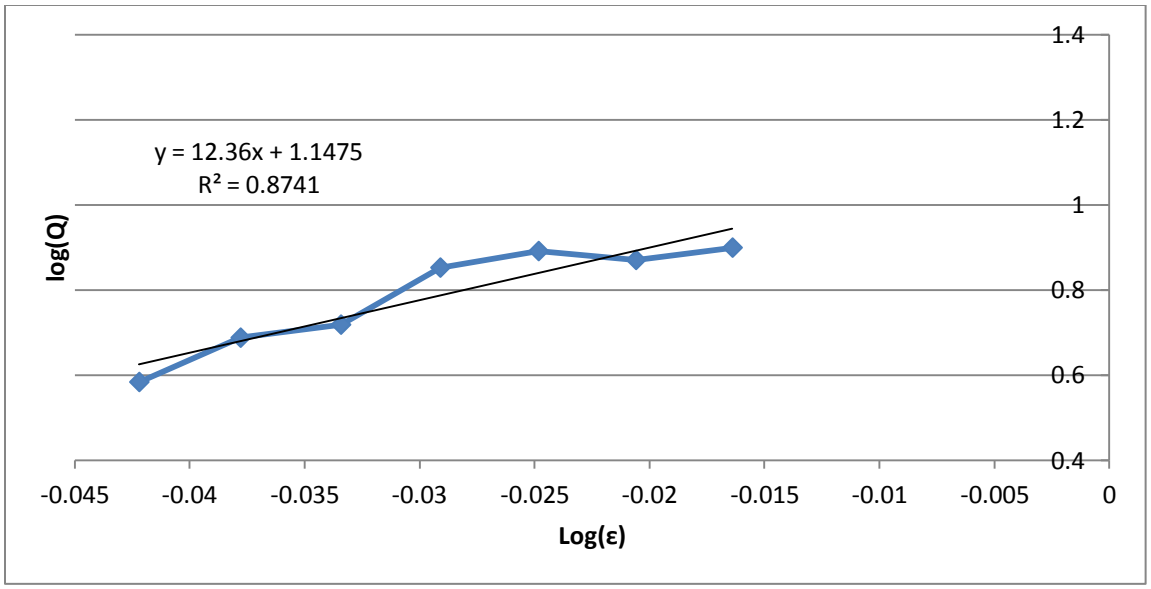

Fig. 7-14: The linear plot for the Richardson & Zaki equation for different weights of calcium carbonate in 1.0% Labrasol®, where slope = 12.36; intercept = 1.1475; and R^2 = 0.8751

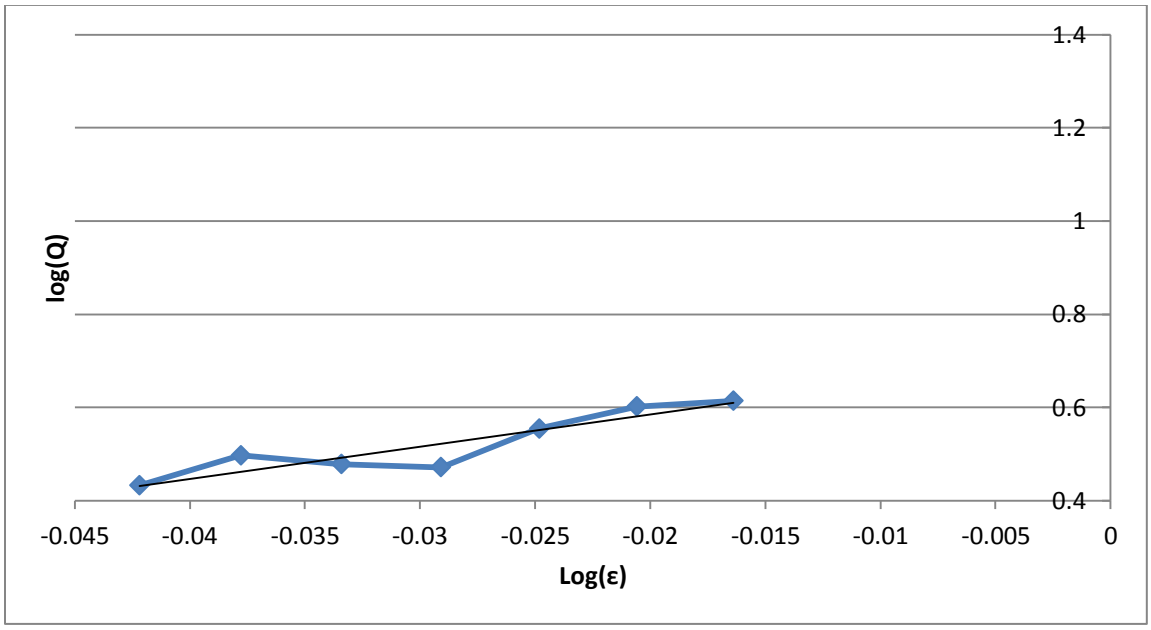

Fig. 7-15: The linear plot for the Richardson & Zaki equation for different weights of Calcium Carbonate in 2.0% Labrasol®, where slope = 6.8908; intercept = 0.7228; and R^2 = 0.8478

Table 7.13: Hindered settling parameters obtained by Richardson & Zaki equation for calcium carbonate suspended in different media

Suspension Media	n	Log V_s	V_s (mm/min)
Water	17.295	1.504	31.959
0.05% Labrasol®	16.285	1.446	27.938
0.5% Labrasol®	14.393	1.193	15.620
1.0% Labrasol®	12.36	1.147	14.044
2.0% Labrasol®	6.890	0.722	5.282

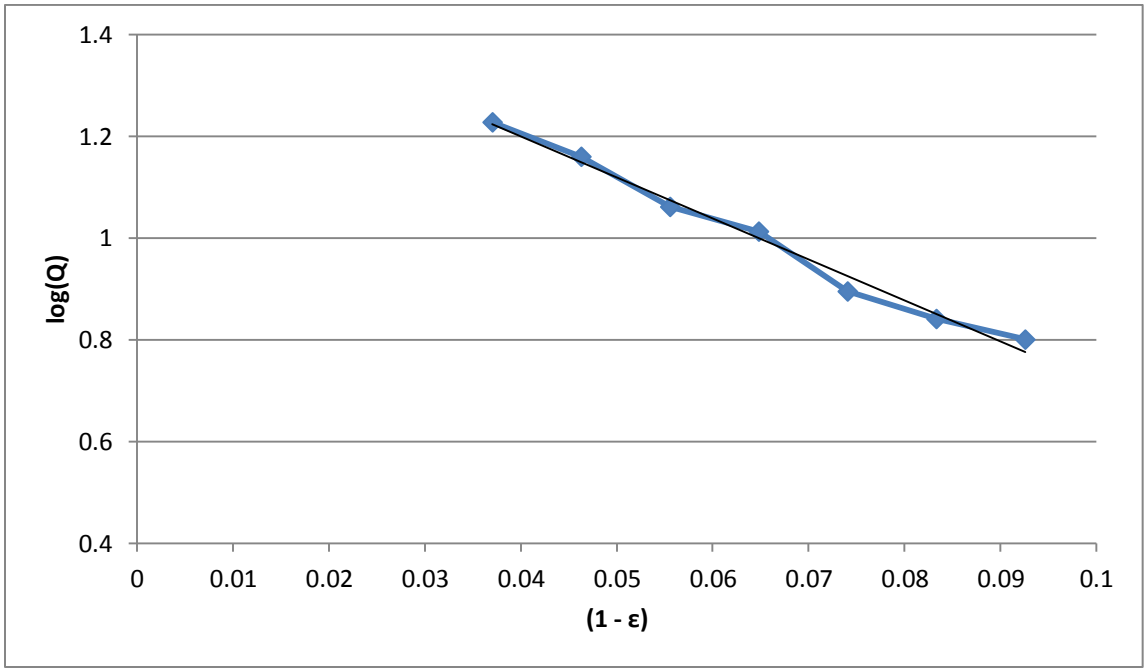

Figure 7-16: The linear plot for the Dollimore &McBride equation for different weights of calcium carbonate in water, where slope = -8.0383; intercept = 1.5208; and R^2 = 0.9868

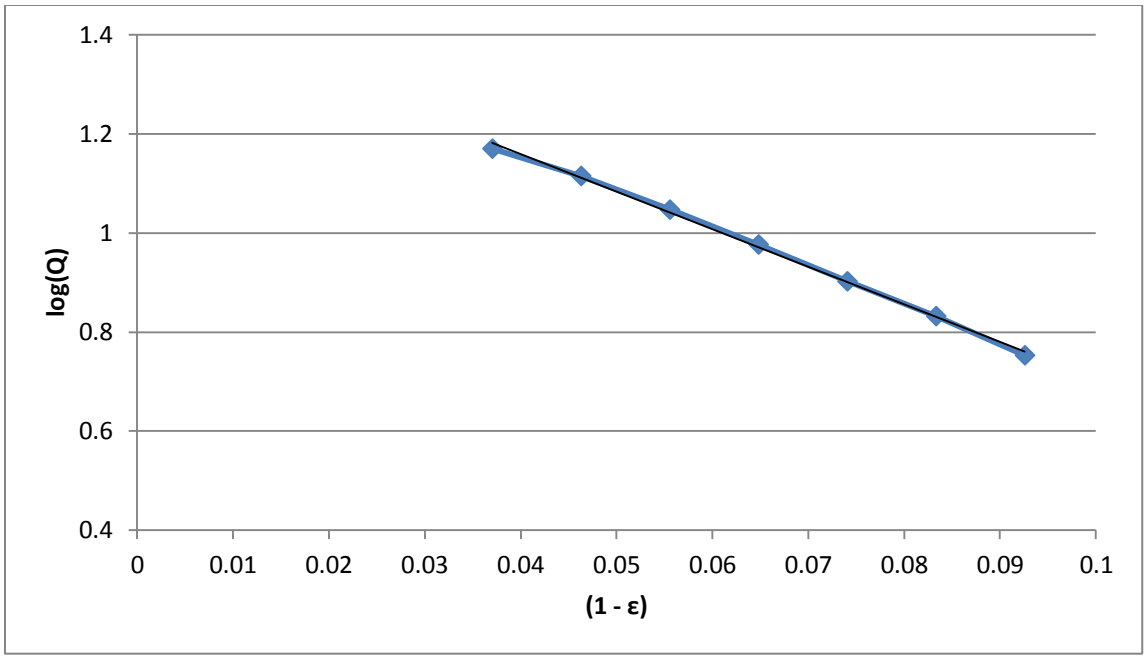

Figure 7-17: The linear plot for the Dollimore &McBride equation for different weights of calcium carbonate in 0.05% Labrasol®, where slope = -7.5623; intercept = 1.461; and R^2 = 0.9981

.

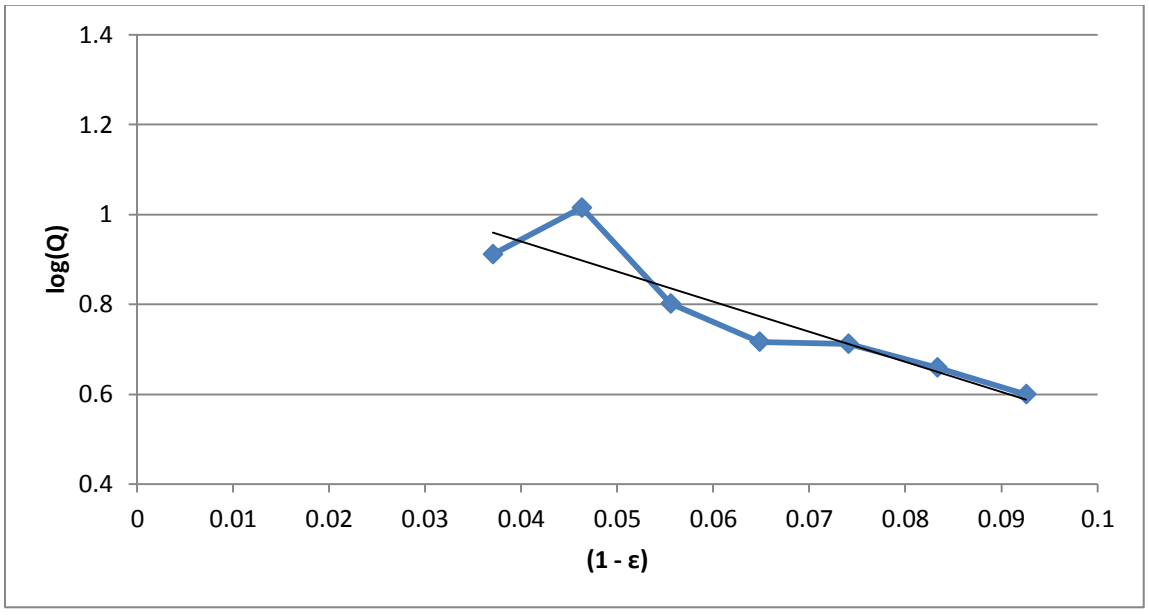

Figure 7-18: The linear plot for the Dollimore &McBride equation for different weights of calcium carbonate in 0.5% Labrasol®, where slope = -6.6889; intercept = 1.2072; and R^2 = 0.8384

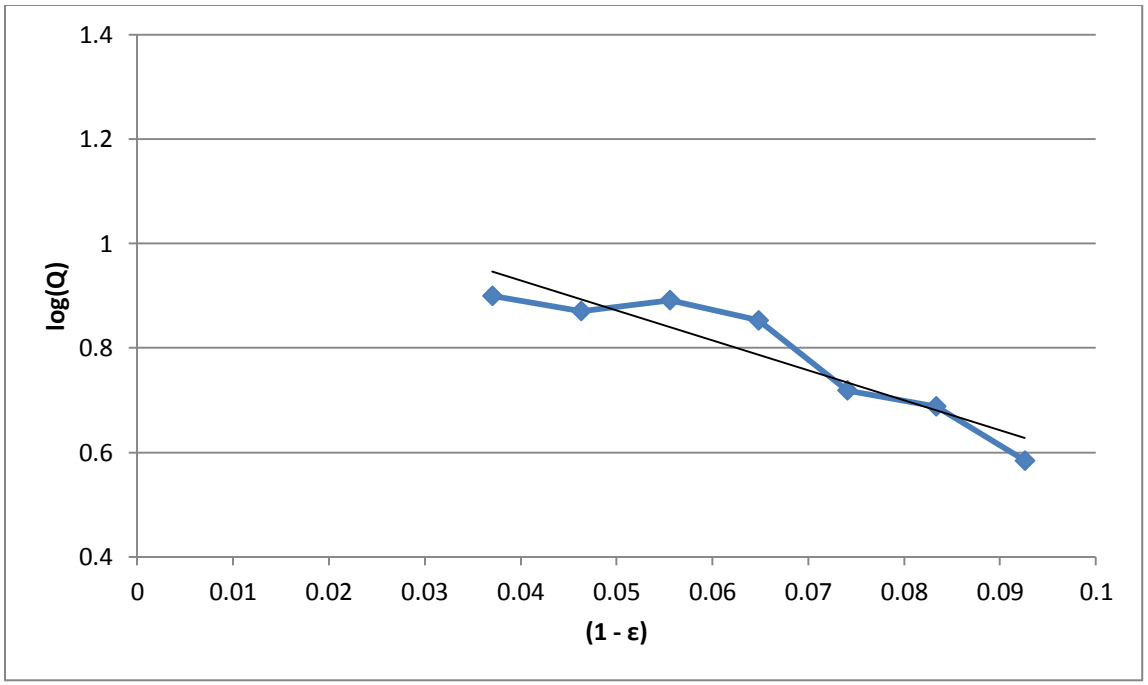

Figure 7-19: The linear plot for the Dollimore &McBride equation for different weights of calcium carbonate in 1.0% Labrasol®, where slope = -5.7258; intercept = 1.1579; and R^2 = 0.8694

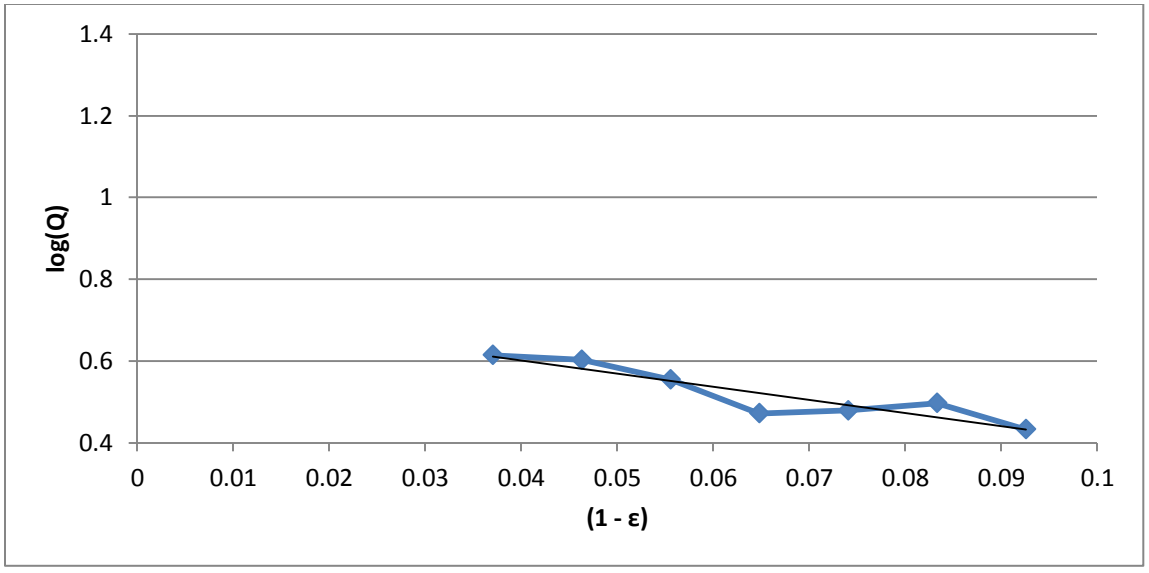

Figure 7-20: The linear plot for the Dollimore &McBride equation for different weights of calcium carbonate in 2.0% Labrasol®, where slope = -3.2058; intercept = 0.7295; and R^2 = 0.8504

Table 7.14: The values for hindered settling parameters obtained by Dollimore & Mcbride equation for calcium carbonate suspended in different media

Suspension Media	b	Log V_s	V_s (mm/min)
Water	2.977	1.520	33.1742
0.05% Labrasol®	2.800	1.461	28.906
0.5% Labrasol®	2.477	1.207	16.113
1.0% Labrasol®	2.120	1.157	14.384
2.0% Labrasol®	1.187	0.729	5.364

Table 7.15: Particle size calculated using the three different equations for calcium carbonate suspended in water

Equation	Vs (cm/s)	r (μm)
Steinour	0.05505	11.6229
Richardson & Zaki	0.05327	11.4331
Dollimore-Mcbride	0.05529	11.6483
Average	0.05454	11.5861

Table 7.16: Particle size calculated using the three different equations for calcium carbonate suspended in 0.05% Labrasol®

Equation	Vs (cm/s)	r (μm)
Steinour	0.0479	11.075
Richardson & Zaki	0.0465	10.911
Dollimore-Mcbride	0.0481	11.099
Average	0.0475	11.028

Table 7.17: Particle size calculated using the three different equations for Calcium Carbonate suspended in 0.5% Labrasol®

Equation	Vs (cm/s)	r (μm)
Steinour	0.0267	8.269
Richardson & Zaki	0.0260	8.159
Dollimore-Mcbride	0.0268	8.287
Average	0.0265	8.238

Table 7.18: Particle size calculated using the three different equations for Calcium Carbonate suspended in 1.0% Labrasol®

Equation	Vs (cm/s)	r (μm)
Steinour	0.0238	7.898
Richardson & Zaki	0.0234	7.821
Dollimore-Mcbride	0.0239	7.915
Average	0.0237	7.878

Table 7.19: Particle size calculated using the three different equations for Calcium Carbonate suspended in 2.0% Labrasol®

Equation	Vs (cm/s)	r (μm)
Steinour	0.0089	4.974
Richardson & Zaki	0.0088	4.946
Dollimore-Mcbride	0.00894	4.985
Average	0.00888	4.968

Table 7.20: Percent deviation of settling velocity and particle size during hindered settling

	Deviation (%)	
Media	V_s	r (μm)
Water	0.000	0.000
0.05% Labrasol®	-12.772	-4.662
0.5% Labrasol®	-51.328	-28.779
1.0% Labrasol®	-56.446	-31.896
2.0% Labrasol®	-83.713	-57.046

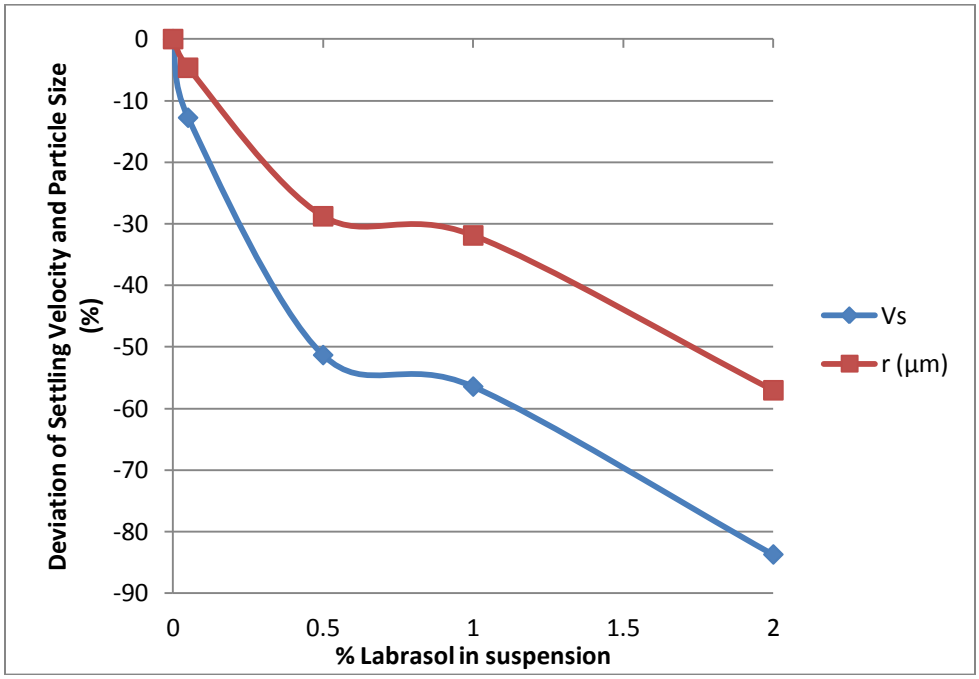

Figure 7-21: Plot of % Labrasol® in suspension against percent deviation of settling velocity and particle size compared to 0.0% Labrasol® concentration.

From the data presented above it is clear that increasing the concentration of Labrasol® led to the deflocculation of the system. Figure 7.21 shows the percent deviation of the settling velocities and the particle sizes when compared to a suspension with only water as the suspending media. The negative sign in the percent deviations denote that the settling velocities and particle sizes decreased as Labrasol® was increased. Figure 7-21 also shows that the settling velocities and particle sizes changed according to the same pattern, however, the change in settling velocity was more severe.

This deflocculation is most likely a result of the Labrasol® increasing the wettability of the calcium carbonate and decreasing particle-particle interactions leading to a decrease in particle size.

7.1.4 Permeability

In hindered settling, the suspended material can be stationary bed with the liquid media flowing upward through it. This is considered to be the permeability of the suspension. The permeability can be calculated from the rate of fall and settling velocity, or the (n) value determined from the Richardson and Zaki equation. The method to determine permeability in the experiment used the (n) value from the Richardson and Zaki equation. The equations used for the permeability calculations are listed below.

$$K = \frac{1}{2\varepsilon^{n-3}(1-\varepsilon)} \quad \text{Eq. 7.5}$$

$$\varepsilon_k = \frac{n-3}{n-2} \quad \text{Eq. 7.6}$$

$$K_{min} = \frac{1}{2\varepsilon_k^{n-3}(1-\varepsilon_k)} \quad \text{Eq. 7.7}$$

$$\varepsilon_1 = \frac{n}{n+1} \quad \text{Eq. 7.8}$$

Where:

K = Kozeny Carman Constant

ε = Bed porosity

n = Dimensionless number derived from Richardson & Zaki Equation

Using these equations, (K), (K_{min}), (ε_k), and (ε_1) are calculated, and these parameters are shown below in Table 7-21. Plots of (K) vs (ε), and (ε_k) vs (ε_1) are constructed and shown below.

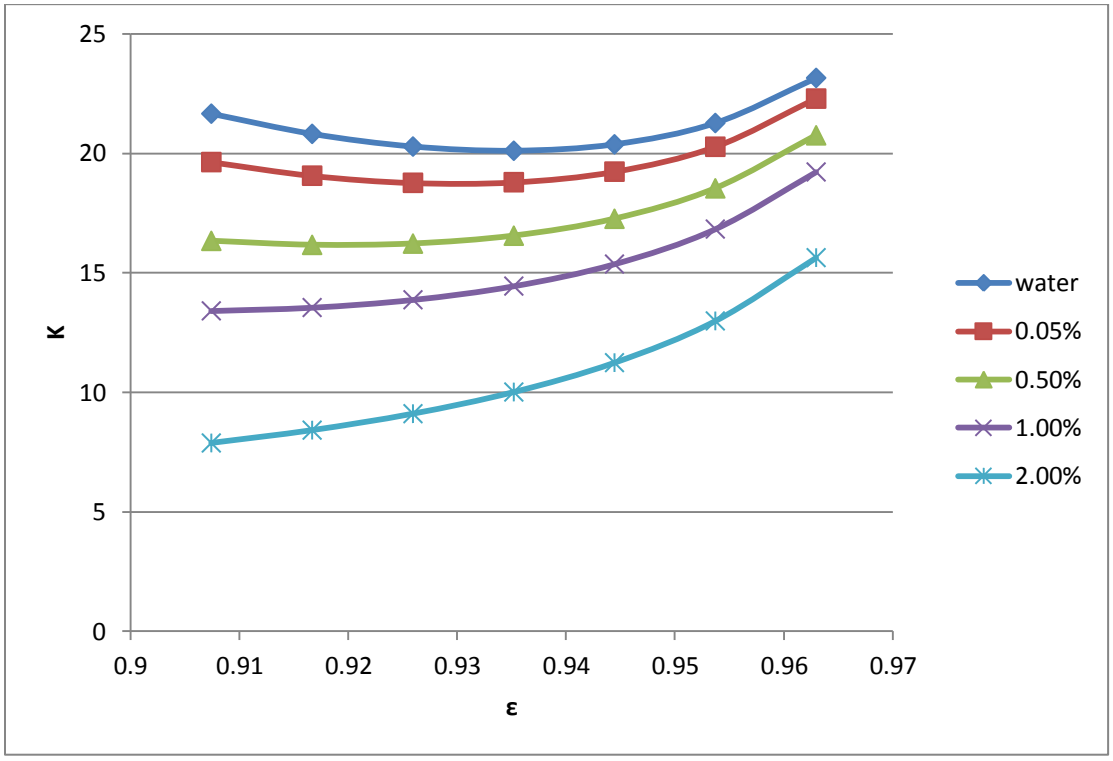

Figure 7-22 A plot of the Kozeny Carman constant for permeability (K) against porosity for calcium carbonate suspended in various experimental Labrasol® media

Table 7.21: The values for the permeability parameters of calcium carbonate suspended in various Labrasol® media

Medium	Weight (g)	K	ε_k	K_{min}
Water	20	23.153	0.934	20.104
	25	21.266		
	30	20.3746		
	35	20.105		
	40	20.281		
	45	20.812		
	50	21.657		
0.05%	20	22.287	0.93	18.731
	25	20.272		
	30	19.231		
	35	18.789		
	40	18.764		
	45	19.062		
	50	19.632		
0.50%	20	20.751	0.919	16.159
	25	18.533		
	30	17.260		
	35	16.552		
	40	16.221		
	45	16.168		
	50	16.336		
1.00%	20	19.218	0.903	13.395
	25	16.830		
	30	15.366		
	35	14.444		
	40	13.872		
	45	13.547		
	50	13.408		
2.00%	20	15.634	0.795	5.954
	25	12.986		
	30	11.240		
	35	10.012		
	40	9.106		
	45	8.417		
	50	7.881		

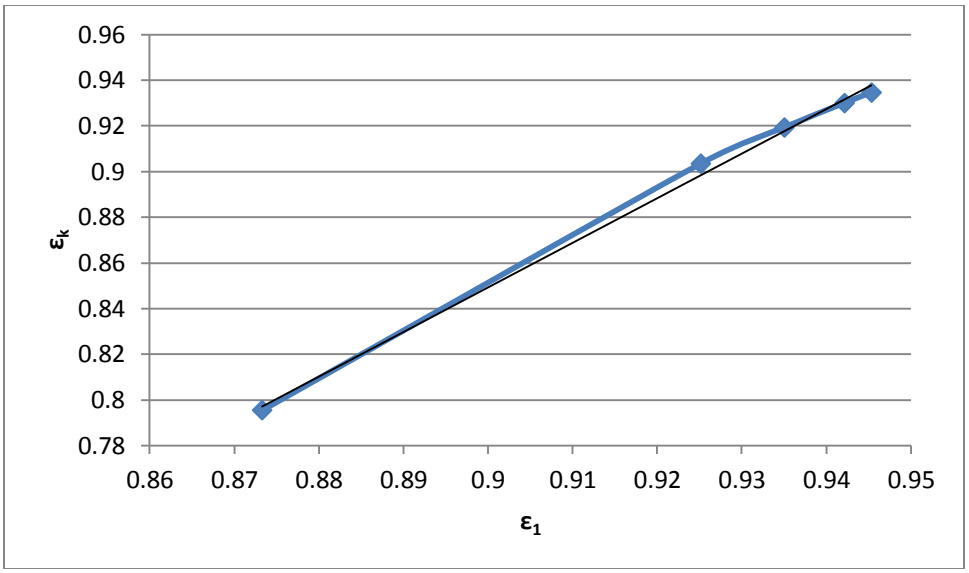

Figure 7-23: A plot of initial porosity and minimum porosity for calcium carbonate suspended in various Labrasol® media, where slope = 1.9542; intercept = -0.9095; and $R^2 = 0.9967$

Table 7.22: The values of initial porosity and minimum porosity for calcium carbonate suspended in various Labrasol® media

Media	ε_1	ε_k
Water	0.94534	0.934619
0.05% Labrasol®	0.942146	0.929996
0.5% Labrasol®	0.935035	0.919309
1.0% Labrasol®	0.92515	0.903475
2.0% Labrasol®	0.87327	0.795534

From the data presented in the above tables and figures, it can be shown that permeability decreased with increased Labrasol® concentration in the suspensions. This is most likely due to Labrasol® deflocculating the suspension leading to smaller particle sizes. Smaller calcium carbonate particles mean that the particles can pack in a tighter conformation compared to larger particles which have greater void space between them. The smaller particles fill in the void spaces in the settling bed and thus permeability to the liquid

media is decreased. This data correlates with the data presented in the previous section showing that Labrasol® decreased particle size and settling velocity. The reduced settling velocity can be related to the decreased permeability. The decreased permeability reduces the flow of the liquid through the settling bed and therefore causes it to be suspended longer, consequently showing a slower settling velocity.

7.2 Laser Diffraction

Laser diffraction studies were performed on suspensions containing 40 grams of calcium carbonate and Labrasol® concentrations from 0% to 2%. Methods used for laser diffraction were described in chapter 6.2.6.

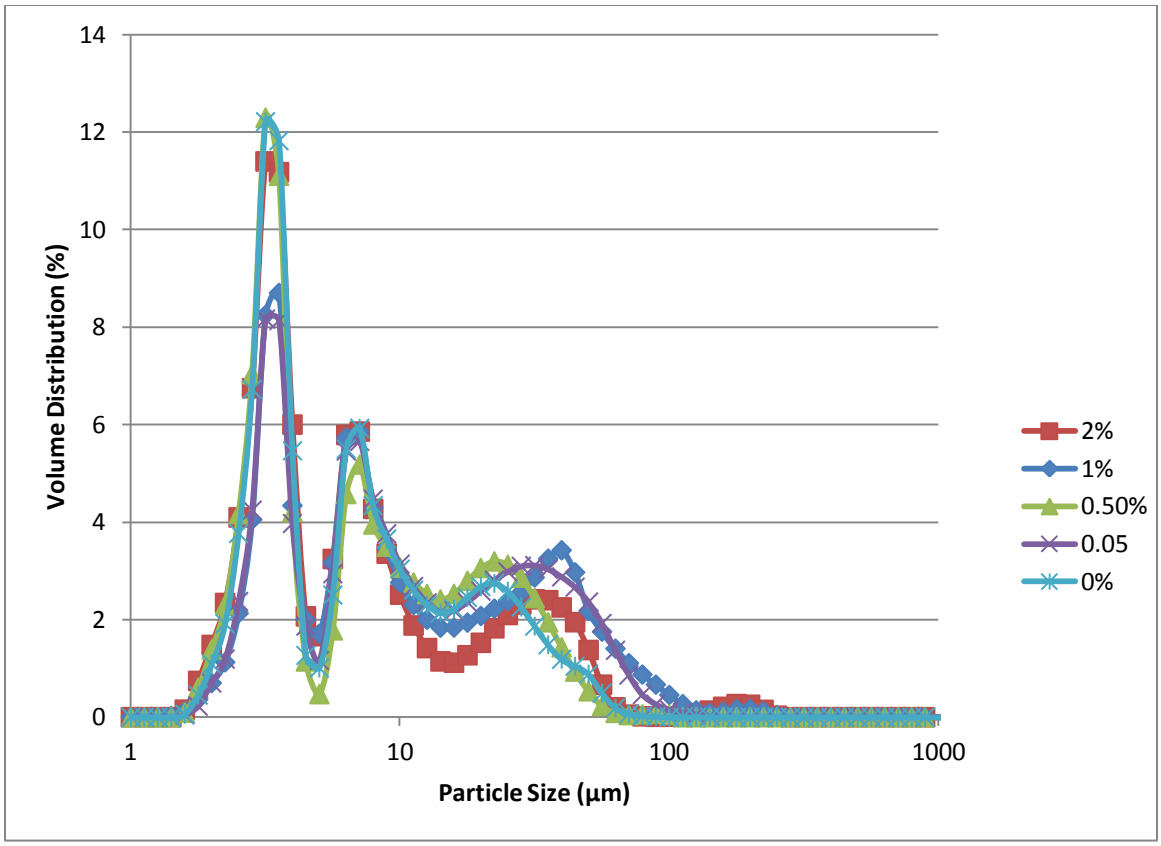

Figure 7-24: Comparison of laser diffraction results for 40gm of calcium carbonate with various Labrasol® concentrations

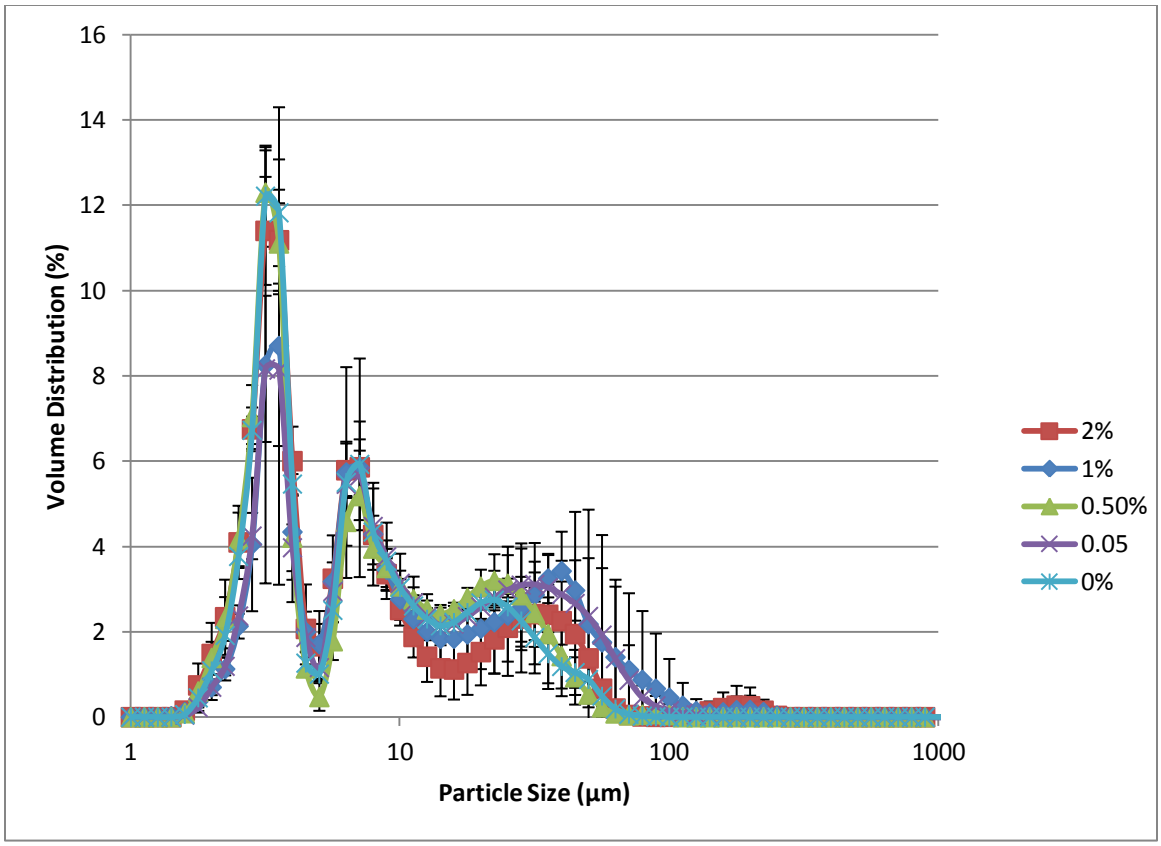

Figure 7-25: Comparison of laser diffraction results for 40gm of calcium carbonate with standard deviation error bars given for various Labrasol® concentrations

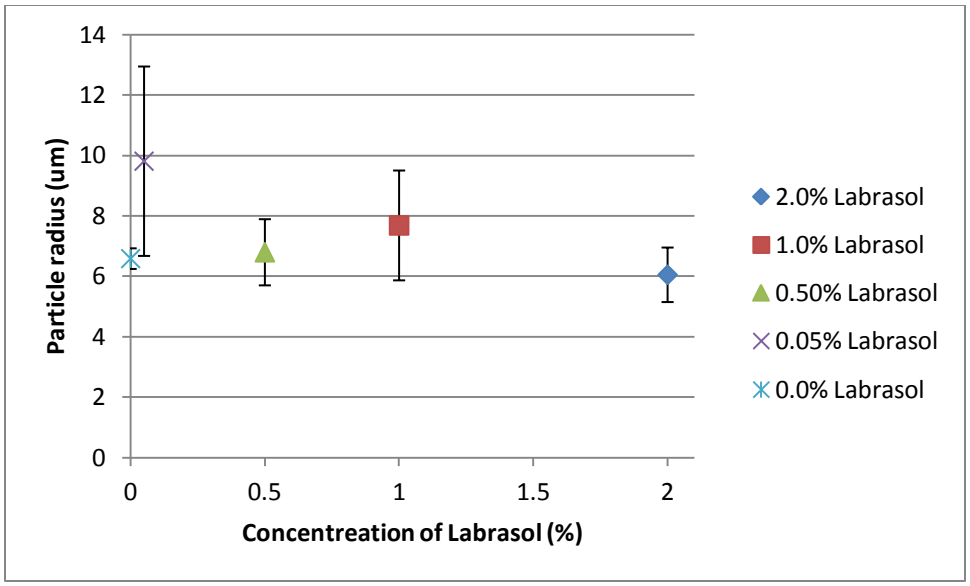

Figure 7-26: Plot of average particle size against the concentration of Labrasol® for 40gm calcium carbonate in suspension.

Table: 7.23 Mean Particle size parameters for calcium carbonate Suspension

	Labrasol® Concentration (%)	d (0.5) (µm)	Std. Dev.	Maximum Particle Size (µm)	Minimum Particle Size (µm)
2	2.00%	6.050	0.901	282.507	1.782
1	1.00%	7.684	1.817	100.237	1.782
0.5	0.50%	6.796	1.094	112.468	1.782
0.05	0.05%	9.810	3.134	158.865	1.782
0	0.00%	6.586	0.341	100.237	1.782

Results from laser diffraction indicate that the Calcium carbonate suspensions have a large particle size range. Table 7.23 shows that while the Labrasol® does seem to affect the maximum particle size, it doesn't change the minimum particle size, which remains constant at all Labrasol® concentrations. From Figures 7-25 and 7-26 we can infer that the particle size distributions of the suspensions containing different concentrations of Labrasol® are all the same. This can be said because the error bars overlap which means that there is no statistical difference between the values and hence are the same. The data

from the laser diffraction studies does not match up with the data obtained from the analysis of the data performed in Chapter 7.1. This is most likely due to the homogenizer used in the laser diffraction experiment which disrupted any particle agglomeration.

7.3 Differential Scanning Calorimetry Results:

Differential Scanning Calorimetry was performed using the method stated in Chapter 6. Exothermic peaks shown on the thermograms represented the crystallization of water, and the endothermic peaks represented the melting and vaporization of water. The heat of crystallization (H_c), heat of fusion (H_m), and heat of vaporization (H_v) are listed below in Table 7.24

Table 7.24: Thermogram data, heat of crystallization (H_c), fusion (H_m), and vaporization (H_v). and temperatures at T_c,T_m and T_v. for calcium carbonate Suspension in water and various experimental concentrations of Labrasol®

Medium	H_c (J/g)	T_c (°C)	H_f (J/g)	T_m (°C)	H_v (J/g)	T_v (°C)
Water	274.940	-6.290	-298.830	4.540	-1831.140	100.860
0.05% Labrasol®	287.440	-7.110	-314.500	5.290	-1345.380	103.190
0.5% Labrasol®	190.010	-7.150	-206.460	3.190	-1164.140	102.220
1.0% Labrasol®	245.930	-7.210	-255.690	4.850	-1468.270	102.610
2.0% Labrasol®	313.650	-4.420	-316.070	4.540	-1501.330	98.000

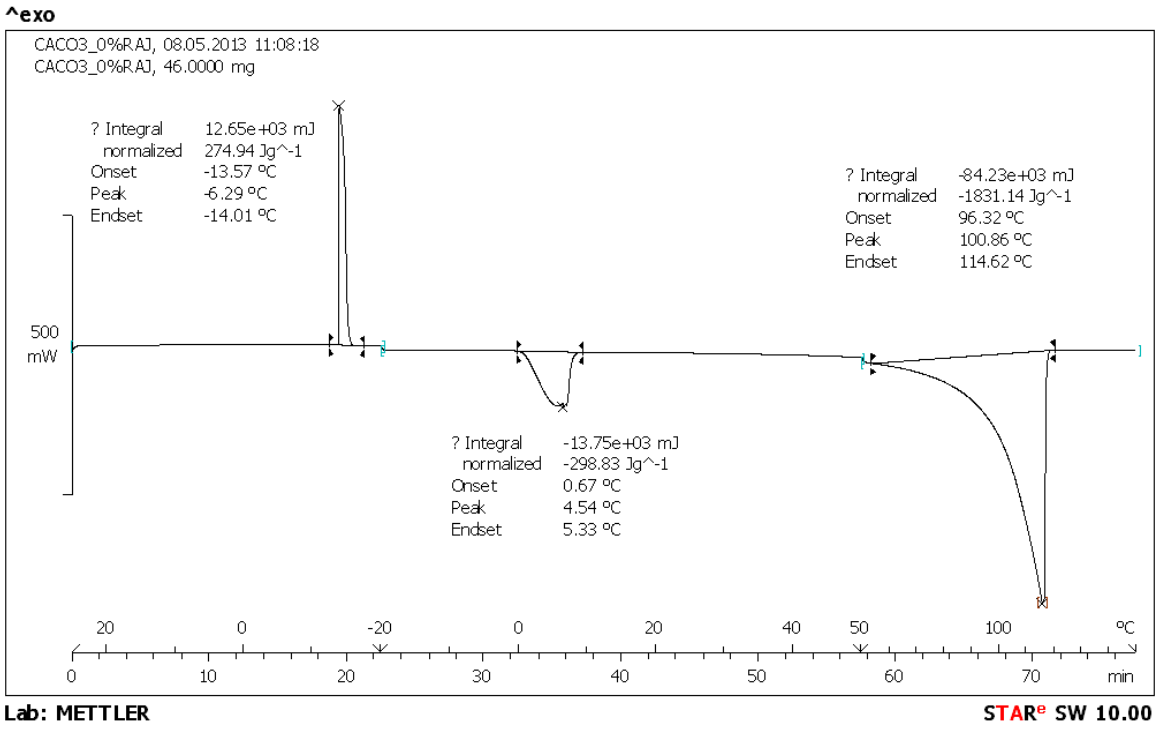

Figure 7-27: DSC thermogram for 30 g of calcium carbonate suspended in water.

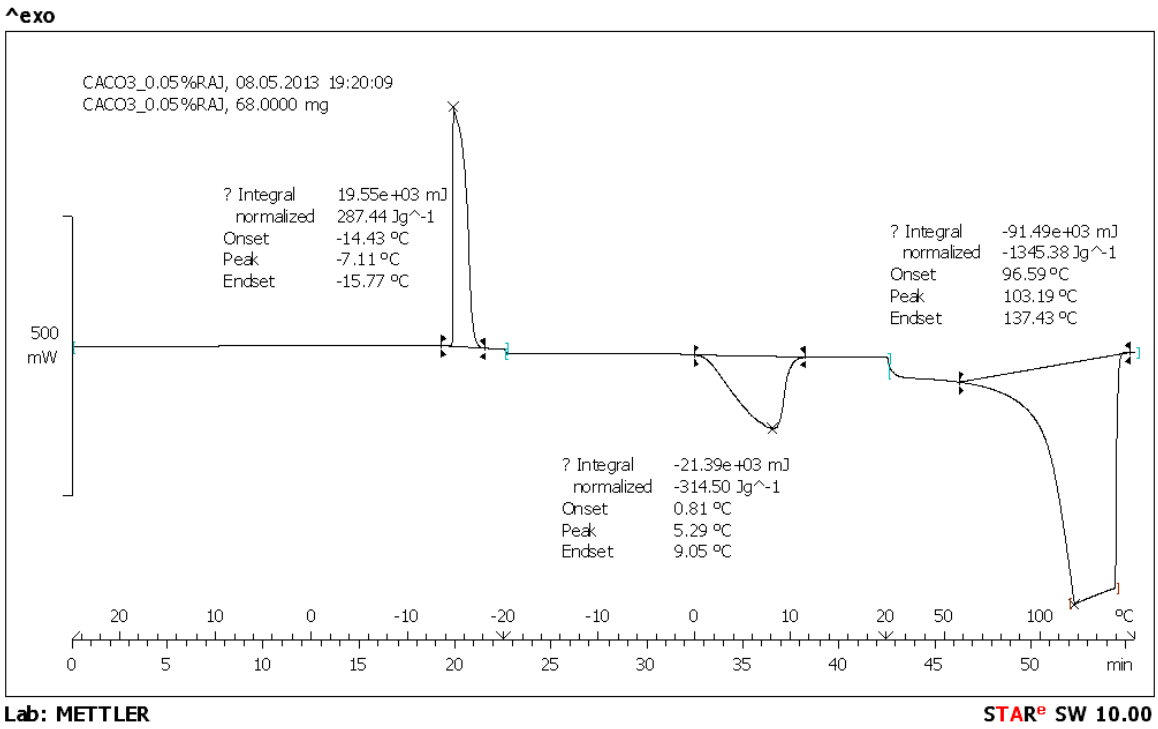

Figure 7-28: DSC thermogram for 30 g of calcium carbonate suspended in 0.05% Labrasol®.

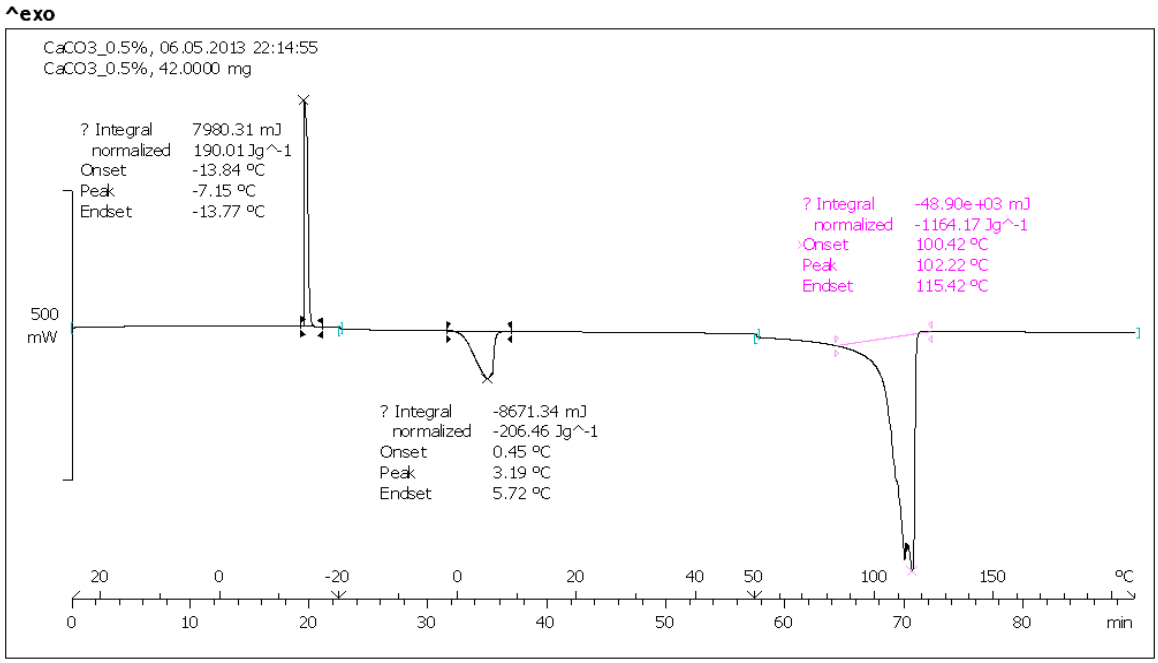

Figure 7-29: DSC thermogram for 30 g of calcium carbonate suspended in 0.5% Labrasol®.

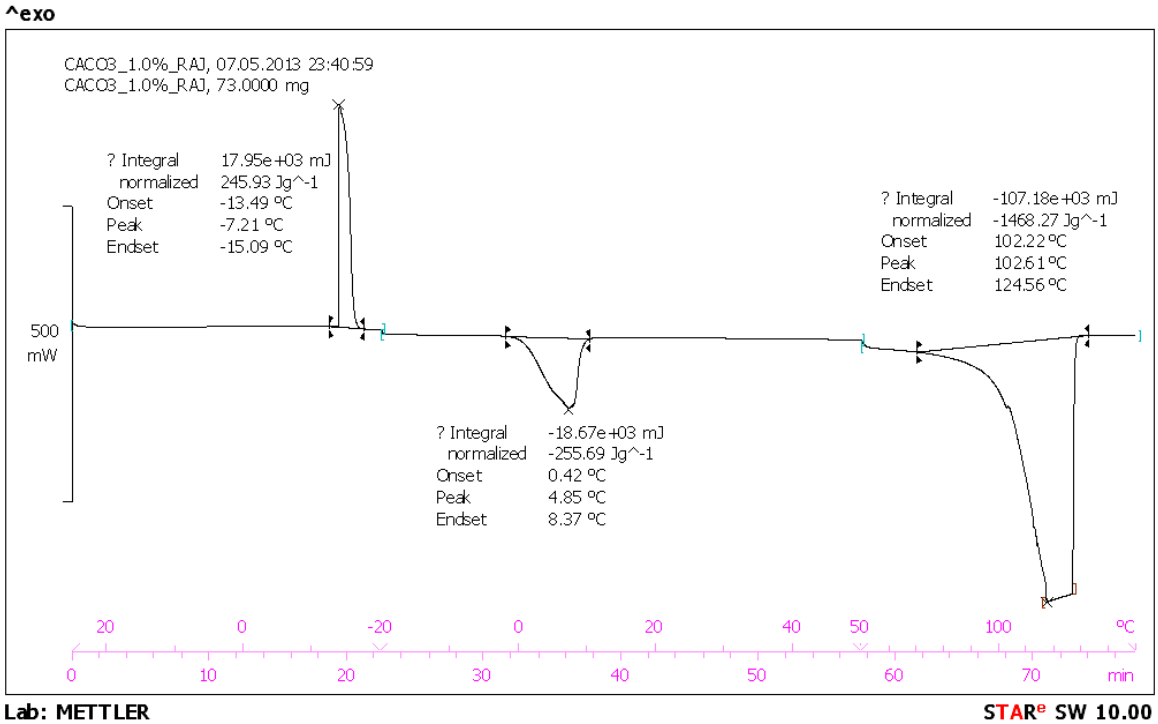

Figure 7-30: DSC thermogram for 30 g of calcium carbonate suspended in 1.0% Labrasol®.

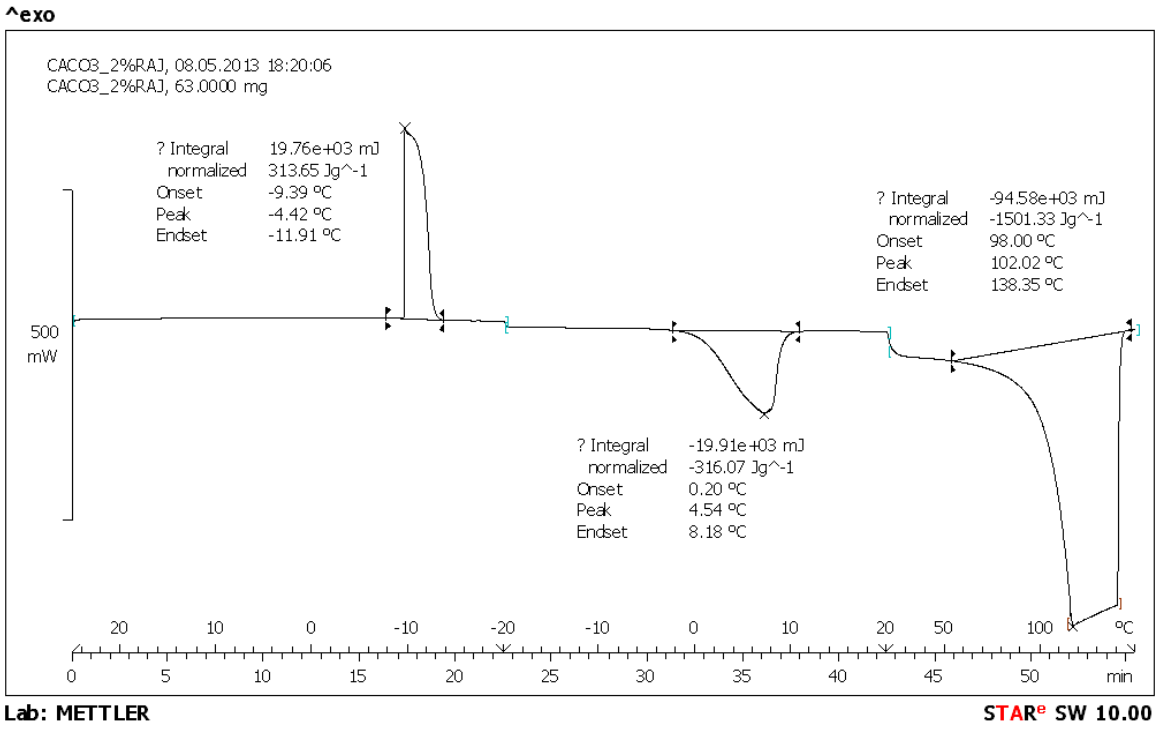

Figure 7-31: DSC thermogram for 30 g of Calcium Carbonate suspended in 2.0% Labrasol®

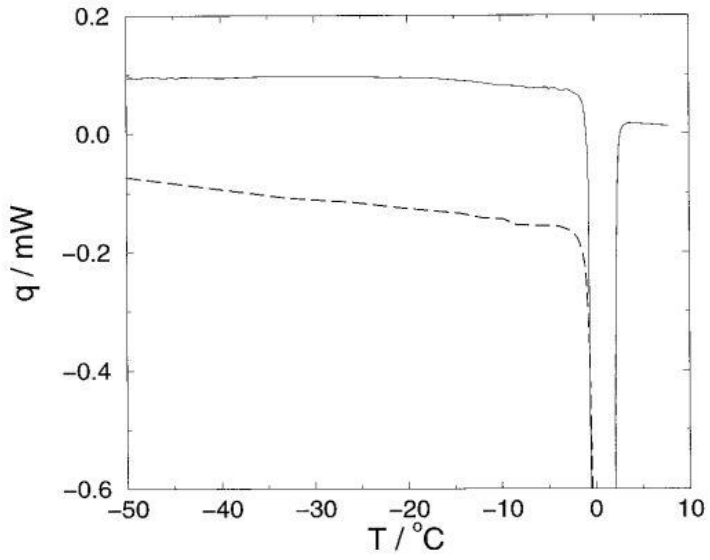

Figure 7-32: DSC thermogram of pure ice melting during a DSC experiment. The solid line has a warming rate of 5^0C/min, and the dashed line has a heating rate of 1^0C/min

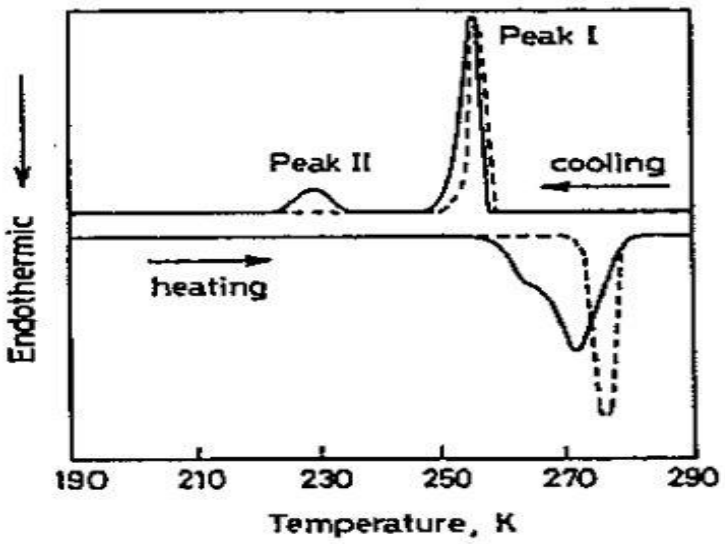

Figure 7-33: DSC thermogram. The unbroken line is sample of water adsorbed on cellulose samples, and dashed line is pure water.

Differential scanning calorimetry was used to examine the bound and unbound water content within the samples. From Table 7.24 is can be shown that when compared to 0.0% Labrasol® suspensions, the other suspensions an alteration in the water vaporization peaks. Pure water is has a heat of fusion of 334 J/g, and a heat of vaporization of 2270 J/g. As seen in the above two figures showing cooling and heating of pure water, the pure water peaks are much sharper, and the melting peak is right at 0^0C. Free water, which can also be called bulk water, has enthalpies closer to that of pure water, however in a system with other components, these peaks can be shifted due to supercooling effects and interactions with the additives. In the data presented, all the heats of vaporization are below the value stated in literature sources. As the concentration of Labrasol® is increased, the heats of vaporization decrease even more when compared to the 0.0% Labrasol® suspension. This suggests that the increasing concentration of Labrasol® is leading to interactions between the Labrasol®, Calcium carbonate, and water. A possible explanation is that, the increased concentration of surfactant is lowering the surface tension between the liquid and the air. This decreased

surface tension allows for water molecules to more easily escape the liquid phase at the boiling point temperature. As to the point of bound water, based on these results it cannot be definitively stated that there is an increase or decrease in the content of bound water. However, given the nature and purpose of a non-ionic surfactant, and in addition to the particle size analysis showing decreased particle sizes, it is possible to infer that there is an increase in bound water due to the surfactant increasing the wettability and surface area of the calcium carbonate allowing for more water adsorption on its surfaces.

7.4 Average Zeta Potential Results:

Zeta potential experiments were performed on suspensions containing 30 grams of calcium carbonate and various concentrations of Labrasol®. The method used was described in chapter 6. The zeta potential measurements are listed below in table 7.25

Table 7.25: Zeta potential values for 30 g calcium carbonate suspensions with various experimental Labrasol® concentrations

Dispersion Media	Average zeta potential	Std Dev
Water	-4.751	1.815
0.05% Labrasol®	-8.366	1.873
0.5% Labrasol®	-10.891	1.633
1.0% Labrasol®	-9.506	2.420
2.0%Labrasol®	-6.817	0.723

It was observed that increasing the concentration of Labrasol® caused the zeta potential to become more negative. This is likely due to the deflocculation of the suspension as a result of the Labrasol®. The decreased particle sizes resulting from the Labrasol® lead to more adsorption sites for ions forming the electric double layer creating a more negative zeta potential. In the case of the zeta potential measure for the 2.0% Labrasol®

suspension, the decrease in zeta potential is more likely due to steric hindrance from the high concentration of Labrasol® which adsorbs onto the particles and blocks out ions limiting the formation of the electric double layer and causing a zeta potential closer to zero.

7.5 X-ray Powder Diffraction (PXRD):

PXRD was performed on calcium carbonate suspensions according to the method described in chapter 6. The diffractogram produced from the experiments is shown below.

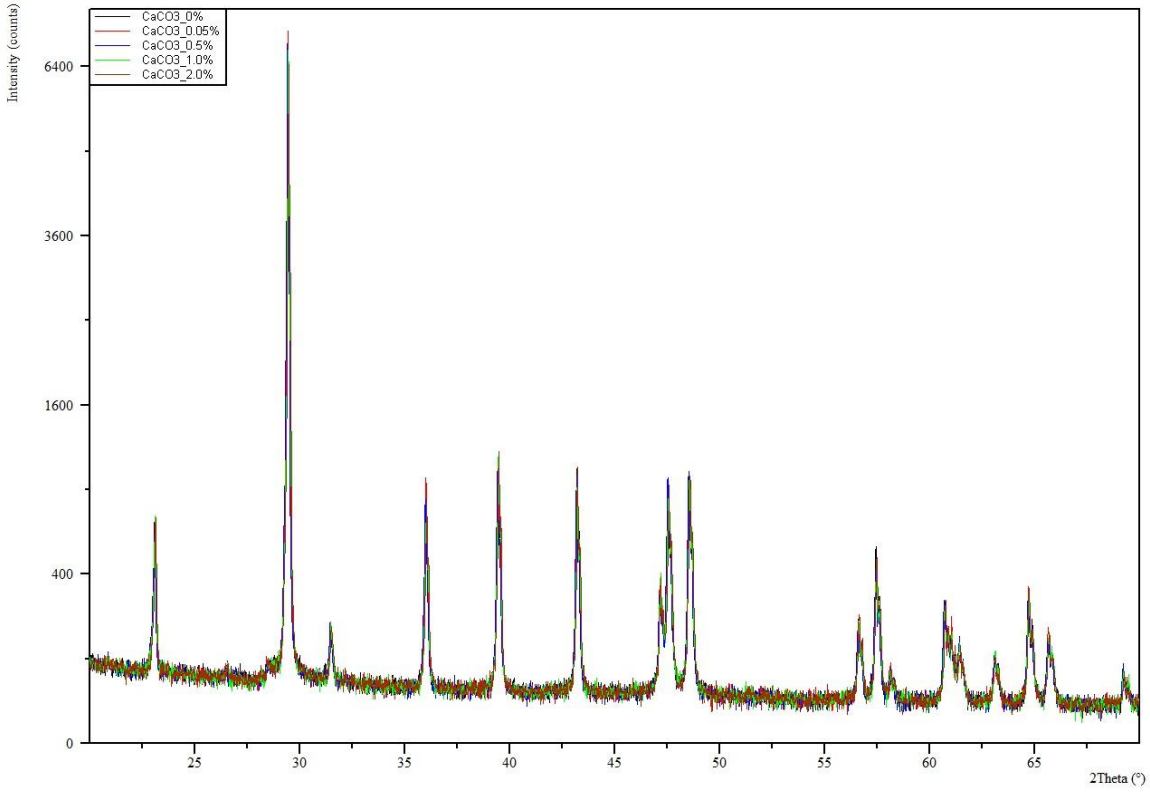

Figure 7-32: Diffractogram calcium carbonate with varying concentrations of Labrasol®

When analyzing the diffractogram produced from the PXRD experiments, it is shown that the variation in the concentration of Labrasol® has no effect on the crystallinity of the Calcium carbonate. At all concentrations of Labrasol®, the diffractogram patterns overlap almost completely making them indistinguishable from one another as seen above in figure 7-32.

7.6 Scanning Electron Microscopy (SEM) results:

Scanning electron microscopy was carried out according to the method explained in Chapter 6. Images of the dried calcium carbonate suspensions are shown below.

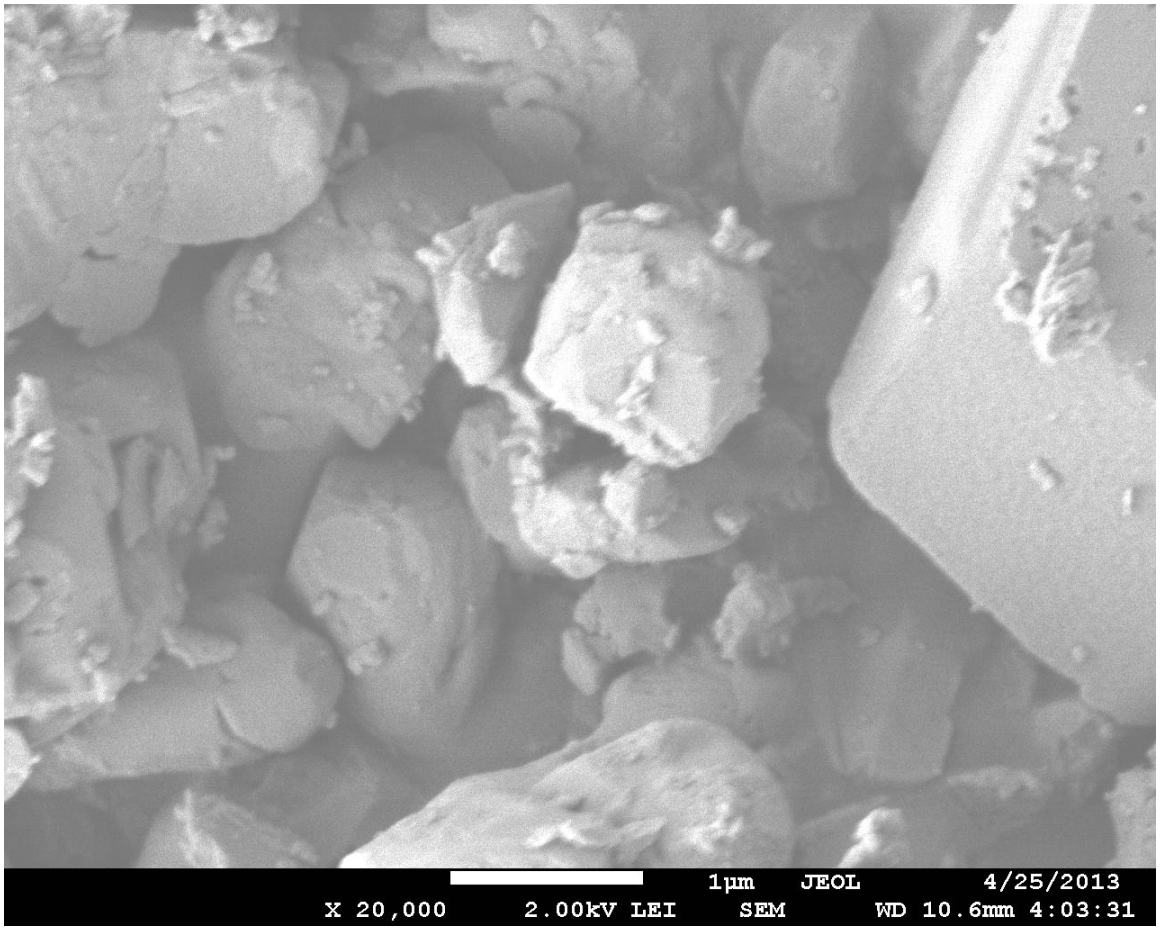

Figure 7-33: SEM image of calcium carbonate dispersed in water.

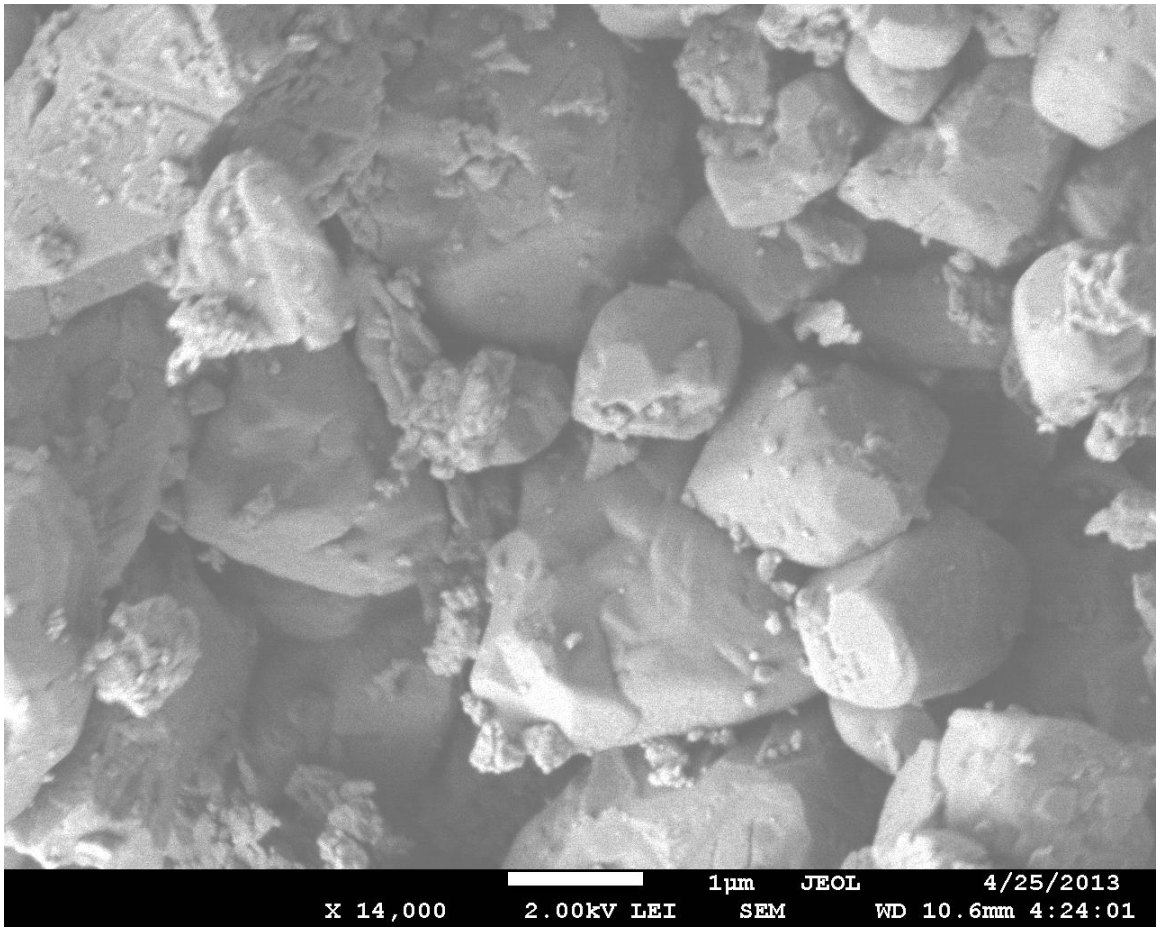

Figure 7-34: SEM image of calcium carbonate dispersed in 0.05% Labrasol®

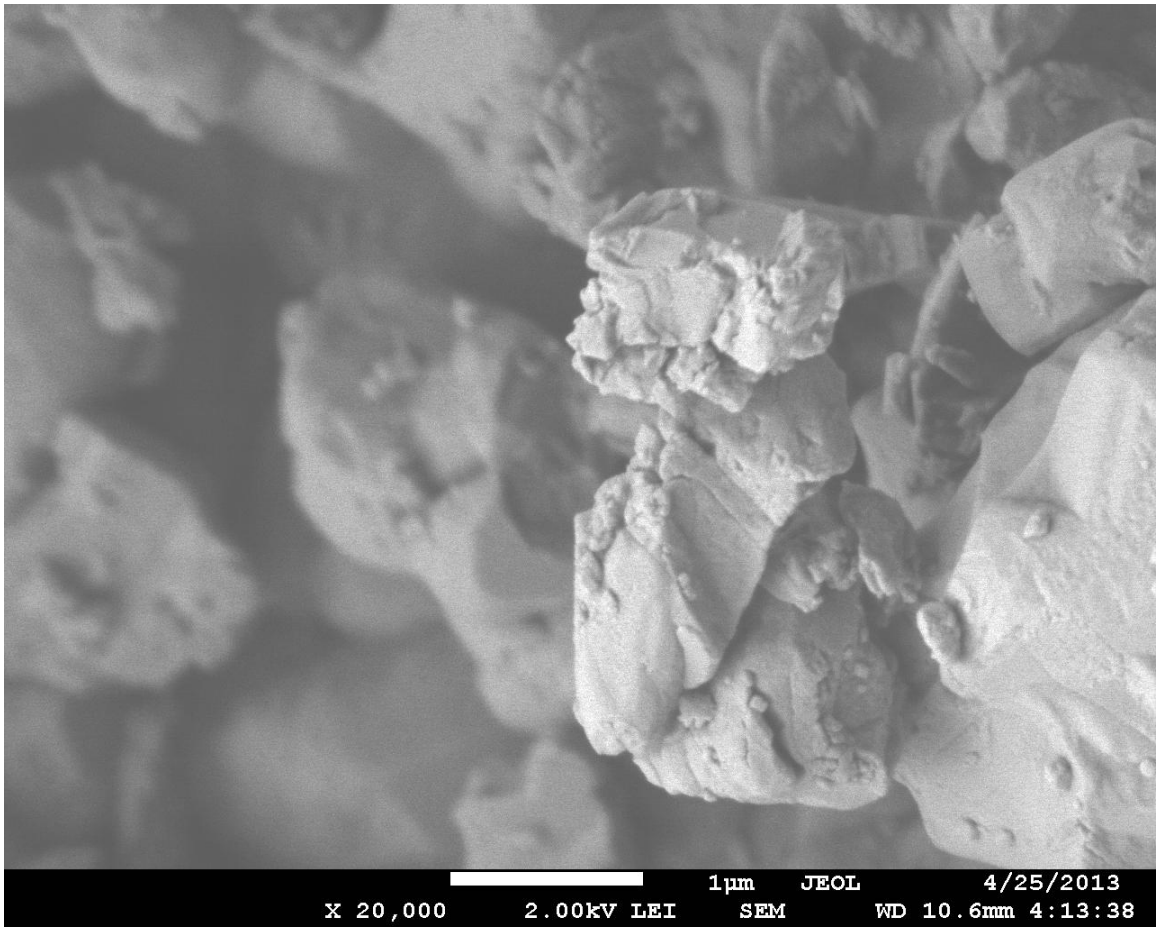

Figure 7-35: SEM image of calcium carbonate dispersed in 0.5% Labrasol®

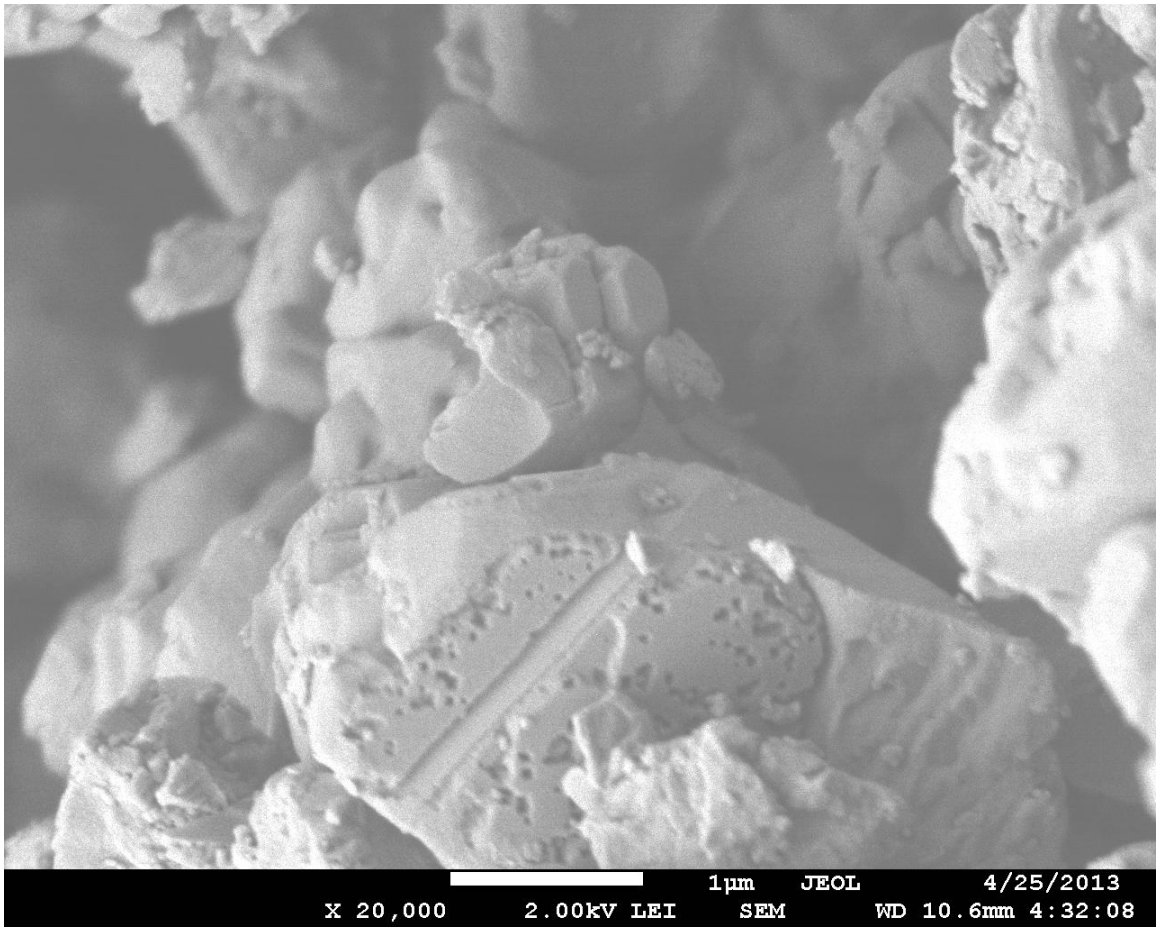

Figure 7-36: SEM image of calcium carbonate dispersed in 1.0% Labrasol®

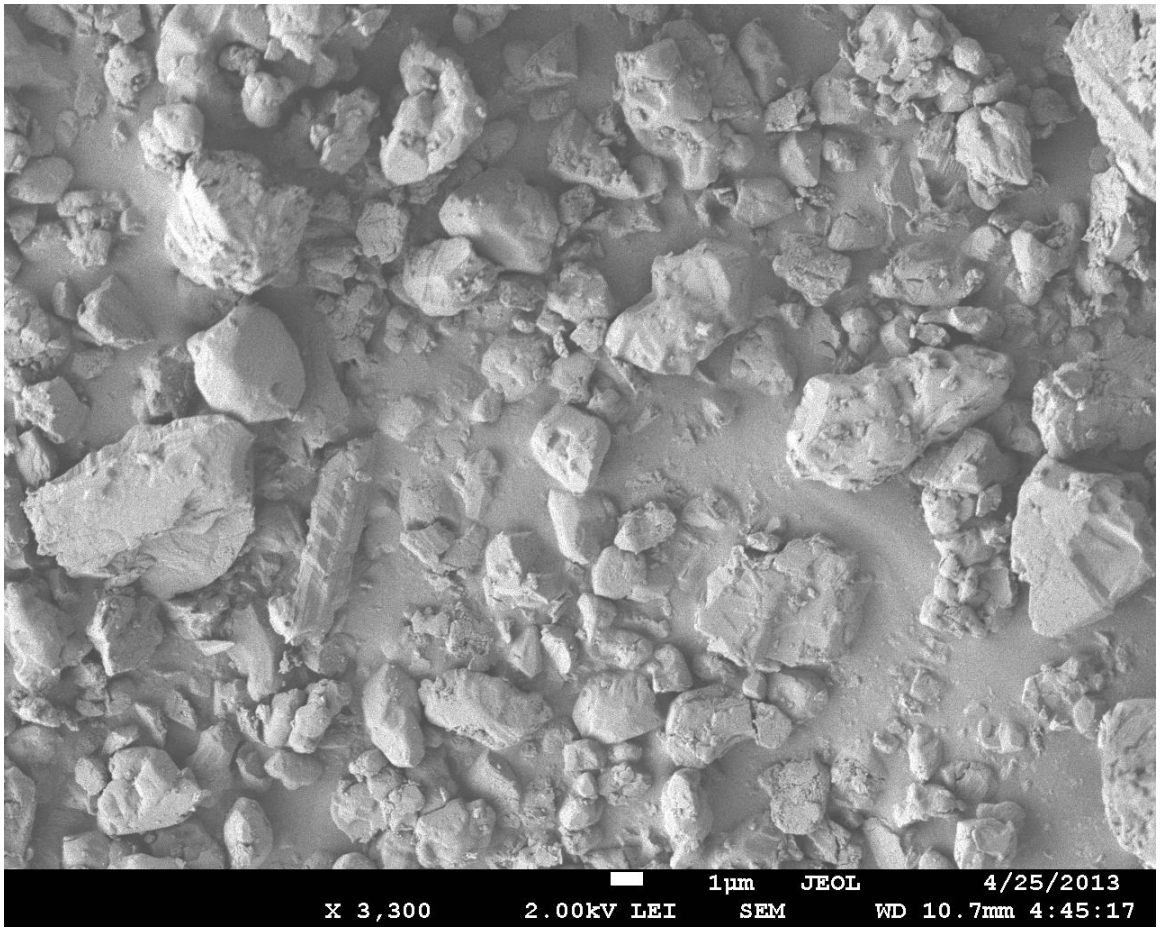

Figure 7-37: SEM image of calcium carbonate dispersed in 2.0% Labrasol®

The samples used for scanning electron microcopy were dried which means that any particle clusters that were present in suspension most likely won't be visible here. As the suspension was dried, the particle agglomerated and therefore you get the appearance seen in the images above. Due to the agglomeration of the particles from drying, it became difficult to see the specific surface morphology of the calcium carbonate, however in some of the images, there is some trace of the rhomohedral structure that was not covered up by the particle coagulation. Particle size analysis was not carried out on the calcium carbonate images due to the intensive nature of it, but based on the scales

present on the images; it appears that particles in the 0 to 100 micrometer range are present which is in agreement with the data shown from the hindered settling calculations.

Chapter 8

Conclusion

8.1 **Conclusions**

Suspensions made from ground calcium carbonate showed hindered settling behavior. Suspensions at all concentrations of Labrasol® were redispersible and didn't show significant signs of caking when compared to the suspension with 0.0% Labrasol®. The hindered settling experiments were shown to be effective in determining particle size and the Steinour, Richardson & Zaki and Dollimore & McBride equations produced results that were in agreement with each other. Laser diffraction is a useful tool in determining particle size, however, in this case it didn't match up perfectly with the data from the hindered settling calculations. This was most likely due to the homogenizer effecting the particle interactions. This is visible in the Figures 7-23 to 7-25 where it is shown that regardless of the Labrasol® concentration, the particle size distribution is the same.

From the data acquired from the hindered settling experiments, it is shown that Labrasol® doesn't act as a flocculating agent with calcium carbonate, and instead causes the suspension to deflocculate, especially at higher concentrations.

Zeta potential measurements show that Labrasol® leads to a more negative zeta potential. This fits with the hindered settling data that shows deflocculation of the suspension due to Labrasol®. The more negative the zeta potential, the greater the repulsive forces between the particles and the more deflocculated the suspension becomes. Labrasol® is a non-ionic surfactant, meaning that it doesn't confer or take away charge from the suspended particles, this suggests that there is some type of steric hindrance effect caused by Labrasol® which is affecting the electric double layer formation. One possibility is that the deflocculation is opening up more adsorption sites for ions to form an electric double layer.

Powder x-ray diffraction shows that the Labrasol® has no effect whatsoever on the crystalline nature of the calcium carbonate. The diffractograms overlap almost completely which means that there is no difference in the cyrstallinity between the different suspensions.

Differential scanning calorimetry results showed that increased amounts of Labrasol® caused a decrease in the heat of vaporization of water. This was likely attributed to decreased surface tension between the liquid media and the air, allowing for easier evolution of liquid vapor upon reaching the boiling point. After analyzing the thermograms for bound and unbound water content, it could not be definitively stated if the Labrasol® altered water content. However, in conjunction with the particle size analysis, which showed significant decreases in particle size, it can be postulated that there is an increase in the bound water content. Due to the decreased particle size, the total surface area available to water adsorption is greatly increased, also, Labrasol® increased the wettability of the calcium carbonate by decreasing the contact angle

between water and calcium carbonate allowing for water to more easily adsorb onto its surface. To be able to state with certainty that there is an increase in bound water content, further thermal analysis would be required.

8.2 **Future studies**

Future hindered settling experimentation on ground calcium carbonate should be performed using other additives such as anionic surfactants, cationic surfactants, electrolytes, viscosity modifiers, and other types of polymers. Experimentation with pH modification can be carried out to see how sedimentation is affected by it. Adsorption characterization experiments should be carried out on the additives used in the suspension. Sedimentation experiments should be carried out, and then analytical techniques such as HPLC can be used to determine the content of the additive in the supernatant which would be characteristic of how much was adsorbed onto the suspended particles.

References

< Chapter 3

1. Azizi, J., et al., *The development of a permeability theory applied to concentrated suspensions.* Colloids and surfaces, 1992. **62**(1-2): p. 1-9.
2. Majumder, A., *Settling velocities of particulate systems- a critical review of some useful models.* Minerals and Metallurgical Processing, 2007. **24**(4): p. 237-242.
3. McKay, R.B., *Hindered settling of organic pigment dispersions in hydrocarbon liquids.* J. Appl. Chem. Biotechnol., 1976. **26**(2): p. 55-66.
4. Bhatty, J.I., et al., *The Use Of Hindered Settling Data To Evaluate Particle-Size Or Floc Size, And The Effect Of Particle-Liquid Association On Such Sizes.* Surface Technology, 1982. **15**(4): p. 323-344.
5. Zimmels, Y., *Theory Of Hindered Sedimentation Of Polydisperse Mixtures.* AIChE Journal, 1983. **29**(4): p. 669-676. 147
6. Steinour, H.H., *Rate of sedimentation Nonflocculated Suspensions of Uniform Spheres.* Industrial & Engineering Chemistry, 1944. **36**(7): p. 618-624.
7. Ramakrishna, V. and S. Rao, *Particle size determination and hindered settling.*

Journal of Applied Chemistry, 1965. **15**(10): p. 473-479.

8. Di Felice, R. and R. Kehlenbeck, *Sedimentation velocity of solids in finite size vessels.* Chemical engineering & technology, 2000. **23**(12): p. 1123-1126.
9. Davies, L., D. Dollimore, and J. Sharp, *Sedimentation of supsensions: implications of theories of hindered settling.* Powder Technology, 1975. **13**(1): p. 123-132.
10. Baldock, T., et al., *Settling velocity of sediments at high concentrations.* Coastal engineering, 2004. **51**(1): p. 91-100.
11. Dollimore, D. and G. McBride, *Comparison of methods of calculating particle size from hindered settling results and its application to inorganic oxysalt precipitates.* Analyst, 1969. **94**(1122): p. 760-767.
12. Davies, L. and D. Dollimore, *Theoretical and experimental values for the parameter k of the Kozeny-Carman equation, as applied to sedimenting suspensions.* Journal of Physics D: Applied Physics, 1980. **13**: p. 2013.
13. Happel, J., *Viscous flow in multiparticle systems: slow motion of fluids relative to beds of spherical particles.* AIChE J., 1958. **4**: p. 197-201.
14. Dollimore, D. and G. McBride, *Alternative methods of calculating particle size from hindered settling measurements.* Journal of Applied Chemistry, 1968. **18**(5): p. 136-140.

Chapter 4

1. Aulton, M.E. and J.W. Cooper, *Pharmaceutics: the science of dosage form design.* 2002.
2. Martin, A.N., J. Swarbrick, and A. Cammarata, *Physical pharmacy : physical chemical principles in the pharmaceutical science*. 2d ed1969, Philadelphia: Lea & Febiger. vii, 637 p.
3. Lachman, L., H.A. Lieberman, and J.L. Kanig, *The theory and practice of industrial pharmacy*1970, Philadelphia,: Lea & Febiger. xii, 811 p.
4. Huang, Yi-Bin and P. Somasundara. "Discrete modeling of sedimentation." 28 April 1988. <http://www.columbia.edu/~ps24/PDFs/Discrete%20Modeling%20of%20Sedimentation.pdf>.
5. Kopeliovich, Dmitri Kopeliovich. Stabilization of colloids. 20 September 2013 <http://www.substech.com/dokuwiki/doku.php?id=stabilization_of_colloids>.
6. Pharmainfo.net. 2005; Available from: http://www.pharmainfo.net/freebooks/pharmaceutical-suspensionsa-review.
7. Stillinger Jr, Frank H. and John G Kirkwood. "Theory of the Diffuse Double Layer." The Journal of Chemical Physics (1960).
8. Rawlings, M.M., C.S.B Fitzpatrick and J Gregory. "The effect of polymeric flocculants on floc strength and filter performance." March 2006. EBSCO HOST. <http://connection.ebscohost.com/c/articles/21209524/effect-polymeric-flocculants-floc-strength-filter-performance>.

Chapter 5

1. AZojomo, T.A.t.Z.o.M.a. *Particle Size Analysis - The Laser Diffraction Technique*. 2011; Available from: http://www.azom.com/article.aspx?ArticleID=1528.
2. Chu, B., *Laser light scattering.* NASA STI/Recon Technical Report A, 1974. **75**:p. 12150.
3. Botiren, C. and D.R. Huffman, *Absorption and scattering of light by small particles.* J Wiley & Sons, New York, 1983
4. de Boer, G.B.J., et al., *Laser diffraction spectrometry: Fraunhofer diffraction versus Mie scattering.* Particle & Particle Systems Characterization, 1987. **4**(1-4): p. 14-19.
5. Malvern. 2011; Available from: http://www.malvern.com/LabEng/industry/colloids/dlvo_theory.htm.
6. Analyser, C.P.S. 2004; Available from: http://www.particle-sizeanalyzer.com/frequently_asked_questions.pdf.
7. malvern. *Zeta potential measurement using laser doppler electrophoresis*. 2012; Available from: http://www.malvern.com/labeng/technology/zeta_potential/zeta_potential_lde.htm.

8. Raj, P.M. and W.R. Cannon, *Electrosteric stabilization mechanisms in nonaqueous high solids loading dispersions.* Surfactant Sci. Ser., 2002. 104(Polymers in Particulate Systems): p. 27-61.

9. Li, L.C. and Y. Tian, *Zeta potential.* Encyclopedia of pharmaceutical technology, 2002. **2**: p. 429–458.

10. Wikipedia. *Electrophoretic light scattering*. 2012; Available from:http://en.wikipedia.org/wiki/Electrophoretic_light_scattering.

11. Reimer, L., *Scanning electron microscopy: physics of image formation and microanalysis*. Vol. 45. 1998: Springer Verlag.

12. Goldstein, J., *Scanning electron microscopy and X-ray microanalysis*. Vol. 1. 2003: Springer Us.

13. Wikipedia. 2011; Available from: http://en.wikipedia.org/wiki/Scanning_electron_microscope.

14. Whittingham, S. *X-ray analysis of a solid*. 1997; Available from: http://materials.binghamton.edu/labs/xray/xray.html.

15. Connolly, J.R. *Introduction to X-ray Powder Diffraction*. 2007; Available from: http://epswww.unm.edu/xrd/xrdclass/01-XRD-Intro.pdf.

16. Mississippi, T.U.o.S. 2005; Available from: http://pslc.ws/macrog/dsc.htm.

17. Tarr, Martin. 29 September 2013 <http://www.ami.ac.uk/courses/topics/0140_pl/index.html>.

18. Laboratory, Nanoscale Devices and Materials Physics. Research: Nanocharacterization. 15 October 2013 <http://nanoscience.skku.edu/index.php?cont=research&subcont=characterization >.

Chapter 6

1. Letco Medical.Material Safety Data Sheet Hubercal 250 USP. MSDS. Decatur: Letco Medical, 2004.
2. Letco Medical. Certificate of Analysis. COFA. Decatur: Letco Medical, 2010.
3. Gattefosse. Labrasol. 2010. 10 September 2013 <http://www.gattefosse.com/node.php?articleid=296>.
4. J.M. Huber Corporation. "Hubercal USP 250 Product Specifications." 18 March 2006. <http://www.barringtonchem.com/docs/Calcium-Carbonate-USP-Powder-HuberCAL-250-JM-Huber.pdf>.

Chapter 7

1. Shulz, P C. "DSC ANALYSIS OF THE STATE OF WATER IN SURFACTANT-BASED MICROSTRUCTURES." Journal of Thermal Chemistry (1998): 135-149.
2. Wen, D S and B X Wang. "Effects of surface wettability on nucleate pool boiling heat transfer for surfactant solutions." International Journal of Heat and Mass Transfer (2001): 1739-1747.
3. Garti, N, et al. "Water Behavior in Nonionic Surfactant Systems I:Subzero Temperature Behavior of Water in Nonionic Microemulsions Studied by DSC." Journal of Colloid and Interface Science (1996): 60-68.
4. Nakamure, Kunio, Tatsuko Hatakeyama and Hyoe Hatakeyama. "Studies on Bound Water of Cellulose by Differential Scanning Calorimetry." Textile Research Journal (1981): 607-613.
5. Wilson, P W, J W Arthur and A D.J. Haymet. "Ice Premelting during Differential Scanning Calorimetry." Biophysical Journal (1999): 2850–2855.